THE STATISTICAL AND DYNAMICAL MODELS OF NUCLEAR FISSION

By

JHILAM SADHUKHAN

Variable Energy Cyclotron Centre, Kolkata

A thesis submitted to
The Board of Studies in Physical Sciences

In partial fulfillment of requirements
for the Degree of
DOCTOR OF PHILOSOPHY

of

HOMI BHABHA NATIONAL INSTITUTE

January, 2012

STATEMENT BY AUTHOR

This dissertation has been submitted in partial fulfillment of requirements for an advanced degree at Homi Bhabha National Institute (HBNI) and is deposited in the Library to be made available to borrowers under rules of the HBNI.

Brief quotation from this dissertation are allowable without special permission, provided that accurate acknowledgement of source is made. Requests for permission for extended quotation from or reproduction of this manuscript in whole or in part may be granted by the Competent Authority of HBNI when in his or her judgement the proposed use of the material is in the interests of scholarship. In all other instances, however, permission must be obtained from the author.

Jhilam Sadhukhan

DECLARATION

I, hereby declare that the investigation presented in the thesis has been carried out by me. The work is original and has not been submitted earlier as a whole or in part for a degree/diploma at this or any other Institution/University.

Jhilam Sadhukhan

Dedicated to my parents

Nemai Chandra Sadhukhan

and

Anima Sadhukhan

ACKNOWLEDGMENTS

LIST OF PUBLICATIONS

(A) Relevant to the present Thesis

In refereed journals

1. **Spin dependence of the modified Kramers width of nuclear fission,**
   Jhilam Sadhukhan and Santanu Pal,
   Phys. Rev. C **78**, 011603(R) (2008); Phys. Rev. C **79**, 019901(E) (2009).

2. **Critical comparison of Kramers' fission width with the stationary width from Langevin equation,**
   Jhilam Sadhukhan and Santanu Pal,
   Phys. Rev. C **79**, 064606 (2009).

3. **Role of shape dependence of dissipation on nuclear fission,**
   Jhilam Sadhukhan and Santanu Pal,
   Phys. Rev. C **81**, 031602(R) (2010).

4. **Fission as diffusion of a Brownian particle with variable inertia,**
   Jhilam Sadhukhan and Santanu Pal,
   Phys. Rev. C **82**, 021601(R) (2010).

5. **Role of saddle-to-scission dynamics in fission fragment mass distribution,**
   Jhilam Sadhukhan and Santanu Pal,
   Phys. Rev. C **84**, 044610 (2011).

In conferences

1. **A statistical model calculation for fission fragment mass distribution,**
   Jhilam Sadhukhan and Santanu Pal,
   Proc. DAE-BRNS Symp. on Nucl. Phys. **52**, 337 (2007).

2. **A statistical model calculation of pre-scission neutron multiplicity with spin dependent fission width,**
   Jhilam Sadhukhan and Santanu Pal,
   Proc. DAE-BRNS Symp. on Nucl. Phys. **53**, 383 (2008).

3. **A critical comparison of Kramers' fission width with the stationary width from Langevin equation,**
   Jhilam Sadhukhan and Santanu Pal,
   Proc. DAE-BRNS Symp. on Nucl. Phys. **53**, 453 (2008).

4. **Fission as diffusion of a Brownian particle with variable inertia,**
   Jhilam Sadhukhan and Santanu Pal,
   Proc. DAE-BRNS Int. Symp. on Nucl. Phys. **54**, 362 (2009).

5. **Role of shape-dependence of dissipation on nuclear fission,**
   Jhilam Sadhukhan and Santanu Pal,
   Proc. DAE-BRNS Int. Symp. on Nucl. Phys. **54**, 364 (2009).

6. **Role of saddle-to-scission dynamics in fission fragment mass distribution,**
   Jhilam Sadhukhan and Santanu Pal,
   Proc. DAE-BRNS Symp. on Nucl. Phys. **55**, 270 (2010).

7. **Fission width for different mass fragmentation from Langevin equations,**
   Jhilam Sadhukhan and Santanu Pal,
   Proc. DAE-BRNS Symp. on Nucl. Phys. **55**, 322 (2010).

8. **Statistical and dynamical models of fission fragment mass distribution,**
   Jhilam Sadhukhan and Santanu Pal,
   Proc. DAE-BRNS Symp. on Nucl. Phys. **56**, 458 (2011).

9. **Fission fragment mass distribution from combined dynamical and statistical model of fission including evaporation,**

   Jhilam Sadhukhan and Santanu Pal,

   Proc. DAE-BRNS Symp. on Nucl. Phys. **56**, 534 (2011).

(B) Other publications (in refereed journals)

1. **The role of neck degree of freedom in nuclear fission,**
   Santanu Pal, Gargi Chaudhuri, *Jhilam Sadhukhan*,
   Nucl. Phys. **A 808**, 1 (2008).

2. **Evaporation residue excitation function from complete fusion of ^{19}F with ^{184}W,**
   S. Nath, P. V. Madhusudhana Rao, Santanu Pal, J. Gehlot, E. Prasad, Gayatri Mohanto,
   Sunil Kalkal, *Jhilam Sadhukhan*, P. D. Shidling, K. S. Golda, A. Jhingan, N. Madhavan,
   S. Muralithar and A. K. Sinha,
   Phys. Rev. C **81**, 064601 (2010).

3. **Evidence of quasifission in the ^{16}O+^{238}U reaction at sub-barrier energies,**
   K. Banerjee, T. K. Ghosh, S. Bhattacharya, C. Bhattacharya, S. Kundu, T. K. Rana,
   G. Mukherjee, J. K. Meena, *Jhilam Sadhukhan*, S. Pal, P. Bhattacharya, K. S. Golda, P.
   Sugathan, and R. P. Singh,
   Phys. Rev. C **83**, 024605 (2011).

4. **Angular momentum distribution for the formation of evaporation residues in
   fusion of ^{19}F with ^{184}W near the Coulomb barrier,**
   S. Nath, J. Gehlot, E. Prasad, *Jhilam Sadhukhan*, P. D. Shidling, N. Madhavan, S. Mu-
   ralithar, K. S. Golda, A. Jhingan, T. Varughese, P. V. Madhusudhana Rao,A. K. Sinha
   and Santanu Pal,
   Nucl. Phys. **A 850**, 22 (2011).

5. **Evaporation residue excitation function measurement for ^{16}O+^{194}Pt reaction,**
   E. Prasad, . K. M. Varier, N. Madhavan, S. Nath, J. Gehlot, Sunil Kalkal, *Jhilam
   Sadhukhan*, G. Mohanto, P. Sugathan, A. Jhingan, B. R. S. Babu, T. Varughese, K. S.
   Golda, B. P. Ajith Kumar, B. Satheesh, Santanu Pal, R. Singh, A. K. Sinha, and S.
   Kailas,
   Phys. Rev. C **84**, 064606 (2011).

SYNOPSIS

It is now well established from the analysis of experimental results that the underlying dynamics governing the fission process of a hot compound nucleus is dissipative in nature. The first dissipative dynamical model for fission was proposed by H. A. Kramers long back in 1940. Presently, the Fokker-Planck equation and the Langevin equations are widely used for realistic calculations of fission dynamics. Among the above prescriptions, Kramers' analytical formulation is the most convenient one as it can be easily implemented in a statistical model code of compound nuclear decay and hence it is used extensively to study hot compound nuclei formed in heavy ion induced fusion-fission reactions. The majority of these investigations concern the understanding of the nature of nuclear dissipation, where the dissipation strength itself is treated as a free parameter. Therefore, a precise and realistic modeling of the fission process is required to extract reliable values of the dissipation strength. However, Kramers made a few simplifying assumptions, such as considering the collective inertia and dissipation strength to be constant, to obtain the expression for the stationary fission width. Hence, it is necessary to study the different aspects of Kramers' fission width for precise understanding and their consequences in the realistic calculations. This is one of the main objectives of the work reported in the present thesis. To this end, after giving an overview and introduction to the Langevin dynamical calculation, we first study, in Chapter 3, the effects of compound nuclear spin dependence of the Kramers' fission width on the different fission observables. We next examine, in Chapter 4, the applicability of Kramers' fission width and its possible generalization under more realistic situation of shape-dependent collective inertia. For this purpose, the one-dimensional Langevin dynamical fission width is used as a benchmark. Similar investigation has also been performed for shape-dependent dissipation in Chapter 5. We have further studied the fission fragment mass distribution using the dissipative dynamical model. In this course of study, we have investigated, in Chapter 6, the role of saddle-to-scission dynamics in fission fragment mass distribution by using a two dimensional Lanngevin dynamical model. Finally, we summarize the results with the possible future outlook in Chapter 7.

Contents

Chapter 1

Overview

1.1 Introduction

1.1.1 Discovery of nuclear fission

In 1934, Enrico Fermi [1] discovered that neutrons can be captured by heavy nuclei to form new radioactive isotopes of higher masses and charge numbers than hitherto known. According to this finding, nearly all the heavy elements around uranium (U) could be activated by bombarding neutrons. The nuclei, formed in such a process, were unstable and reverted to the stability by ejection of negatively charged beta-particles. For thorium (Th), two half lives of one minute and 15 minutes have been found experimentally [2]. Similarly, four activities with some indication of a few more were detected for U. Since there were three known isotopes of U, the larger number of half-lives confirmed the occurrence of some unusual process. The pursuit of these investigations, particularly through the works of Lise Meitner, Otto Hahn and Fritz Stassmann as well as of Irene Curie and Paul Savitch, revealed a number of unsuspected and startling results which finally guided Hahn and Strassmann [3] to the discovery that elements of much smaller atomic weight and charge are also produced from the irradiation of U. The new type of nuclear reaction thus discovered was given the name "fission" by Meitner and Frisch [4] in 1939. They emphasized the analogy between the above process and the liquid drop model (LDM) which describes the division of a electrically charged liquid drop into two smaller droplets. In this connection, they also drew attention to the fact that the mutual repulsion between the positively charged protons annuls the effect of the short-range attractive nuclear

1

forces to a large extent. Therefore, a small energy is required to produce a critical deformation beyond which a nucleus proceeds to break apart. As a consequence of this type of splitting, a very large amount of energy is released in the form of kinetic energy of the resulting fragments. It is the great ionizing power of these fragments which guided Frisch [5] and others to observe the fission process directly. Also, the penetrating power of these fragments allowed an efficient way to separate the new nuclei formed in the fission [6]. In addition, it was found that the fission process is accompanied by emission of neutrons, some of which seemed to be directly associated with the fission and others associated with the subsequent beta-decay of the heavy fragments.

Today, after more than seven decades of its discovery, nuclear fission still remains a vibrant field of research. In the following sections, we shall present a brief overview of the theoretical developments in the field which are relevant for the present thesis.

1.1.2 The first theory on fission

The discovery of fission induced by thermal neutrons dispelled the accumulated difficulties concerning the active substances produced from U and Th. However, it also raised a number of questions of which the principal one was: how can the fairly moderate excitation of the nucleus resulting from capture of a neutron lead to such a cataclysmic disruption? Further, fission is observed for certain heavy nuclei while the other nuclei are stable against fission. The first theoretical model for fission came from Meitner and Frisch [4] who pointed out that a nucleus is similar to a charged liquid drop in many ways. An uncharged liquid drop of a given volume assumes a spherical shape since the surface tension, which is proportional to the surface area, becomes minimum for a spherical shape. The nature of the attractive nuclear forces are analogous to the cohesive forces between the atoms in a drop of liquid. Hence, a nucleus experiences the effects similar to the surface tension in a liquid drop. Therefore, for a given volume, the spherical shape would be the most stable one if only the nuclear forces were present. However, the repulsive electrostatic forces between protons tend to produce an opposite effect. A nucleus remains stable as long as the sum of the surface energy and electrostatic energy has a minimum for the spherical shape. Identical to a charged liquid drop, the total energy of a nucleus increases with the deformation and thus it gives the restoring force towards the spherical shape.

However, the total energy reaches a maximum at a certain deformation and the nucleus may split into two smaller nuclei when it crosses this maximum. This becomes more probable for a heavy nuclei because of an effective reduction of the restoring force resulting from a higher nuclear charge. In fact, the barrier of energy that prevents the nucleus from fission, reduces with the increase of charge (Z) of the nucleus and, eventually, it disappears altogether for some critical value of Z. Nuclei of Z values greater than this critical Z will then immediately break apart. Meitner and Frisch estimated that this happens for values of Z more than 100. The stability of nuclei has been discussed in several papers by others [7] and also in the seminal paper by Niels Bohr and John A. Wheeler [8].

Since the theory of Meitner and Frisch, the understanding of nuclear forces has undergone considerable improvements. However, the basic understanding regarding the nature of deformation energy as a function of the nuclear deformation remains unchanged. A detail calculation
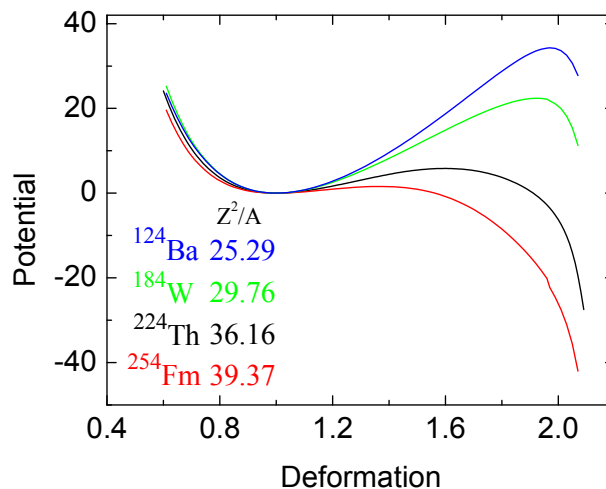
Figure 1.1: Liquid drop model potential as a function of deformation for different combinations of A and Z. The values of Z^2/A are also indicated. The value of deformation (definition given in Sec. 2.1) equal to 1 corresponds to the spherical shapes.

of nuclear potential based on the finite range liquid drop model (FRLDM) is discussed in the Chapter 2. Here, in Fig. 1.1, we present the calculated potential energies of different nuclei plotted as a function of the nuclear deformation. Evidently, the potential becomes flatter as Z

3

increases and the restoring force against larger deformation is almost zero for the Fm ($Z = 100$) nucleus.

1.2 Statistical models of fission

1.2.1 The Bohr-Wheeler's theory on fission

The first comprehensive work on the theory of fission was presented by Niels Bohr and John A. Wheeler [9]. They assumed that any nuclear process, initiated by collision or irradiation, takes place in two steps. In the first step, a highly excited compound nucleus (CN) is formed with a comparatively long lifetime during which the excitation energy is distributed among all the degrees of freedom as the thermal energy. Then, in the second step, the CN disintegrates or decays to a less excited state by the emission of radiation. The disintegration of a CN may happen through emission of a neutron or light charged particle, which requires the concentration of a large part of the excitation energy on one or a few number of particles at the nuclear surface. On the other hand, it may break apart via fission where a reasonable part of the excitation energy transforms into the potential energy of deformation.

In order to discuss briefly the Bohr-Wheeler theory on nuclear fission [8], the LDM potential energy of a nucleus is shown in Fig. 1.2 as a function of the nuclear deformation. Here, the critical deformation, or the saddle point, corresponds to the deformation where potential energy reaches a maximum forming the barrier V_B. To determine the fission probability, we consider a microcanonical ensemble of nuclei with intrinsic excitation energies between E^* and $E^* + \delta E^*$. We assume that the CN is formed in a fusion reaction where E_{cm} is the centre of mass energy of the target-projectile combination and Q is the Q-value of the reaction. Then, the intrinsic excitation energy E^* can be written as

$$E^* = E_{cm} + Q - V - E_{rot}, \tag{1.1}$$

where V (Fig. 1.2) and E_{rot} are the LDM potential energy and rotational energy of the CN, respectively. E_{rot} depends on the shape of the CN as the moment of inertia changes with the compound nuclear shape. We consider $\rho(E^*)$ as the density of states at the ground-state configuration which is the local minimum ($V = 0$) of the LDM potential. Then, the number of

quantum states between the energy E^* and $E^* + \delta E^*$ is given by $\rho(E^*)\delta E^*$. The ensemble is chosen in such a way that the number of nuclei is exactly equal to the number of levels in the selected energy interval and there is one nucleus in each state. Therefore, the number of nuclei which divide per unit time can be represented as

$$R = \frac{\Gamma_{BW}}{\hbar}\rho(E^*)\delta E^*, \tag{1.2}$$

where Γ_{BW} is the fission width.

Again, the rate R can be expressed in the following way. The number of fission events is equal to the number of nuclei in the "transition state" which pass outward over the fission barrier. Here, the transition state corresponds to the nuclear configuration at the saddle point
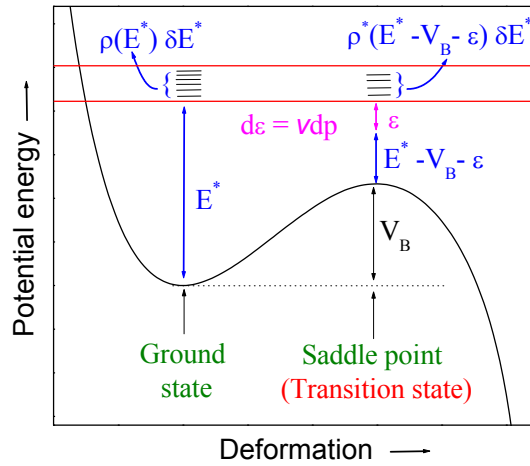
Figure 1.2: A schematic representation of the Bohr-Wheeler theory of fission [8].

of the compound nuclear potential. Now, in a unit distance measured in the direction of fission, there are $(dp/h)\rho^*(E^* - V_B - \epsilon)\delta E^*$ number of quantum states for which the momentum associated with the fission distortion lies in the interval $(p,\ p+dp)$ and the kinetic energy is ϵ. The density of states ρ^* is different from ρ in a sense that it does not contain the degree of freedom associated with the fission itself. Initially, we have one nucleus in each of the quantum states and, therefore, the number of nuclei crossing the saddle point per unit time lying in the momentum interval $(p, p+dp)$ is given by $v(dp/h)\rho^*(E^* - V_B - \epsilon)\delta E^*$, where v is the magnitude of the speed of the fission distortion. Hence, the rate of fission events R can be written as

$$R = \delta E^* \int v(dp/h)\rho^*(E^* - V_B - \epsilon). \tag{1.3}$$

5

Now, comparing Eq. 1.2 with the above expression, we get

$$\Gamma_{BW} = \frac{1}{2\pi\rho(E^*)} \int_0^{E^*-V_B} d\epsilon \rho^*(E^* - V_B - \epsilon),\qquad(1.4)$$

where the relation: $vdp = d\epsilon$ is used. This derivation for the fission width is valid only if the number of states in the transition state is sufficiently large compared to unity. It corresponds to the conditions under which the statistical mechanics can be applied for fission. On the other hand when the excitation energy exceeds V_B by a small amount, or falls below V_B, specific quantum-mechanical tunneling effect becomes important.

1.2.2   Nuclear density of states and Bohr-Wheeler fission width

Nuclear density of states:

The nuclear level density $\rho(E)$ plays a central role in the theoretical modeling of decay of hot compound nuclei. It is not only the crucial ingredient in the Bohr-Wheeler fission width [Eq. (1.4)], the particle and statistical γ-ray evaporation widths, as discussed in the Appendix B, are also very much sensitive to the level density formula. Number of sophisticated models have been developed to calculate the nuclear level density so far. These models employ various techniques ranging from microscopic combinatorial methods [10, 11], Hertree-Fock approaches [12, 13] and relativistic mean field theory [14] to phenomenological analytical expressions [15]. It is desirable to model the nuclear density of states using a microscopic approach since it contains the detail information of nuclear levels. With the progresses in the theoretical nuclear physics and with the increasing power of computers, it is now possible to tabulate the level density values for the entire nuclear chart. However, these tabulated values of the level densities are required to supplement with adjustable empirical expressions for optimization with respect to the experimental data. Another problem with microscopic models is that their use in practical calculations is rather complicated. On the other hand, most of the studies related to nuclear reaction calculations prefer the analytical level density formulae because, especially for stable nuclei, they allow to reproduce the experimental data very well. In present days, two phenomenological models, constant temperature model (CTM) of Gilbert-Cameron [16] and back-shifted fermi gas model (BSFGM) [17] based on the Bethe formula are used in the level density calculations. These simple models take into account the shell, pairing and deformation

effects via adjustable parameters.

The level density formula used in the present work is obtained from the BSFGM where a nucleus is assumed as a gas of Fermions within the nuclear volume. However, we have not included the free parameter δ' in our calculations, which is used in the BSFGM to back-shift the excitation energy from E^* to $E^* - \delta'$. Here, δ' accounts for the first excited-state energy of the CN and its effect becomes negligible at higher excitation energies which is the domain of interest of the present work. With the above consideration, the standard form of the level-density formula can be written as [18]

$$\rho(E^*, \ell) = \frac{2\ell + 1}{24} \left(\frac{\hbar^2}{2I}\right)^{3/2} \frac{\sqrt{a}}{E^{*2}} \exp\left(2\sqrt{aE^*}\right) \tag{1.5}$$

where the factor $(2\ell + 1)$ accounts for the degeneracy due to the compound nuclear spin ℓ. I is the rigid body moment of inertia of the CN and the quantity 'a' is called the level-density parameter which, according to the Fermi gas model, is related to the nuclear temperature T by the equation [18]: $E^* = aT^2$. Often, a is treated as a free parameter to fit the experimental data and, with $a \sim A/9$ MeV^{-1} [19], the properties of particle emission processes in coincidence with the heavy ion induced fission seem to be consistent. However, the physical origin of a, according to the Fermi gas model, can be defined as [18]

$$a = \frac{\pi^2}{6} g = \frac{\pi^2 A}{4\epsilon_F} \tag{1.6}$$

where $g = 3A/2\epsilon_F$ is the density of single-particle levels near the Fermi energy ϵ_F of a homogenous Fermi gas with A particles and a volume sufficiently large for effects associated with the diffuse surface region to be negligible. To incorporate the shell effects in the level density parameter, an extension of Eq. (1.6) was given by Ignatyuk et al. [20]. In their approach the level density parameter was taken as a function of the ground-state nuclear masses, which introduces the shell structure explicitly, but with an smooth energy dependent factor:

$$a(E^*) = \overline{a} \left(1 + \frac{f(E^*)}{E^*} \delta M\right) \tag{1.7}$$

with

$$f(E^*) = 1 - \exp(-E^*/E_D) \tag{1.8}$$

where $\overline{a}$ is the level density parameter given by Eq. (1.6), E_D determines the rate at which the shell effects disappear at high excitations and δM is the shell correction in the LDM masses,

7

i.e. $\delta M = M_{experimental} - M_{LDM}$.

In a subsequent study by Tōke *et al.* [21], $\bar{a}$ was modified to include the effect of nuclear surface diffuseness. They derived an expression for $\bar{a}$ by using the Thomas-Fermi treatment and the leptodermous expansion in powers of $A^{-1/3}$. With this improvement, $\bar{a}$ changes substantially, since the surface diffuseness, even for the heaviest nuclei, is not very small compared to its radius. Also, $\bar{a}$ now becomes a function of the nuclear shape parameters $\overrightarrow{q}$ (Chapter 2) with the following expression:

$$\bar{a}(\overrightarrow{q}) = a_v A + a_s A^{2/3} B_s(\overrightarrow{q}) + a_\kappa A^{1/3} B_\kappa(\overrightarrow{q}) \tag{1.9}$$

where $B_s(\overrightarrow{q})$ and $B_\kappa(\overrightarrow{q})$ are the fractions of integrated surface area and curvature, respectively, with respect to that of a spherical configuration. The values of the constant coefficients a_v, a_s and a_κ in Eq. (1.9) are given as 0.068, 0.213 and 0.383, respectively, in Ref. [21]. Here, level density parameter $\bar{a}(\overrightarrow{q})$ depends on the nuclear mass and shape in a fashion similar to that of the binding energy of a liquid drop and hence $\bar{a}(\overrightarrow{q})$ is often referred to as liquid drop level density parameter. At the same time, exploring a microscopic approach, Reisdorf [22] calculated the level density parameter that takes into account the smoothed volume, surface and curvature dependence of the single particle level density at the Fermi surface. In 1970 and later years, Balian and Bloch [23] published a series of papers in which they considered the mathematical problem of the eigenfrequency density in an arbitrary-shaped cavity. Reisdorf brought the relevance of this problem in nuclear physics, particularly in the Fermi gas model. Eventually, he derived the expression for $\bar{a}$ which is same as Eq. (1.9), apart from the fact that the coefficients are now given as: $a_v = 0.04543 r_0^3$, $a_s = 0.1355 r_0^2$ and $a_\kappa = 0.1426 r_0$. Here, r_0 is the nuclear radius parameter with its value as 1.153 fm [22].

Before concluding the discussions on level density parameter, it should be mentioned that many authors prefer to treat the ratio a_f/a_n, where a_f and a_n are the level density parameters corresponding to the fission width and the particle emission widths (described in the Appendix B) respectively, as a free parameter, while keeping a constant shape-independent value for a_n, to reproduce the experimental data [24, 25, 26]. In the present work, a_f is considered to be the shell corrected shape-dependent level density parameter given by Eq. (1.7) with $\bar{a}$ as prescribed by Reisdorf [22]. However, the particle emissions are assumed to occur always from a spherical

configuration and therefore, a shape-independent a_n with $B_s = B_\kappa = 1$ is used.

The Bohr-Wheeler fission width :

With the above description of the density of states and the level density parameter the Bohr-Wheeler fission width can be calculated numerically [27] from Eq. (1.4). On the other hand, if we assume that the moment of inertia I and the level density parameter a in Eq. (1.5) are to be shape-independent then, by substituting the expression of the density of states [Eq. (1.5)]
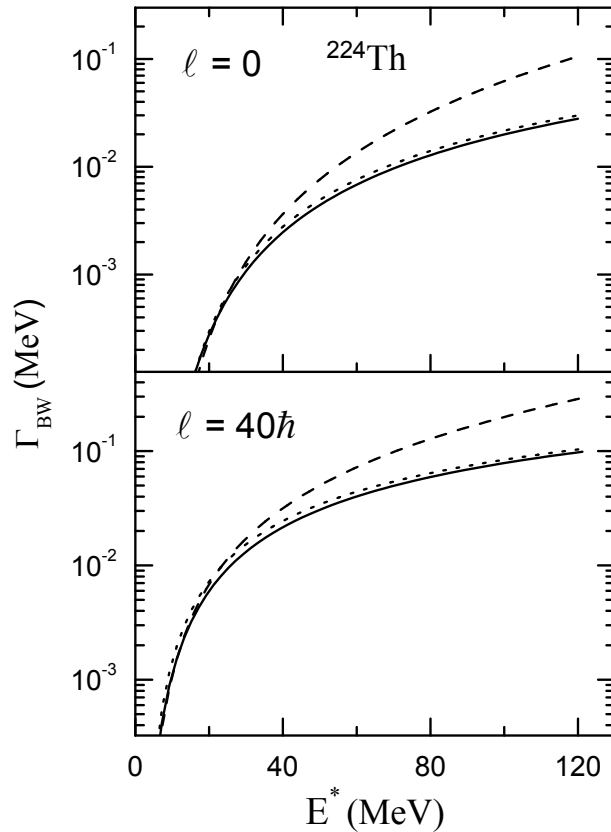
Figure 1.3: Bohr-Wheeler fission width at different excitations [27]. The solid lines are the approximate widths from Eq. (1.12); the short-dashed lines are obtained from Eq. (1.10) with shape-independent parameters of the level-density formula. The long-dashed line represents the widths [Eq. (1.4)] obtained with shape-dependent parameters of the shell corrected level-density formula [Eq. (1.7)].

in Eq. (1.4), we get

$$\Gamma_{BW} = \frac{1}{2\pi} \int_0^{E^*-V_B} \frac{E^{*2}}{(E^*-V_B-\epsilon)^2} e^{2\sqrt{a(E^*-V_B-\epsilon)}-2\sqrt{aE^*}} d\epsilon. \tag{1.10}$$

In Fig. 1.3, the above equation is compared with the exact Bohr-Wheeler fission width given by Eq. (1.4) for two different values of spin of the ^{224}Th nucleus. There is a substantial difference between these two expressions at higher excitation energies. Therefore, the shape-dependence of I and a becomes crucial as the excitation energy goes higher. If we consider $E^* \gg V_B$ then the Eq. (1.10) can be simplified further. Now, $[E^*/(E^*-V_B-\epsilon)]^2 \approx 1$ which implies

$$\Gamma_{BW} \approx \frac{1}{2\pi} \int_0^{E^*-V_B} e^{2\sqrt{a(E^*-V_B-\epsilon)}-2\sqrt{aE^*}} d\epsilon. \tag{1.11}$$

After performing the above integration and then using the condition $E^* \gg V_B$ once again, we get

$$\Gamma_{BW} = \frac{T}{2\pi} \exp(-V_B/T) \tag{1.12}$$

where the temperature T is related with E^* through the Fermi gas model ($T = \sqrt{E^*/a}$). The Γ_{BW}, given by Eq. (1.12), is also plotted in Fig. 1.3 for ^{224}Th ($V_B \approx 5$ MeV at $\ell = 0$). It is apparent from this figure that the approximate form of Γ_{BW} [Eq. (1.12)] agrees well with Eq. (1.10) where the shape-dependence of I and a are ignored.

1.2.3   Fission fragment mass distribution - a scission point model

Fission fragment mass distribution (FFMD) continues to be an important topic since the discovery of fission. The experimental results on thermal neutron induced fission, which was the only possible fusion-fission route known during 1940s, indicated that a somewhat asymmetrical splitting of the nucleus is more probable than a symmetrical one. During that time, Back and Havas first pointed out theoretically that an asymmetric division is more probable than a symmetrical one. For various splittings of a CN, they calculated the available energy in excess of the fission barrier and found that it is more for an asymmetrical division. In their calculations, fission fragments were assumed to be well separated and, hence, only the electrostatic force between the fragments was considered. In a subsequent study by Flügge and Von Droste , the same idea was represented in a somewhat different manner. Their results indicated maximum yield of the fission fragments in the neighborhood of $Z = 35$ and $Z = 55$ for the fission of U. A

review of these initial works can be found in Ref. [28].

The theoretical calculation of the FFMD got a new dimension with the work of Peter Fong in the early 1950s. He was motivated with the findings of Frankel, Metropolis and Hill. In 1947, Frankel and Metropolis [29] showed that the nuclear shape remains symmetric at the saddle point configuration. However, at this point, they did not find any indication of the formation of a narrow 'neck' at which the deformed nucleus might break. Also, the calculations by Hill [30] demonstrated that the fission process is slow enough such that a deformed nuclear shape can oscillate many times before a definite neck develops and fission occurs. As a consequence of these results, Fong [31] proposed that the mode of fission is still undetermined at the saddle point. He extended the concept of statistical equilibrium, used by Bohr and Wheeler [8], from the saddle point to a much latter stage where the CN is just about ready to come apart. Accordingly, the number of quantum states at that later stage gives the relative probability of different mass fragmentation. For convenience Fong simplified the situation at the breaking point by considering the two fragment nuclei in contact.

The calculation of FFMD, as prescribed by Fong, can be summarized in the following manner. The number of quantum states for asymmetric fission is larger than that for symmetric fission. It is mainly because of the fact that the intrinsic excitation energy of the system at the breaking point is larger for the asymmetric fission than for the symmetric mode. According to the model adopted, the excitation energy at the breaking point is given by [31]

$$E^* = M^*(A, Z) - M(A_1, Z_1) - M(A_2, Z_2) - E_{el} - D. \tag{1.13}$$

Here $M^*(A, Z)$ indicates the mass of the original excited fissioning nucleus with mass number A and charge Z, $M(A_1, Z_1)$ and $M(A_2, Z_2)$ are the masses of the two fission fragments in their ground states, and E_{el} is the electrostatic repulsion between the two fragments. Since the nuclei are presumably deformed, a deformation energy D is introduced which reduces the excitation energy available to the fission fragments. D does not effect the fragment mass distribution as it is almost independent of the mode of mass splitting. Now, the relative probability of a particular mode of splitting is completely determined by E^*. In Eq. (1.13),$-E_{el}$ always favors asymmetric fission as it is proportional to the product $Z_1 Z_2$. On the other hand, the mass terms, when calculated from the LDM, favor symmetric fission. However, the scenario may change

if the experimentally obtained masses are considered. It is described in the following example which is taken from Ref. [31]. For the fission of a U nucleus, LDM predicts that the sum of the masses of two equal fragments (^{118}Cd) is lower by 4.2 MeV than that of two fragments of the experimentally observed most probable masses,i.e., ^{100}Zr and ^{136}Te. However, the experimental results show that the mass of two ^{118}Cd nuclei is higher than the ^{100}Zr+^{136}Te combination by 2 MeV, supporting asymmetric fission. This fact, together with the contribution from the $-E_{el}$ term, causes E^* for asymmetric splitting to be larger than E^* for symmetric splitting by 4.5 MeV. In order to establish the quantitative relation between the excitation energy and the number of quantum states, the following formula was derived by Fong [31]:

$$
\begin{aligned}
N \;\sim\; & c_1 c_2 \left(\frac{A_1^{5/3} A_2^{5/3}}{A_1^{5/3} + A_2^{5/3}} \right)^{\frac{3}{2}} \left(\frac{A_1 A_2}{A_1 + A_2} \right)^{\frac{3}{2}} \frac{(a_1 a_2)^{1/2}}{(a_1 + a_2)^{5/2}} \\
& \times \left(1 - \frac{1}{2[(a_1 + a_2)E^*]^{1/2}} \right) E^{*9/4} \exp\left\{ 2[(a_1 + a_2)E^*]^{1/2} \right\}
\end{aligned}
\tag{1.14}
$$

where c_1, a_1; c_2, a_2 are constants of the simplified level density formula,

$$
\rho(E^*) = c \exp\left[2(aE^*)^{1/2} \right],
\tag{1.15}
$$

for the two fragment nuclei A_1 and A_2, respectively. According to the statistical assumption, N is proportional to the relative probability of occurrence of fission products (A_1, Z_1) and (A_2, Z_2). For thermal neutron induced fission of U, the average value of E^* is about 11 MeV [31]. Therefore, the difference of 4.5 MeV between the asymmetric and symmetric modes is large enough to give a very high yield ratio. As a result, a double-humped shape of the FFMD appears. However, with the increase of the average excitation energy, difference in E^* for the symmetric and asymmetric fission becomes insignificant and then FFMD tends to be a single-picked distribution. In the initial calculations of Fong, E^* values for all possible mass splitting were extrapolated from the experimental masses of stable nuclei and from the parabolic dependence [31] of mass on charge number. The constants in Eq. (1.15) were determined from the fast neutron capture cross-section data. The mass distribution curve thus obtained for thermal neutron induced fission of ^{235}U is shown in Fig. 1.4.

As evident from Fig. 1.4, the FFMD for slow neutron fission could be reproduced well with Eq. (1.14). Nevertheless, the theoretical calculations, as mentioned above, largely depend on the experimentally obtained values of nuclear masses. Therefore, a more fundamental
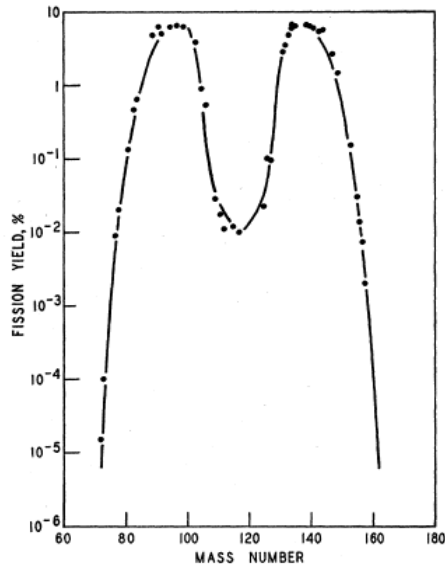
Figure 1.4: Mass distribution curve of thermal neutron induced fission of ^{235}U calculated from Eq. (1.14). Solid circles indicate the corresponding fission yield as determined by radiochemical methods. (taken from Ref. [31])

theoretical calculation of FFMD was required. It came into picture with the advancement in the concept of LDM potential which was triggered by Strutinsky [32] with the attempt to understand the effects of "shell correction" in the nuclear binding energy. Within the framework of the shell correction method, nuclear potential is obtained from the superposition of a macroscopic smooth liquid drop part and a shell correction, obtained from a microscopic single particle model. As a result, for heavy nuclei like U, the potential shows the double-humped character as a function of the quadrupole deformation. Subsequently, Möller and Nix [33] extended the work of Strutinsky by introducing the octupole deformation which is directly related to the mass asymmetry of the nucleus. In this course of study, considering a new set of deformation parameters which also include the mass asymmetry, Mustafa *et al.* [34] calculated the shell-corrected potential energy surface from the saddle points (collectively called the saddle ridge) down the potential hill all the way to a neck radius of about 1 fm. It was the intersection of the potential energy surface and the neck radius of 1 fm that was considered by them as the potential energy at the scission points (collectively the scission line). This particular choice of the neck radius obeyed the consideration that the LDM can not be applied to a dimension less than the nucleonic dimension. Earlier, FFMD had been calculated statistically [31, 35]

13
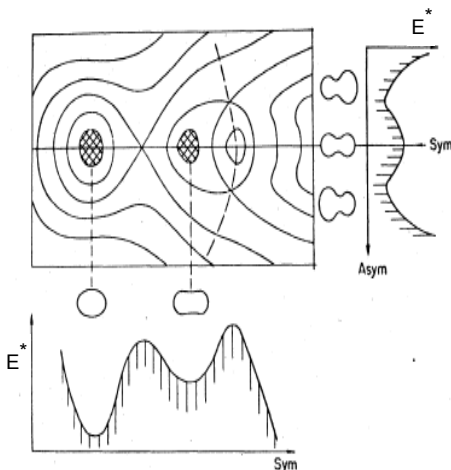
Figure 1.5: Schematic illustration of the nuclear potential energy surface as a function of symmetric and asymmetric deformations [36].

by using a different scission configuration with two deformed fragments in contact. Although the shell correction effects were included by Fong in some later calculations, the new scission criterion of Mustafa *et al.* provided a better matching with the experimental data. Therefore, the statistical model calculations, as described, suffer from an arbitrariness in the choice of the scission line which, unlike the saddle ridge, is not defined by the statics of the problem. However, as shown in the schematic diagram (Fig. 1.5) of the shell-corrected potential landscape along the symmetry (quadrupole) and asymmetry (octupole) axes, the FFMD will be asymmetric in nature if it follows the potential along the asymmetry axis. Parallel to the developments in the statistical model calculations of FFMD, a fragmentary study of the dynamical aspects of fission was performed by Hill and Wheeler [37] in connection with the question of mass asymmetry. The next three sections provide detail discussions on the dynamical features of the fission process.

1.3 Nuclear dissipation

Before the suggestion came from Bohr and Wheeler [8] for the theory of fission, Weisskopf [38], in 1937, developed the statistical model theory for particle evaporation from a hot CN. Afterward, in the late 70s, Pühlhofer [39], Blann [40] and others implemented the computer codes

14

for fission process by combining these statistical theories of particle evaporation and fission. For a long time, these codes were quite successful in explaining the experimental fission data. Now, let us state briefly how the scenario changed from 40s to late 70s. The early successes of the statistical theory of fission and its conceptual simplicity firmly established its popularity. Therefore, the major effort in the development of nuclear theory had been concerned with the static problem of calculating the potential energy of a deformed and charged liquid drop [41]. Although statics had been studied extensively, little was known about the dynamics of nuclear division. For a few special cases, the division of a charged drop was traced out numerically along the potential profile over a very short distance before the actual division of the CN. However, no dynamical study had been performed starting from the initial conditions. In 1964, Nix and Swiatecki [42] were the first to treat statics, dynamics and statistical mechanics of the fission process in a systematic manner. In their work, the statistical equilibrium was assumed to hold near the saddle ridge in order to calculate the probability of finding the CN in a given state of motion close to the saddle configuration. The kinetic energy of the CN was calculated accordingly as a function of the collective coordinates and their conjugate momenta. Subsequently, the Hamilton's classical equations of motion were solved to accomplish first the division of the nucleus and then the separation of the fragments from some given initial configuration to infinity. Here, the concept of dissipation was not invoked.

The status changed dramatically in the 1980s when measurements revealed enhanced neutron multiplicities as compared to statistical model calculations [43]. This experimental finding was accompanied by theoretical investigations based on the Fokker-Planck equation by Grangé and Weidenmüller [44, 45] predicting reduced fission probabilities due to dissipative effects which should also influence the emission of neutrons. Further, experimental evidences of fission as a slow process came from the measurements of pre-scission multiplicities of neutron [46, 47, 48, 49, 50, 51, 52, 53, 54, 55], charged particles [56], Giant Dipole Resonance (GDR) γ-rays [57, 58, 59, 60], fission fragment mass and kinetic energy distributions [51, 52, 53], and evaporation residue cross section [24, 61, 62]. These experimental results suggested that the collective motion of an excited CN is overdamped and possibly provided an answer to the question raised by Kramers as early as 1940 in his seminal paper [63] where justifications were given in favor of the presence of viscous effects in nuclear fission. It was found that the pre-scission

neutron multiplicities increase more rapidly with bombarding energy than the statistical model predictions, no matter how one varies the parameters of the model, i.e., the fission barrier, the level density parameter and the spin distribution, within physically reasonable limits [64]. Therefore, the inadequacy of the statistical or dynamical model treatments without considering dissipation was strongly established. A systematic study was carried out by Thoennessen *et al.* [65] to find the threshold excitation energy from where the statistical model starts losing its validity. Their work opened up the problem of understanding the properties of nuclear dissipation and its dependence on the excitation energy. Consequently, the excess yield of particles and γ-rays from heavy compound systems were analyzed by incorporating the dissipation parameter and also the transient effects which allow the fission flux to build up from zero value. The importance of nuclear dissipation and the corresponding theoretical evolution has been surveyed in detail in the thesis work of Chaudhuri [66].

It is thus well established that a dissipative force operates in the dynamics of a fissioning nucleus. In a dissipative dynamical model, the intrinsic motions, comprising of all the degrees of freedom other than fission, are assumed to form a thermalized heat bath. Then, fission can be viewed as a diffusion process of the fission degree of freedom over the fission barrier, where dissipation corresponds to the irreversible flow of energy from the collective fission dynamics to the heat bath. From the microscopic point of view, it represents the average effect of the interactions between the collective and intrinsic motions. In this picture, the residual part of the interactions gives the fluctuating force on the collective dynamics, which in effect causes the diffusion of the dynamical variables. Therefore, one can conclude qualitatively that dissipation and diffusion are not independent of each other. In fact, they are related through the Einstein's fluctuation-dissipation theorem which we shall discuss later. Here, the important observation is that dissipation may influence the distribution of those fission observables which are generated through diffusion of collective coordinates. On the other hand, dissipation affects the dynamical motion in a more direct way by increasing the time required to go from one shape to another which results in enhancement of prescission particle emission. Another crucial effect is the heating of the compound system at the expense of collective kinetic energy.

1.3.1 Origin and nature of nuclear dissipation

Two kinds of dissipation mechanisms are generally considered in the dissipative dynamical models of nuclear reactions. One is the one-body dissipation and the other is the hydrodynamical two-body dissipation. In the first case, the interactions between the nucleons are approximated with a mean field potential and the collective dynamics is described by the shape evolution of this potential. For a heavy nucleus, such a potential is ideally represented by the Wood-Saxon shape which exerts force on the nucleons only within a narrow width at the nuclear surface. Therefore, in a classical-mechanical treatment, nucleons can be assumed to undergo collisions with the moving nuclear surface and thereby damp the surface motion [67]. The irreversible feature of friction comes out after taking a proper time average. On the other hand, in the linear response theory approach [68], quantum states in the mean field potential are allowed to scatter from one another. Details of this theory can be found in Ref. [69]. A classical version of the linear response theory was also applied to calculate the nuclear friction [70]. The models of hydrodynamical viscosity [71] are based on the assumption that nuclear dissipation arises from individual two body collisions of nucleons. It was however concluded from analysis of extensive experimental data that the hydrodynamical two body viscosity cannot give consistent explanation of both neutron multiplicity and fission fragment kinetic energy distribution [72]. A strong two-body viscosity is required to reproduce the observed neutron multiplicity. Whereas, the total kinetic energy calculated with this value of two-body viscosity is far smaller than given by the Viola systematics [73]. A consistent explanation of neutron multiplicities and fragment kinetic energies indeed supports the one-body friction and not the two-body viscosity [74]. Similarly, the studies of macroscopic nuclear dynamics such as those encountered in low-energy collisions between two heavy nuclei or nuclear fission have established that one-body dissipation is the most important mechanism for collective kinetic energy damping. The nucleus is basically a one-body system at low excitation energies corresponding to temperatures up to a few MeV. It can be understood from the following theoretical interpretation. The Fermi energy of a nucleus is around 40 MeV. Therefore, at a few MeV of temperature, nucleon-nucleon collisions are suppressed by the Pauli's exclusion principle which, in effect, limits the available phase space for two colliding nucleons. As a result, the mean free path of the nucleons is greater than the nuclear dimensions and hence two-body processes are less favored compared to one-body processes. The above argument is also consistent with the idea of mean field approximation

where the nucleonic motions are assumed to be independent of each other.

Theoretical work on the detailed nature of the nuclear friction has made considerable progress during 1970s. The concept of the one-body dissipation mechanism was introduced first by D. H. E. Gross [75]. He deduced a classical equation of motion including frictional forces from the general many-body Schrödinger equation for two colliding heavy ions. A detail description of the one-body dissipation mechanism, used in the present thesis, is given in Chapter 2. The structure of the friction coefficient has been also investigated within the microscopic transport theories based on random matrix approach [76], the linear response theory [68, 70], and the one-body wall-plus-window dissipation model [67]. A compilation of data on the magnitude of dissipation strength has been given in Ref. [77]. However, a complete theoretical understanding of the dissipative force in fission dynamics is yet to be developed. The results obtained in various one-body or two-body viscosity models differ very much in their strength and coordinate dependence and also with respect to its dependence on the temperature. They sometimes differ by an order of magnitude, a feature which not only reflects the complexity of the problem, but also urges for finding the solution.

1.4   Dissipative dynamical models

Nuclear fission is picturised as an evolution of the nuclear shape from a relatively compact mononucleus to a dinuclear configuration. In a macroscopic description [66, 72, 78, 79] of this shape evolution, the gross features of the fissioning nucleus can be described in terms of a small number of parameters also called the collective degrees of freedom. The time development of these parameters is the result of an complicated interplay between various dynamical effects which are similar to that experienced by a massive Brownian particle floating in a equilibrated heat bath under the action of a potential field. Here, the heat bath is comprised of a large number of intrinsic degrees of freedom representing the rest of the nucleus and the potential energy is associated with a given shape of the nucleus. Moreover, the fission degrees of freedom are connected with the heat bath through dissipative interactions and, as a result, the shape evolution is both damped and diffusive. The diffusion happens essentially duo to the fluctuating force exserted by the heat bath on the Brownian particle. In most cases, the inertia associated

with the fission parameters are large enough so that their dynamics can be treated entirely by the laws of classical physics. The above scenario is illustrated schematically in Fig. 1.6.
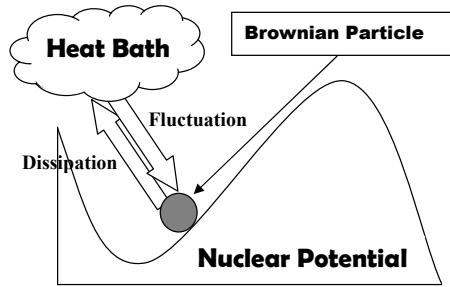
Figure 1.6: A schematic diagram for the dynamical model of fission.

The separation of the whole system into a Brownian particle and a heat bath relies on the basic assumption that the equilibration time of the intrinsic degrees of freedom (τ_{equ}) is much shorter than the typical time scale of collective motions (τ_{coll}), i.e, the time over which the collective variables change significantly. Then, one can decompose the total Hamiltonian of a nucleus into two parts corresponding to the collective parameters and intrinsic motions. In addition, it is assumed that the intrinsic motions lose the memory of any previous instant very quickly. Under these conditions, a transport equation for the collective degrees of freedoms can be derived easily. Let $\tau_{poincaré}$ be the time taken by the entire system to return to a point very close to its original position in phase space. Then it should be much larger than τ_{coll} so that the collective dynamics is irreversible. Thus, for a transport description to be valid, the time scales governing the dynamics of a thermally equilibrated system must obey the following inequalities:

$$\tau_{equ} \ll \tau_{coll} \ll \tau_{poincaré}. \tag{1.16}$$

Initially, transport theories were used extensively in the study of deep inelastic heavy-ion reactions [80]. Later it was found that transport theories can also be applied to investigate the decay of composite nuclear systems via fission [81]. In case of fission process, the fission decay time τ_f is a measure of τ_{coll} and thus a transport theory can be applicable to fission when the

internal equilibration time τ_{equ} is much smaller than τ_f. We assume that the transport (diffusion) equation will be applicable to nuclear fission at high excitation energies in the dissipative dynamical model. In a realistic situation, the decay of a CN is a competitive process between fission and evaporation of light-particles and statistical γ-rays. The evaporation channels are incorporated in a dynamical model code with the assumption that the corresponding decay times are much larger than the equilibration time τ_{equ}. Now, we shall explain two alternative but equivalent mathematical formulations which describe the motion of a Brownian particle in an external force field.

1.4.1   Langevin equation

The Fokker-Planck equation and the Langevin equation are the two equivalent prescriptions that can used to describe the motion of a Brownian particle in a heat bath. Langevin approach was first proposed by Y. Abe [82] as a phenomenological framework to portray the nuclear fission dynamics. It deals directly with the time evolution of the Brownian particle while the Fokker-Planck equation deals with the time evolution of the distribution function (in classical phase space) of Brownian particles and hence the earlier one is much more intuitive. Although the two approaches describe different aspects of the dynamics, they are equivalent with respect to their physical content. In the Langevin dynamical approach, the motion of a Brownian particle is written as

$$\begin{aligned} \frac{d\overrightarrow{r}}{dt} &= \frac{\overrightarrow{p}}{m} \\ \frac{d\overrightarrow{p}}{dt} &= \overrightarrow{F}(t) + \overrightarrow{H}(t) \end{aligned} \tag{1.17}$$

where $\overrightarrow{F}(t)$ is the externally applied conservative force. It is related to the external potential field $V(\overrightarrow{r})$ through the relation $\overrightarrow{F}(t) = -\overrightarrow{\nabla}V(\overrightarrow{r})$. The non-conservative force $\overrightarrow{H}(t)$ describes the coupling of the collective motion with the heat bath and it is given by

$$\overrightarrow{H}(t) = -\frac{\eta}{m}\overrightarrow{p} + \overrightarrow{R}(t). \tag{1.18}$$

The foregoing equation has two parts; a slowly varying part which describes the average effect of heat bath on the particle and is called the friction force $(\frac{\eta}{m}\overrightarrow{p})$, and the rapidly fluctuating part $\overrightarrow{R}(t)$ which has no precise functional dependence on t. Since it depends on the instantaneous effects of collisions of the Brownian particle with the molecules of the heat bath, $\overrightarrow{R}(t)$ is a

random (stochastic) force and it is assumed to have a probability distribution with the mean value equals to zero. It is further assumed [72, 78] that $\overrightarrow{R}(t)$ has an infinitely short time-correlation which means the process is Markovian. Therefore $\overrightarrow{R}(t)$ is completely characterized by the following moments,

$$\begin{aligned} \langle R_i(t) \rangle &= 0 \\ \langle R_i(t)R_j(t') \rangle &= 2D\delta_{ij}\delta(t-t'), \end{aligned} \tag{1.19}$$

where the suffix i denotes the i-th component of the vector $\overrightarrow{R}(t)$. D is the diffusion coefficient and it is related to the friction coefficient η and the temperature of the heat bath T by the Einstein's fluctuation-dissipation theorem:

$$D = \eta T. \tag{1.20}$$

It should be noted that the Langevin equations are different from ordinary differential equations as it contains a stochastic term $\overrightarrow{R}(t)$. In order to calculate physical quantities such as mean values or distributions of the observables from such a stochastic equation, one has to deal with a sufficiently large ensemble of trajectories for a true realization of the stochastic force. The physical description of the Brownian motion is therefore contained in a large number of stochastic trajectories rather than in a single trajectory, as would be the case for the solution of a deterministic equation of motion.

It has been mentioned earlier that the fission of a hot nucleus involves two distinct time scales; one being associated with the slow motion of the fission parameters and the other with the rapid motion of the intrinsic degrees of freedom. The Markovian approximation in Eq. (1.17) remains valid as long as there exists a clear separation between these two time scales. However, when the the two time scales become comparable, one has to generalize the Langevin equation to allow for a finite memory and hence the process turns out to be non-Markovian [72]. For fast collective motion, Eq. (1.17) is generalized as

$$\begin{aligned} \frac{d\overrightarrow{r}}{dt} &= \frac{\overrightarrow{p}}{m} \\ \frac{d\overrightarrow{p}}{dt} &= \overrightarrow{F}(t) - \frac{1}{m}\int^{t} dt'\eta(t-t')\overrightarrow{p}(t') + \overrightarrow{R}(t). \end{aligned} \tag{1.21}$$

The above equation implies that the friction η has a memory time, i.e., the friction depends on the previous stages of the collective motion. It is, therefore, also called a retarded friction.

The time-correlation property of the stochastic force is then generalized accordingly and it is given by the following equation,

$$\langle R_i(t)R_j(t')\rangle = 2\delta_{ij}\eta(t-t')T. \tag{1.22}$$

Recently, Kolomietz and Radionov [83] have studied the time and energy characteristics of symmetric fission using non-Markovian multidimensional Langevin approach. According to their observation, the peculiarities of the non-Markovian dynamics are reflected in the mean saddle-to-scission time with the growth of strength of memory effects in the system. The non-Markovian nature in the fission dynamics is mostly seen during the saddle-to-scission transition, because the nuclear LDM potential falls very sharply in this region, which effectively makes the corresponding collective dynamics faster. Another distinguishing feature of the nuclear collective dynamics, from that of an ideal Brownian particle, is the fact that the heat bath itself is affected by its coupling to the collective motion (in particular, its temperature does not remain constant). In deep-inelastic collisions or during the fission process, we suppose that the bath represents the intrinsic degrees of freedom of the nucleus. Here again, though the thermal capacity (intrinsic nuclear excitation ~ 100 MeV) of the heat bath is much larger than the collective kinetic energy of the fission degree of freedom (~ 10 MeV), the variation in the temperature of the bath due to energy dissipation from the collective modes cannot be neglected. In order to conserve the total energy, net kinetic energy loss of the collective excitations manifests as energy gain in the heat bath. Consequently, the strength of the random force does not remains a constant, but changes continually with the heating up of the bath. The underlying condition to hold this scheme is that the intrinsic motions equilibrate faster than the time scale of macroscopic collective motions. The above assumption thus implies that the Langevin dynamics can be applied with confidence for slow collective motion of a highly excited nuclear system which is best fulfilled in the fission of a highly excited CN. Hence, we shall assume a phenomenological Markovian friction term in our work and it is allowed that the temperature and, therefore, also the strength of the fluctuating Langevin force can modify with time, but at a rate which is slower than the time scale of the thermal equilibration.

It is necessary to mention here that the transport coefficients, m and η, are multidimensional symmetric tensors for the nuclear collective dynamics with more than one degree of freedom. Also, these quantities are in general functions of collective coordinates. Therefore, the Langevin

22

equations [Eq. (1.17)] are modified as

$$
\begin{aligned}
\frac{dq_i}{dt} &= (m^{-1})_{ij}p_j \\
\frac{dp_i}{dt} &= -\frac{p_j p_k}{2}\frac{\partial}{\partial q_i}(m^{-1})_{jk} - \frac{\partial V}{\partial q_i} - \eta_{ij}(m^{-1})_{jk}p_k + g_{ij}\Gamma_j(t),
\end{aligned}
\tag{1.23}
$$

where q_is are the collective coordinates and p_is are the conjugate momenta. Here $g_{ij}\Gamma_j(t)$ is the random force with the the time-correlation property:

$$
\langle \Gamma_k(t)\Gamma_l(t')\rangle = 2\delta_{kl}\delta(t-t').
$$

and the strength of the random force is related to the dissipation coefficients through the fluctuation-dissipation theorem:

$$
g_{ik}g_{jk} = \eta_{ij}T.
\tag{1.24}
$$

The numerical technique to solve the Langevin equations [Eq. (1.23)] in one dimension and two dimensions are described in Chapter 2 and Chapter 6, respectively.

1.4.2   Fokker-Planck equation

The Fokker-Planck equation which is an alternative description of the Brownian motion can be derived starting from the Langevin equations [84]:

$$
m\frac{d\overrightarrow{r}}{dt} = \overrightarrow{p}, \qquad \frac{d\overrightarrow{p}}{dt} = -\frac{\eta}{m}\overrightarrow{p} - \overrightarrow{\nabla}V + \overrightarrow{R}(t),
\tag{1.25}
$$

which describe the motion of a Brownian particle of mass m in the presence of the potential $V(\overrightarrow{r})$ and friction coefficient η. Let Δt denotes an interval of time which is long compared to the period of fluctuations of $\overrightarrow{R}(t)$, but short enough compared to intervals during which the momentum of the Brownian particle changes by an appreciable amount. Then, from Eq. (1.25), the increments $\Delta\overrightarrow{r}$ and $\Delta\overrightarrow{p}$ can be written as

$$
\Delta\overrightarrow{r} = \frac{\overrightarrow{p}}{m}\Delta t, \qquad \Delta\overrightarrow{p} = -(\frac{\eta}{m}\overrightarrow{p} + \overrightarrow{\nabla}V)\Delta t + \overrightarrow{\Omega}(\Delta t),
\tag{1.26}
$$

where

$$
\overrightarrow{\Omega}(\Delta t) = \int_t^{t+\Delta t}\overrightarrow{R}(\xi)d\xi.
\tag{1.27}
$$

The physical meaning of $\overrightarrow{\Omega}(\Delta t)$ is that it represents the net random force on a Brownian particle during an interval of time Δt. As $t \to \infty$, $\overrightarrow{p}$ must obey the Maxwellian distribution

23

and it is fulfilled if one asserts that the probability of occurrence of different values for $\vec{\Omega}(\Delta t)$ is governed by the distribution function:

$$f(\vec{\Omega}[\Delta t]) = \frac{1}{(4\pi q\Delta t)^{3/2}} \exp\left(-|\vec{\Omega}(\Delta t)|^2/4q\Delta t\right), \tag{1.28}$$

where $q = \eta m T$, T being the temperature of the heat bath in energy unit.

Under this circumstances we should expect to derive the probability distribution function $\rho(\vec{r}, \vec{p}; t + \Delta t)$ governing the probability of occurrence of the state $(\vec{r}, \vec{p})$ of the Brownian particle at time $t + \Delta t$ from the distribution $\rho(\vec{r}, \vec{p}; t)$ at time t and a knowledge of the transition probability $\Psi(\vec{r}, \vec{p}; \Delta\vec{r}, \Delta\vec{p})$ that $(\vec{r}, \vec{p})$ suffers an increment $(\Delta\vec{r}, \Delta\vec{p})$ in time Δt. More precisely, one expects the relation [84]:

$$\rho(\vec{r}, \vec{p}; t + \Delta t) = \int \rho(\vec{r} - \Delta\vec{r}, \vec{p} - \Delta\vec{p}; t)\psi(\vec{r} - \Delta\vec{r}, \vec{p} - \Delta\vec{p}; \Delta\vec{r}, \Delta\vec{p})d(\Delta\vec{r})d(\Delta\vec{p}) \tag{1.29}$$

to be valid. In constructing the above expression, it is assumed that the motion of a Brownian particle depends only on the instantaneous values of its physical parameters and is entirely independent of its whole previous history. As mentioned earlier, a stochastic process which has this characteristic is said to be a Markovian process. According to Eq. (1.26) we can write

$$\psi(\vec{r}, \vec{p}; \Delta\vec{r}, \Delta\vec{p}) = \psi(\vec{r}, \vec{p}; \Delta\vec{p})\delta(\Delta x - p_x\Delta t)\delta(\Delta y - p_y\Delta t)\delta(\Delta z - p_z\Delta t), \tag{1.30}$$

where the δs denote Dirac's delta function and $\psi(\vec{r}, \vec{p}; \Delta\vec{p})$ is the transition probability in momentum space. With this form for the transition probability in phase space the integration over $\Delta\vec{r}$ in Eq. (1.29) is immediately performed and we get

$$\rho(\vec{r}, \vec{p}; t + \Delta t) = \int \rho(\vec{r} - \frac{\vec{p}}{m}\Delta t, \vec{p} - \Delta\vec{p}; t)\psi(\vec{r} - \frac{\vec{p}}{m}\Delta t, \vec{p} - \Delta\vec{p}; \Delta\vec{p})d(\Delta\vec{p}). \tag{1.31}$$

Alternatively, we can write

$$\rho(\vec{r} + \frac{\vec{p}}{m}\Delta t, \vec{p}; t + \Delta t) = \int \rho(\vec{r}, \vec{p} - \Delta\vec{p}; t)\psi(\vec{r}, \vec{p} - \Delta\vec{p}; \Delta\vec{p})d(\Delta\vec{p}). \tag{1.32}$$

According to the Eq. (1.28) and Eq. (1.26) the transition probability is given by

$$\psi(\vec{r}, \vec{p}; \Delta\vec{p}) = \frac{1}{(4\pi q\Delta t)^{3/2}} \exp\left(-|\Delta\vec{p} + (\frac{\eta}{m}\vec{p} + \nabla V)\Delta t|^2/4q\Delta t\right). \tag{1.33}$$

Now, expanding the various functions in Eq. (1.32) in the form of Taylor series and using the foregoing expression for the transition probability, we get, in the limit $\Delta t \to 0$ [84],

$$\frac{\partial\rho(\vec{r}, \vec{p}; t)}{\partial t} + \frac{\vec{p}\cdot\vec{\nabla}}{m}\rho(\vec{r}, \vec{p}; t) - (\vec{\nabla}V\cdot\vec{\nabla}_p)\rho(\vec{r}, \vec{p}; t) = \frac{\eta}{m}\vec{\nabla}_p\cdot(\vec{p}\rho(\vec{r}, \vec{p}; t)) + \eta T\nabla_p^2\rho(\vec{r}, \vec{p}; t). \tag{1.34}$$

This equation is known as the Fokker-Planck equation. The fact that it is possible to derive the Fokker-Planck equation from the Langevin equations clarifies the relation between the two equations and establishes their equivalence. The Fokker-Planck equation is a probabilistic dynamical description and it deals with the time-evolution of the distribution function of a Brownian particle.

1.4.3 Steady state solution - Kramers' equation

In 1940 Kramers [63] solved the one-dimensional Fokker-Planck equation to get the stationary current of Brownian particles over a potential barrier described by two harmonic oscillators as shown in Fig. 1.7, where q is the generalized coordinate. He considered the particles to be of unit mass ($m = 1$). Then the corresponding Fokker-Planck equation can be written as

$$\frac{\partial \rho}{\partial t} + p\frac{\partial \rho}{\partial q} - \frac{dV}{dq}\frac{\partial \rho}{\partial p} = \eta \frac{\partial (p\rho)}{\partial p} + \eta T \frac{\partial^2 \rho}{\partial p^2}. \qquad (1.35)$$

Now, following the Ref. [63], we solve Eq. (1.35) to obtain the stationary current of the Brownian particles over the potential barrier V_B (Fig. 1.7). First, the LDM potential near the ground-state ($q = q_g$) and the saddle-point ($q = q_s$) configurations are approximated with two harmonic oscillator potentials as

$$
\begin{aligned}
V &= \frac{1}{2}\omega_g^2 \left(q - q_g\right)^2 & \text{near} \quad q = q_g \\
&= V_B - \frac{1}{2}\omega_s^2 \left(q - q_s\right)^2 & \text{near} \quad q = q_s,
\end{aligned} \qquad (1.36)
$$

where ω_g and ω_s are the frequencies of the respective oscillator potentials. We consider an ensemble of a great number of similar particles each in its own potential field. At the beginning, the number of particles in the region B is smaller than would correspond to thermal equilibrium with the number near A. As a result, a diffusion process will start to establish the equilibrium. Let us assume that the hight V_B is large compared to the temperature of the heat bath T and, therefore, this process will be slow enough to be considered as a quasi-stationary diffusion process. Under this condition, Eq. (1.35) reduces to

$$p\frac{\partial \rho}{\partial q} - \frac{dV}{dq}\frac{\partial \rho}{\partial p} = \eta \frac{\partial (p\rho)}{\partial p} + \eta T \frac{\partial^2 \rho}{\partial p^2}. \qquad (1.37)$$

If the initial distribution near A happens to be not an equilibrated one, a Boltzmann distribution near A will be established a long time before an appreciable number of particles have escaped.
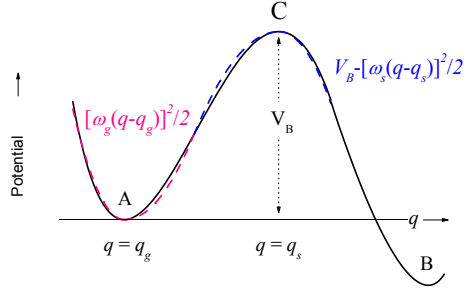
Figure 1.7: Schematic illustration of the nuclear potential energy to calculate the Kramers' fission width [63].

Hence, by using the first part of Eq. (1.36), the distribution function near A can be written as

$$\rho = K \exp\left[-\frac{p^2 + \omega_g^2(q - q_g)^2}{2T}\right] \tag{1.38}$$

where K is a normalization constant. Further, the quasi-stationary diffusion corresponds to a flow from a quasi-infinite supply of Boltzmann distributed particles at A to the region B. Also, in case of large viscosity, effect of the Brownian forces on the velocity of the particles is much larger than the external force dV/dq. Assuming dV/dq to be remaining almost unchanged over a distance $\sqrt{T/\eta}$ [63], we expect that, starting from an arbitrary ρ distribution, a Boltzmann velocity distribution will be established very soon at every value of q. Therefore, the desired solution of Eq. (1.37) near C can be written as

$$\rho = KF(q,p)e^{-V_B/T}\exp\left[-\frac{p^2 - \omega_s^2(q - q_s)^2}{2T}\right] \tag{1.39}$$

such that $F(q,p)$ satisfies the condition

$$\begin{aligned} F(q,p) &\simeq 1 &&\text{at } q = q_g, \\ &\simeq 0 &&\text{at } q \gg q_s. \end{aligned} \tag{1.40}$$

The first boundary condition corresponds to a continuous change of the potential and the second one implies that the number of particles near B is negligibly small. Substituting Eq. (1.39) in Eq. (1.37), we get

$$\eta T\frac{\partial^2 F}{\partial p^2} = p\frac{\partial F}{\partial X} + \frac{\partial F}{\partial p}\left(\omega_s^2 X + \eta p\right), \tag{1.41}$$

where $X = q - q_s$. Following Kramers [63], we next assume the form of F as

$$F(X,p) = F(\zeta), \tag{1.42}$$

26

where $\zeta = p - aX$ and a is a constant. The value of a is determined as follows. Substituting Eq. (1.42) in Eq. (1.41), we obtain

$$\eta T \frac{d^2 F}{d\zeta^2} = -(a - \eta) \left\{ p - \frac{\omega_s^2}{a - \eta} X \right\} \frac{dF}{d\zeta}. \tag{1.43}$$

Now, the above equation will be consistent with Eq. (1.42) if we demand

$$\frac{\omega_s^2}{a - \eta} = a, \tag{1.44}$$

which leads to

$$a = \frac{\eta}{2} + \sqrt{\omega_s^2 + \frac{\eta^2}{4}}. \tag{1.45}$$

Here, the positive root of a is considered because it satisfies the following boundary conditions: $F(X, p) \to 1$ for $X \to -\infty$ (assuming the ground state to be far on the left of the saddle point), and $F(X, p) \to 0$ for $X \to \infty$. Eq. (1.43) then becomes

$$\eta T \frac{d^2 F}{d\zeta^2} = -(a - \eta) \zeta \frac{dF}{d\zeta}. \tag{1.46}$$

The solution of Eq. (1.46) satisfying the above boundary conditions is

$$F(\zeta) = \sqrt{\frac{(a - \eta)}{2\pi\eta T}} \int_{-\infty}^{\zeta} e^{-(a-\eta)\zeta^2/2\eta T} d\zeta. \tag{1.47}$$

The stationary density in the saddle region is finally obtained by substituting this F in Eq. (1.39).

We next obtain the net flux or current across the saddle as

$$
\begin{aligned}
j &= \int_{-\infty}^{+\infty} \rho(X = 0, p) p \, dp \\
&= KT e^{-V_B/T} \sqrt{\frac{a - \eta}{a}} \\
&= KT e^{-V_B/T} \left\{ \sqrt{1 + \left(\frac{\eta}{2\omega_s}\right)^2} - \frac{\eta}{2\omega_s} \right\}.
\end{aligned} \tag{1.48}
$$

The total number of particles in the potential pocket at the ground-state deformation is

$$n_g = \int_{-\infty}^{+\infty} \int_{-\infty}^{+\infty} \rho(near \ \ A) dq dp = \frac{2\pi KT}{\omega_g}, \tag{1.49}$$

where we have used the Boltzmann distribution for ρ as given in Eq. (1.38). Therefore, the width corresponding to the probability of escape over the fission barrier V_B is given by

$$\Gamma_K = \hbar \frac{j}{n_g} = \frac{\hbar \omega_g}{2\pi} e^{-V_B/T} \left\{ \sqrt{1 + \left(\frac{\eta}{2\omega_s}\right)^2} - \frac{\eta}{2\omega_s} \right\}. \tag{1.50}$$

The expression of Γ_K can be generalized for constant m of arbitrary value by keeping $m \neq 1$ in Eq. (1.35) and following the same procedure as described above. The resulting equation for Γ_K will then become [84]

$$\Gamma_K = \frac{\hbar \omega_g}{2\pi} e^{-V_B/T} \left\{ \sqrt{1 + \left(\frac{\eta}{2m\omega_s}\right)^2} - \frac{\eta}{2m\omega_s} \right\}. \tag{1.51}$$

The foregoing equation is often used as the fission width in a dissipative decay of excited compound nucleus. In the above derivation, it is assumed that the mass of the particle and the dissipation strength are independent of the dynamical variable q. However, these assumptions do not hold strictly in case of nuclear collective dynamics. Also, ω_g and ω_s can not be defined uniquely as the nuclear potential does not match exactly with the potential-shape assumed in Fig. 1.7. We will discuss these issues one-by-one in Chapter 3, Chapter 4 and Chapter 5.

For the condition $\eta \ll 2m\omega_s$, Γ_K, as in Eq. (1.51), reduces to a simpler form given by

$$\Gamma_K = \frac{\hbar \omega_g}{2\pi} e^{-V_B/T} \tag{1.52}$$

which is similar to the Bohr-Wheeler fission width given by Eq. (1.12) apart from the pre-exponential factor. In 1973, Strutinsky [85] has shown that this similarity is not accidental. He recalculated the Bohr-Wheeler fission width by taking the phase-space corresponding to the collective degrees of freedom into account. Accordingly, Γ_{BW} in Eq. (1.12) should be multiplied with $\hbar \omega_g / T$ and then it matches exactly with Γ_K in Eq. (1.52).

The Kramers' theory was later generalized by Zhang and Weidenmüller [86] to a diffusion problem in n dimensions. This was desirable as several degrees of freedom are necessary to describe the shape deformations occurring during the fission process. Solving the multidimensional Fokker-Planck equation in the quasistationary approximation, they found for the fission width the expression

$$\Gamma = \frac{\hbar}{2\pi} e^{-V_B/T} \left(\frac{\det \mathbf{V}_g}{|\det \mathbf{V}_s|} \right)^{1/2} \Lambda, \tag{1.53}$$

where the real, symmetric and positive definite $n \times n$ matrix $\mathbf{V}_g$ defines the quadratic form which osculates the potential at the ground-state deformation, a local minimum of the potential landscape. The real, symmetric $n \times n$ matrix $\mathbf{V}_s$ defines the potential at the saddle point. The existence of a saddle is ascertained by the fact that $\mathbf{V}_s$ has $(n-1)$ positive and one negative eigenvalues. The symbols V_B and T have the same meaning as in Eq. (1.51), and Λ is the only positive root of the equation

$$\det(m\Lambda^2 + \eta\Lambda + \mathbf{V}_s) = 0. \tag{1.54}$$

Here, m and η are real, symmetric $n \times n$ matrices representing the inertia tensor and dissipation tensor, respectively. In Chapter 6, we shall compare the two-dimensional Kramers' width with the corresponding Langevin dynamical fission width.

1.5   Application of dynamical models in nuclear fission

As mentioned earlier, dynamical models attracted much attention after 1980 when the presence of dissipative effects in nuclear fission was started to be observed. It was initiated by Weidenmuller and his group [44] who followed the approach of Kramers to investigate how the quasistationary flow over the fission barrier is attained. They solved the two-dimensional Fokker-Planck equation after making a number of simplifying assumptions and obtained the time dependent fission width. Their study first established the importance of transients, i.e., those processes which occur before the stationary value of the fission width is attained. The existence of the transient time as well as the effect of the Kramers' factor in the Bohr-Wheeler fission with have studied also by other groups [87, 88]. Theoretical developments were made for a proper description of the competitive decays of particle evaporation and fission [89, 90], which becomes especially important when one considers the fission of hot nuclei. Subsequently, multidimensional Fokker-Planck equation was applied in fission [91] with the increasing importance of dynamical effects.

The Fokker-Planck equation is a partial differential equation which can be solved analytically under simplifying assumptions. On the other hand, the Langevin equations are stochastic differential equations and therefore not amenable to analytic treatment. This is possibly the reason why the Langevin approach was not used in nuclear physics for a long time, while the

Fokker-Planck equation was preferred for applications in heavy-ion collisions, especially for the deep inelastic processes. Initially, quasi-linear method was used to solve the Fokker-Planck equation analytically. In this method, the driving terms are expanded to the lowest order and only the first and second moments of the Fokker-Planck equation together with a Gaussian ansatz are used to calculate the distribution function at large times. However, the Gaussian ansatz is not a good approximation in many cases. Further, the Fokker-Planck equation or the Langevin equations are to be solved numerically for practical applications where more than one degree of freedom are involved and the transport coefficients (friction, inertia) are coordinate dependent. Numerically, the Langevin equations are more straightforward to handle for a number of reasons. Most importantly, it is easier to accommodate more degrees of freedom in these ordinary differential equations. On the other hand, the Fokker-Planck equation is a partial differential equation and adding more degrees of freedom generates a multidimensional partial differential equation, the solution of which is very time consuming even with modern computers. The price one has to pay to avoid this difficulty is the multiple repetition of the Langevin-trajectory calculation. Secondly, the approximate methods applied for a direct solution of Fokker-Planck equation are numerically not so stable as the solution of the Langevin equations [72]. Moreover, the non-Markovian processes can be included very easily in the Langevin approach [72]. It may also be mentioned that there is a quantal version of the Langevin equations based on which a full-fledged transport theory has been formulated in [92] within a quasi-classical approach. In the recent years, Langevin approach is mostly followed by virtue of its intuitiveness, generality, and other practical advantages.

The application of Langevin equations in nuclear physics was suggested in 1979 [93, 94]. A few years later, in 1985, Barbosa *et al.* [95] performed the first calculation using Langevin equations for deep-inelastic procesess. It was subsequently applied for fission by Abe *et al.* [82] and for fusion by Fröbrich [96]. Since then a large volume of work have been reported, which have applied Langevin equations with the aim to describe data for deep-inelastic heavy-ion collisions, fusion, and heavy ion induced fission. Reviews of such work are given in the Refs. [66, 72, 78]. Detailed studies of Langevin dynamics with a combined dynamical and statistical model (CDSM) were made and the influence of friction on prescission neutron, charged particles and γ-ray multiplicities, on the energy spectra of these particles, on fission time distributions,

and on evaporation and fission cross sections were investigated by Fröbrich and his collaborators [78]. Their phenomenological analysis yielded a strong deformation dependent nuclear friction. Later, in 2001, Chaudhuri and Pal [97] accounted this strong shape dependence of friction by incorporating chaos-weighted one-body dissipation in the Langevin dynamical calculations and, with this modified form of nuclear dissipation, they reproduced the experimental neutron multiplicity [98] more precisely. In some recent studies, the effect of nuclear friction on the mass-energy distribution of the fission fragments has been investigated in detail [99, 100, 101] using three dimensional Langevin equations. Also, the multidimensional Langevin dynamics are presently used to study the fusion-fission and quasi-fission dynamics in the super-heavy region [102]. We have carried out the two-dimensional Langevin dynamical calculations to study the role of the saddle-to-scission dynamics in the fission fragment mass distribution [103]. This work will be explained in the Chapter 6.

It is now established that the Langevin dynamical model is the appropriate one to study the division of a hot compound nucleus. However, the application of the Kramers' theory in fission is still a very much active field of research. In fact, the Kramers' formula [Eq. (1.51)] is much easier to implement in a statistical model code compared to the numerical solution of the Langevin equations. Consequently, the statistical modeling of the fission-evaporation process has gone through a great deal of refinements: (1) the thermodynamic averaging of the fission widths associated with the different orientations of the axially symmetric compound nuclear shapes is incorporated [104], (2) fission barrier is calculated from the proper thermodynamic potential instead of using the nuclear potential [105, 106], and (3) the compound nuclear spin dependence of the harmonic oscillator frequencies in Eq. (1.51) are taken into account [107, 108]. The third consideration and its effects in the fission process are described in Chapter 3 of the present thesis. The Chapter 4 and Chapter 5 concern the applicability and the possible generalization of the Kramers' formula in case of more realistic situation with shape-dependent inertia [27, 109] and dissipation [110], respectively. To this end, the one-dimensional Langevin dynamical calculations are performed to benchmark the corresponding statistical model results. Before all these developments, in the next chapter, we describe the dynamical variables (potential, inertia, dissipation) required for a Langevin dynamical calculation and the numerical technique to solve the Lanvevin equations.

Chapter 2

One-dimensional Langevin dynamical model for fission

2.1 Introduction

A suitable model to describe the fission of a hot compound nucleus (CN) is that of a Brownian particle in a heat bath. In this model, the collective motion involving the fission degree of freedom is represented by a Brownian particle while rest of the intrinsic degree of freedom of the CN correspond to the heat bath. In addition to the random force experienced by the Brownian particle in the heat bath, its motion is also controlled by the average nuclear potential. Fission occurs when the Brownian particle picks up sufficient kinetic energy from the heat bath to overcome the fission barrier. The dynamics of such a system is dissipative in nature and is governed by the appropriate Langevin equations or equivalently by the corresponding Fokker-Planck equation. An analytical solution for the stationary diffusion rate of Brownian particles across the barrier was first obtained by Kramers [63] from the Fokker-Planck equation. The Fokker-Planck equation was subsequently used for extensive studies of nuclear fission . However, as discussed in the previous chapter, the Langevin equations found wider applications in recent years mainly because unlike the Fokker-Planck equation, the Langevin equations do not require any approximation and it is easier to solve the latter for multidimensional cases by numerical simulations [72, 78]. Fairly successful Langevin dynamical calculations for several observables such as fission and evaporation residue cross-sections, pre-scission multiplicities of

light particles and giant dipole resonance γs and mass and kinetic energy distributions of the fission fragments have been reported [72, 78].

In this chapter, a systematic study of the fission rate is made using the one-dimensional Langevin equations for different values of spin and initial temperature of the CN. To this end, we first explain the different shape-parametrizations for the collective coordinates which are the dynamical variables in a dynamical description of fission. Then the nuclear properties, required to solve the Langevin equations, are discussed in detail. Finally, the dynamical fission widths are obtained by solving the Langevin equations numerically.

2.2   Nuclear shape

The shape of a nucleus gets deformed when its collective modes are excited. This deformation may leads to fission as the excitation energy goes up. Therefore, to describe the phenomena of fission, nuclear shape has to be defined in a proper way by choosing the appropriate collective coordinates. The surface of a nucleus was first expressed by Bohr and Wheeler [8] in terms of spherical harmonics. The coefficients of different harmonics represent the collective coordinates in this parametrization and it is often used in explaining the low-lying collective modes of oscillation. However, in this approach, large number of harmonic terms are required to describe a highly deformed shape which may appear in a fission process. Therefore, a major difficulty is that one has to control simultaneously a large number of parameters to handle the shapes of the emerging fragments late in the fission process. On the other hand, various other parametrizations are much more effective [111, 112, 113, 114] in order to describe the relevant shapes during the dynamical evolution of a fission process. All these parameterizations are mostly restricted to three collective coordinates, namely elongation, neck and mass asymmetry. In a work by Möller *et al.* [115] three different shape parametrizations have been used simultaneously to get an optimal parametrization in each region of deformation. They have used: (1) Nilsson perturbed spheroid parametrization for small and moderate deformations, (2) an axially symmetric multipole expansion of the nuclear surface, as mentioned earlier, for intermediate deformations and (3) a five-dimensional deformation space given by the three-quadratic-surface

parametrization for highly deformed shapes.

The well known "Funny Hill" [113] parameters $\{c, h, \alpha\}$ turn out to be most suitable for the present work. This conveniently provides a three-parametric family of shapes that have been employed in numerous studies of static [113, 116] as well as dynamical [99, 97, 117] characteristics of fissioning nuclei. It was shown [113, 116] that this simple parametrization describes with rather good quantitative accuracy the properties of the saddle-point shapes obtained in liquid drop model (LDM) calculations [118, 119], where practically no restrictions were imposed on nuclear shapes. Actually, in our dynamical calculations we use $\{c, h, \alpha'\}$ parametrization where the relation between α' and α is given by: $\alpha' = \alpha c^3$. An elaborate study on the $\{c, h, \alpha'\}$ parametrization can be found in Ref. [120]. The advantage of using α' instead of α is that there is no forbidden shape within the range $|\alpha'| \leq 1$ [120]. In cylindrical coordinate system, assuming the cylindrical symmetry, the surface of a deformed nucleus can be given in terms of c, h and α' as

$$
\begin{aligned}
\rho_s^2(z) &= \left(1 - \frac{z^2}{c^2}\right)\left(ac^2 + bz^2 + \frac{\alpha' z}{c^2}\right) && \text{if} \quad b \geq 0, \\
&= \left(1 - \frac{z^2}{c^2}\right)\left(ac^2 + \frac{\alpha' z}{c^2}\right)\exp\left(bcz^2\right) && \text{if} \quad b < 0, \quad (2.1)
\end{aligned}
$$

where z is the coordinate along the symmetry axis and ρ is the radial coordinate and ρ_s is the magnitude of ρ on the nuclear surface. The quantities a, b are defined in terms of the c and h as

$$
b = \frac{c-1}{2} + 2h,
$$

and

$$
\begin{aligned}
a &= \frac{1}{c^3} - \frac{b}{5} && \text{if} \quad b \geq 0, \\
&= -\frac{4}{3}\frac{b}{\exp(p) + \left(1 + \frac{1}{2p}\right)(\sqrt{-\pi p})\mathrm{erf}(\sqrt{-p})} && \text{if} \quad b < 0, \quad (2.2)
\end{aligned}
$$

where $p = bc^3$ and $\mathrm{erf}(x)$ is the error function with x as the argument. The parameter a is always positive for physically acceptable shapes. In the above equations, the parameter h describes the variation of the thickness of the neck without changing the length, $2c$ (in units of R_0, the nuclear radius corresponding to the spherical shape), of the nucleus along the symmetry

axis. In the present work $R_0 = 1.16A^{\frac{1}{3}}$, A being the mass number of the nucleus. The mass asymmetry parameter α' is related to the ratio of the masses of the nascent fragments as

$$\frac{A_1}{A_2} = \frac{1 + \frac{3}{8}\alpha'}{1 - \frac{3}{8}\alpha'}, \tag{2.3}$$

where the masses A_1 and A_2 are the two parts of the nucleus obtained by its intersection with the plane $z = 0$ [121]. The volume is kept constant in the above parametrization for all variations of the nuclear shape. Since we do not consider neck dynamics in the present work, we set $h = 0$ in the above equations. Also the value of α' is considered to be 0 for the one-dimensional
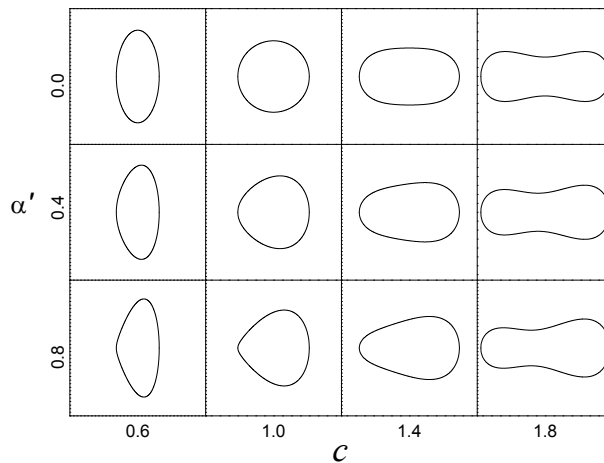
Figure 2.1: Shapes of a nucleus for different values of c and α' ($h = 0$).

calculations. The nuclear shapes with $h = 0$ are shown in Fig. 2.1 for different values of c and α'. The shapes corresponding to non-zero h can be found in [66].

The appearance of a neck in the nuclear shape is associated with the instant at which the surface $\rho_s(z)$ starts to have three extrema, two maxima corresponding to the nascent fragments and a minimum between them, which corresponds to the minimum neck thickness. The minimum appears at the point [114]

$$z_N = 2\sqrt{\frac{x}{3}} \cos\left(\frac{4\pi + \arccos\left(\frac{y\sqrt{27}}{2x^{3/2}}\right)}{3}\right) - \frac{\alpha c}{4b}, \tag{2.4}$$

where

$$x = -\frac{c^2}{4b}\left(\frac{2}{c^3} - \frac{12}{5}b - \frac{3\alpha^2}{4b}\right),$$

35

$$y = -\frac{\alpha c^3}{4b} \left(\frac{\alpha^2}{8b^2} - \frac{2}{5} - \frac{1}{2bc^3} \right).$$

Before the appearance of the neck, the shapes are mono-nuclear shapes. The condition of the existence of a neck in the nuclear shape can be written in the form

$$\frac{y^2}{4} - \frac{x^3}{27} < 0. \tag{2.5}$$

Before concluding this section, we would like to discuss the problem with nonphysical shapes that arises in dynamical calculation using the $\{c, h, \alpha'\}$ parametrization. Usually, the restriction of a rectangular grid along the shape parameters h and α' is the only way to avoid this problem. It is done in the present work by restricting c and α' within the rectangular domain: $c \in \{0.6, 2.09\}$ and $\alpha' \in \{-1.0, 1.0\}$. Alternatively, Nadtochy et $al.$ [114] have introduced a new set of collective coordinates $\{q_1, q_2, q_3\}$ to avoid the nonphysical shapes in dynamical calculations and keep all possible shapes given by the $\{c, h, \alpha'\}$ parametrization in the rectangular grid. Here q_1, q_2 and q_3 are defined as

$$
\begin{aligned}
q_1 &= c \\
q_2 &= \frac{h + 3/2}{\left(\frac{5}{2c^3} + \frac{1-c}{4}\right) + 3/2} \\
q_3 &= \begin{cases} \alpha/(a+b) & \text{if } b \geq 0 \\ \alpha/a & \text{if } b < 0. \end{cases}
\end{aligned}
\tag{2.6}
$$

In this deformation space, all possible mass asymmetric shapes of the nucleus for any values of c and h can be generated by the parameter $|q_3| \leq 1$. However, in the present work, the two-dimensional dynamical model is mainly used to study the nascent fragment-mass distribution at different stages of the dynamical evolution. Therefore, it is rather straightforward to use the $\{c, h, \alpha'\}$ parametrization as α' is directly related to the nascent fragment-masses by Eq. (2.3).

2.3   Nuclear collective properties

In this section, nuclear collective properties are described on the basis of different phenomenological models and these properties are then used in the next section to calculate the fission rate by solving the Langevin equations. Apart from the level density parameter which is described in the previous chapter, three other major inputs to be discussed here are the potential energy (V), collective inertia (m) and dissipation strength (η).

2.3.1 Potential energy

Since the discovery of fission in 1938, nuclear potential energy is the most important ingredient in the study of nuclear fission. Therefore, it is necessary to begin the characterization of the process by calculating the potential energy of a nucleus as a function of shape. The potential energy was first described in terms of a LDM in which it is represented as the sum of shape-dependent surface and Coulomb energy terms. This description was first invoked by Meitner and Frisch [4] and soon put on a more quantitative basis in the seminal paper by Bohr and Wheeler [8]. In this model the Coulomb and surface energies are expressed in an expansion of the reflection and axially symmetric shape in Legendre polynomials, where up to the fourth power in the lowest order polynomial was retained. With this approximation, they could determine the fission barrier heights and the corresponding deformations of various nuclei. Then, almost a decade later, in 1947, Frankel and Metropolis [29] calculated the Coulomb and surface energies of highly deformed nuclear shapes using numerical integration. This was one of the first basic physics calculations done on a digital computer. For more than a decade afterward, several attempts have been made to model the macroscopic energies by more complicated expansions in deformation parameters, which was never completely satisfactory because of convergence difficulties. When numerical calculations were resumed in earnest around 1960, progress in understanding the LDM rapidly followed and after a decade a major development came into picture with the rotating liquid drop model (RLDM) of Cohen *et al.* [122]. Earlier in 1955, Swiatecki [123] suggested that a more realistic fission barrier could be obtained by adding a "correction energy to the minimum in the LDM barrier. The correction was calculated as the difference between the experimentally observed nuclear ground-state mass and the mass given by the LDM. A much improved theoretical spontaneous-fission half-lives were obtained on the basis of these modified barriers. These observations was the beginning of shell correction method. Then Strutinssky [32] presented a macroscopic-microscopic method to calculate these shell corrections theoretically.

Microscopically, shell effects in a nucleus can be treated self-consistently by the finite-temperature Hartree-Fock-Bogoliubov (FT-HFB) method [124, 125, 126]. This type of calculations using a reasonable effective nucleon-nucleon interaction of the Skyrm type or Gogny type are much more elegant than the macroscopic-microscopic model. A major thrust for the

37

microscopic calculations is the study of super-heavy elements (SHE) which are predicted to be stable due to the shell effects. Recently, Pei *et al.* [127] used the FT-HFB technique to investigate the isentropic fission barriers by means of the self-consistent nuclear density functional theory. They have done calculations for ^{264}Fm, ^{272}Ds, ^{278}112,^{292}114, and ^{312}124 and predicted the variation of fission barrier with the excitation energy of the CN. Here, we should mention that the fission barrier, obtained in a finite temperature theory, vanishes at a sufficiently higher excitation energy [127]. A considerable amount of progress is still going on in the field of complete microscopic calculations of potential energy and the search for the heaviest nuclei remains to be a open broblem.

A microscopic calculation mainly contributes in the shell correction which is not expected to be significant at large excitation energies [128]. Also, a complete microscopic calculation demands tremendous computer time even with the most powerful computers. We, therefore, use a still simpler macroscopic approach where the deformation dependent potential energy is obtained from the finite range liquid drop model (FRLDM) [128, 129]. The RLDM [122], where the nucleus is assumed to be formed of an incompressible fluid with a constant charge density and a sharp surface, provides a simplified model of the potential energies of rotating nuclei. However, it overestimates the hight of fission barriers [130, 131, 132, 133, 134] when applied to reproduce experimental data on heavy-ion-induced fission and evaporation residue cross section. In a LDM, the surface thickness and the range of the force are considered to be much smaller than any geometrical parameter of the nuclear configuration. This assumption breaks down in the highly deformed shapes of a fissioning nucleus with a small neck where the neck dimension becomes comparable to the small surface thickness. The following changes are therefore incorporated in the FRLDM relative to the RLDM. (1) The surface energy is replaced by the Yukawa-plus-exponential nuclear energy, which models the effects of the finite range of the nuclear force, nuclear saturation, and the finite surface thickness. (2) The Coulomb energy is calculated for a charge distribution with a realistic surface diffuseness. (3) The moment of inertia is calculated for rigidly rotating nuclei with realistic surface density profile. The different contributions are described briefly as follows.

38

(1) _Nuclear energy:_

As explained, the surface energy of the LDM suffers from several deficiencies. One method to improve the modeling of the macroscopic nuclear energy is to calculate it as a Yukawa-plus-exponential double folding potential. This generalized nuclear energy is a double integral of an empirical Yukawa-plus-exponential folding function over the nuclear volume. With this technique, using one additional parameter (the range of the potential) relative to the RLDM, one can describe heavy-ion scattering potentials, fusion barriers for the light and medium-mass nuclei and also satisfy the condition of nuclear saturation [129]. The Yukawa-plus-exponential nuclear energy, expressed as a function of collective coordinates $\overrightarrow{q} = \{q_1, q_2, ..q_k\}$, is [128]

$$E_N(\overrightarrow{q}) = -\frac{c_s}{8\pi^2 R_0^2 a^3} \int d^3r \int d^3r' \left[\frac{\sigma}{a} - 2 \right] \frac{e^{-\sigma/a}}{\sigma}, \tag{2.7}$$

where $\sigma = \overrightarrow{r} - \overrightarrow{r}'$, $c_s = a_s(1 - \kappa_s I^2)$ and I is the neutron-proton asymmetry that can be written, in terms of mass number A and atomic number Z, as $(A - 2Z)/A$. The integrals are over the volume of sharp-surfaced nucleus. Here, the range a is the only additional parameter with respect to the RLDM and it is determined from heavy-ion scattering experiments. The value of R_0 is determined from average charge radii of nuclei found in electron scattering experiments. The surface energy and surface asymmetry constants a_s and κ_s are determined from the macroscopic fission barriers of nuclei with mass numbers from 109 to 252 at low angular momentum. The values of the constants used in the present work are as follows [128]:

$$
\begin{aligned}
R_0 &= 1.16\text{fm} \\
a &= 0.68\text{fm} \\
a_s &= 21.13\text{MeV} \\
\kappa_s &= 2.3.
\end{aligned}
$$

(2) _Coulomb energy:_

The charge distribution of a nucleus is made diffuse by folding a Yukawa function with range a_C over a sharp surfaced liquid-drop distribution. The Coulomb energy is written as [128]

$$E_C(\overrightarrow{q}) = \frac{Z^2 e^2}{\left(\frac{4}{3}\pi R_0^3\right)^2} \left[\int d^3r \int d^3r' \frac{1}{\sigma} - \int d^3r \int d^3r' \left(1 + \frac{\sigma}{2a_C}\right) \frac{e^{-\sigma/a_C}}{\sigma} \right], \tag{2.8}$$

where the first double-integral in the square bracket corresponds to the sharp-surface Coulomb energy and the second one is the correction due to the diffuseness of the surface. This correction lowers the Coulomb energy since charge is spread over a greater effective volume when the surface is made diffuse. The range parameter a_C is chosen to reproduce the surface-width
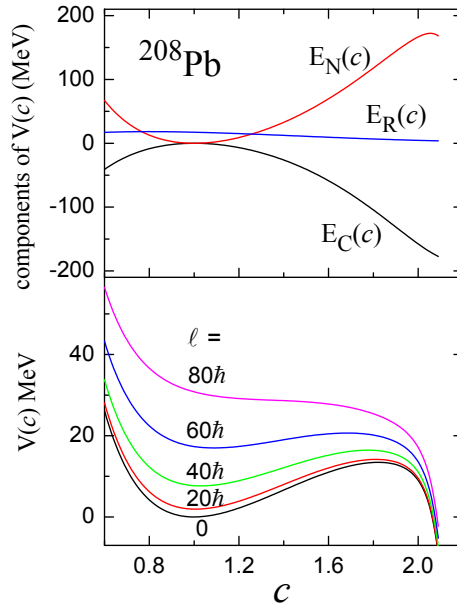
Figure 2.2: The total potential energy $V(c)$ (lower panel) and its different components (upper panel). In both the cases $V(c=1)$ is set to zero for $\ell = 0$. In the upper panel, $E_R(c)$ is plotted for $\ell = 60\hbar$.

parameter of 0.99 fm [128], which gives $a_C = 0.704$ fm.

(3) _Rotational energy:_

The rotational energy of a nucleus, having angular momentum ℓ, is given by

$$E_R(\overrightarrow{q}) = \frac{(\ell\hbar)^2}{2\mathtt{I}(\overrightarrow{q})}, \tag{2.9}$$

where $\mathtt{I}(\overrightarrow{q})$ is the largest of the principle-axis moment of inertia. For a matter distribution made diffuse by folding a Yukawa function over a sharp-surfaced one, the moment of inertia has a particularly simple form, [128] $\mathtt{I}(\overrightarrow{q}) = \mathtt{I}(\overrightarrow{q})^{sharp} + 4M_0 a_M^2$ where M_0 is the nuclear mass and a_M is the range parameter of the folding function. The same diffuseness parameter is used for both the charge and matter distribution, i.e., $a_M = a_C = 0.704$ fm [128].

40
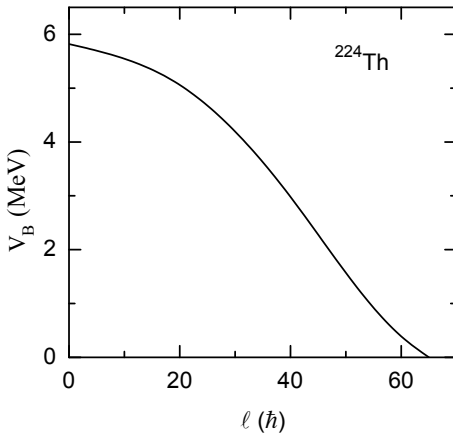
Figure 2.3: The fission barrier as a function of ℓ.

The six-dimensional integrals in Coulomb and surface energies are reduced to three-dimensional integrals by Fourier transform technique [66]. The method used for evaluating these potentials is described in Appendix A. The fission barriers calculated from this FRLDM have been found to be within 1 MeV of those which optimally reproduce fission and evaporation-residue cross sections for a variety of nuclei with masses ranging from 150 to above 200 [128]. For the one-dimension case, the different contributions, $E_N(c)$, $E_C(c)$, $E_R(c)$ and the total potential energy $V(c) = E_N(c) + E_C(c) + E_R(c)$ are plotted in Fig. 2.2. It can be seen that as the value of ℓ increases the fission barrier hight decreases and also the position of the saddle point moves toward more compact shapes. The variation of the fission barrier hight (V_B) as a function of ℓ is plotted in Fig. 2.3.

Thermodynamic potential for fission dynamics:

The heated and rotating CN formed in a reaction with a heavy ions represents a thermodynamic system. It is well known that the conservative force operating in such a system should be determined from its thermodynamic potential (for example, the free energy [117] or entropy [78]). The driving force K in the Langevin equation can then be derived by looking at the change of the total energy

$$dE_{tot} = TdS - Kdq \tag{2.10}$$

where T and S are temperature and entropy and q is the dynamical collective coordinate. Using the expression for the free energy $F = E_{tot} - TS$ in this formula, one obtains

$$K = -(\partial F/\partial q)_T, \tag{2.11}$$

i.e., the driving force is the negative gradient of the free energy with respect to the fission coordinate q at a fixed temperature T. Again, the total energy is a sum of the kinetic energy, which can be neglected for overdamped motion, the potential energy $V(q)$, and the internal energy E^*, $E_{tot} = V(q) + E^*$. Because the total energy does not change during the fission process between two subsequent light-particle emission events, $dE_{tot} = 0$, we obtain from Eq. (2.10),

$$K = TdS/dq, \tag{2.12}$$

i.e., the driving force can also be expressed by the temperature times the gradient of the entropy at fixed total energy. In the Fermi gas model entropy and temperature can be written as $S = 2\sqrt{a(q)E^*}$ and $T = \sqrt{E^*/a(q)}$ respectively. Then, the driving force is given by

$$K = -dV(q)/dq + (da(q)/dq)T^2, \tag{2.13}$$

i.e., it consists of the usual conservative force $-dV(q)/dq$ plus a term which comes from the thermodynamical properties of the fissioning nucleus, which enter via the level density parameter $a(q)$, whose deformation dependence now becomes essential. To avoid the uncertainties related to the temperature dependence of free energy, we have neglected the term associated with the derivative of level density parameter in our work. If the free energy were used instead of zero temperature potential energy the effective fission barrier would have been lower. Consequently, a stronger dissipation strength would have been required to fit the experimental results. However, we shall not explore this aspect in this thesis work.

2.3.2 Collective inertia

We make the Werner-Wheeler approximation [135, 42] for incompressible irrotational flow to calculate the collective inertia m [71, 42]. By virtue of the equation of continuity the velocity field $\overrightarrow{v}$ for an incompressible fluid satisfies $\nabla \cdot \overrightarrow{v} = 0$. The total kinetic energy of the system can be given in terms of $\overrightarrow{v}$ as

$$T = \frac{1}{2}\rho_m \int v^2 d^3r \tag{2.14}$$

where $\rho_m = M_0/(\frac{4}{3}\pi R_0^3)$, is the constant mass density and the integration is over the volume of the nucleus. Now, if the position vector $\vec{r}$ of a fluid element depends only on the collective coordinates $\{q_1, q_2, ...q_k\}$, then $\vec{v} = \sum(\partial\vec{r}/\partial q_i)\dot{q}_i$, where $\dot{q}_i s$ are the generalized velocities and the kinetic energy T can be written as

$$T = \frac{1}{2}\sum m_{ij}(\overrightarrow{q})\dot{q}_i\dot{q}_j. \tag{2.15}$$

For axially symmetric shapes, velocity is given in cylindrical coordinates by $\vec{v} = \dot{\rho}\hat{e}_\rho + \dot{z}\hat{e}_z$, where $\hat{e}_\rho$ and $\hat{e}_z$ denotes unit vectors in the ρ and z directions, respectively. The Werner-Wheeler method is equivalent to assuming that $\dot{z}$ is independent of ρ and that $\dot{\rho}$ depends linearly upon ρ, i.e.,$\dot{z} = \sum_i A_i(z; \overrightarrow{q})\dot{q}_i$ and $\dot{\rho} = \frac{\rho}{\rho_s}\sum_i B_i(z; \overrightarrow{q})\dot{q}_i$, where ρ_s is the value of ρ on the surface of the shape at the position z. Substituting the expressions for $\dot{\rho}$ and $\dot{z}$ in Eq. (2.15) and comparing Eq. (2.14) with Eq. (2.15), we obtain for the elements of the inertia tensor the result [71]

$$m_{ij}(\overrightarrow{q}) = \pi\rho_m \int_{z_{min}}^{z_{max}} \rho_s^2(A_iA_j + \frac{1}{8}\rho_s^2 A_i'A_j')dz, \tag{2.16}$$

where the primes denote differentiation with respect to z. The expansion coefficients A_i are determined from the condition that for an incompressible fluid the total (convective) time derivative of any fluid volume must vanish. The formula for $A_i(z; \overrightarrow{q})$ is given by the following expression [71]

$$A_i(z; \overrightarrow{q}) = \frac{1}{\rho_s^2(z; \overrightarrow{q})}\frac{\partial}{\partial q_i}\int_{z_{min}}^{z}\rho_s^2(z'; \overrightarrow{q})dz'. \tag{2.17}$$

In case of two-dimensional calculation with $\{q_1, q_2\} \equiv \{c, \alpha'\}$ the inertia tensor has the following form

$$m \equiv \begin{pmatrix} m_{cc} & m_{c\alpha'} \\ m_{\alpha'c} & m_{\alpha'\alpha'} \end{pmatrix}. \tag{2.18}$$

For the one-dimensional calculation, with c as the collective coordinate, m is a scaler quantity which may be denoted as $m(c)$. A plot of $m(c)$ for the ^{208}Pb nucleus is given in Fig. 2.4.

Before concluding the discussion on collective inertia, I should mention that the microscopic calculation of the collective inertia can be done within the cranking adiabatic approximation [113, 136, 137]. In the adiabatic description of the collective behavior of a nucleus, the nucleons are assumed to move in a average deformed potential. Using a Hamiltonian that includes pairing interactions, introducing the collective coordinates by means of the Lagrange multipliers, it is
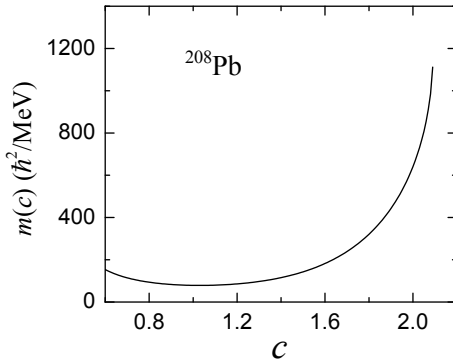
Figure 2.4: The collective inertia calculated using the Werner-Wheeler approximation.

possible to obtain the response of the nuclear system for slow changes of the shape within the cranking model.

2.3.3 One-body dissipation

As discussed in the previous chapter, it is already established that the one-body mechanism is the primary mode of energy dissipation in nuclear fission [74]. If E is the collective kinetic energy of a system then the dissipation tensor $\eta_{ij}(\overrightarrow{q})$ is defined in terms of the time rate of energy dissipation as [138]

$$-\dot{E}_{dis} = \sum_{i,j} \eta_{ij}(\overrightarrow{q})\dot{q}_i\dot{q}_j, \tag{2.19}$$

where $\overrightarrow{q} = \{q_1, q_2..q_k\}$ are the collective coordinates as mentioned earlier. Now, to extract $\eta_{ij}(\overrightarrow{q})$, we shall discuss different mechanisms of one-body dissipation relevant for fission dynamics.

(1) _**Wall Friction (WF):**_
To explain the wall friction [67], let us consider a classical ideal gas in a container supported by a smoothly moveable piston. In a slow compression by the piston, the collective energy of the piston is converted into the kinetic energy of the gas particles. If the rate of energy transfer from the collective to the microscopic (molecular) degrees of freedom is calculated to first order in the 'wall' (piston) speed, the resultant expression will be linear in speed and hence the energy flow has to be reversible, i.e., all the microscopic energy reappears as macroscopic work done on the piston when it is slowly retraced to the original position. By calculating the

44

energy flow between the wall and the particles to the next order in the ratio of wall to particle speeds one finds a term quadratic in the wall speed, which, therefore, represents an irreversible flow of energy from the collective degree of freedom to the random motions. Such a calculation results, under certain assumptions, in the following simple expression for the rate of dissipation of collective energy [67],

$$-\dot{E}^{wall} = \rho_m \overline{v} \oint \dot{n}^2 ds, \qquad (2.20)$$

where ρ_m is the mass density of the gas composed of independent particles of average speed $\overline{v}$. The gas particles are considered to be contained in a vessel of fixed volume, whose walls deform with normal velocities $\dot{n}$. The integral is over the surface of the vessel. This formula is known as the "wall formula" in the literature and it can be applied in the case of nuclear dynamics where the total volume remains constant. As the nucleus is a system of fermions, $\overline{v}$ should be replaced with $(3/4)v_F$, v_F being the Fermi velocity of the nucleons [67]. In deriving the wall formula [Eq. (6.9)] the bulk of the gas is assumed to be at rest. It can be generalized to account for an overall translation or rotation of the container. Then, the relative normal velocity of a surface element with respect to the particles about to strike it will be $\dot{n} - \dot{D}$, where $\dot{D}$ (a function of position on the surface) is the normal component of the relevant drift velocity of the particles about to strike the element of surface in question. Thus the wall formula will be given as

$$-\dot{E}^{wall} = \rho_m \overline{v} \oint (\dot{n} - \dot{D})^2 ds. \qquad (2.21)$$

We consider only the axially symmetric shapes which can be described in cylindrical coordinates by a surface function $\rho_s = \rho_s(z; \overrightarrow{q})$. The quantity $\dot{n}$ entering the wall formula is then given by

$$\dot{n} = \sum_i \dot{q}_i \frac{1}{2} \frac{\partial \rho_s^2}{\partial q_i} \left[\rho_s^2 + \left(\frac{1}{2} \frac{\partial \rho_s^2}{\partial z} \right)^2 \right]^{-1/2}. \qquad (2.22)$$

By putting Eq. (2.22) in the wall formula [Eq. (6.9)] and then comparing it with Eq. (2.19), we get [138]

$$\eta_{ij}^{wall}(\overrightarrow{q}) = \frac{\pi \rho_m \overline{v}}{2} \int_{z_{min}}^{z_{max}} dz \frac{\partial \rho_s^2}{\partial q_i} \frac{\partial \rho_s^2}{\partial q_j} \left[\rho_s^2 + \left(\frac{1}{2} \frac{\partial \rho_s^2}{\partial z} \right)^2 \right]^{-1/2}. \qquad (2.23)$$

So far, the discussion has been within the framework of classical mechanics except incorporating the fermionic nature of nucleons. Quantum mechanical calculation has also been performed

[67] where finite diffuseness of the nuclear surface was considered. In this calculation, the single particle Schrodinger equation was solved numerically in a time dependent Wood-Saxon potential well and a reduction of the wall friction strength from its classical value was observed for systems with diffused surfaces. However, as the potential becomes sharper the quantal results almost match with the classical wall formula. We shall see in the subsequent chapters that the dissipation strength still remains to be determined unambiguously and hence we shall use the one-body dissipation as given by Eq. (2.23), since it is expected to give the form factor for one-body dissipation.

It was found [78] that the wall friction substantially overestimates the strength of one-body dissipation as required to fit experimental data on the pre-scission neutron multiplicity. Also, in order to reproduce simultaneously the measured pre-scission neutron multiplicities and the variance of the fission fragment mass-energy distribution the wall formula [Eq. (2.23)] is often multiplied with a reduction factor κ [99, 100, 139]. However, the constant κ is not defined uniquely and the value of κ, determined through fitting experimental data, is different for different compound nuclear systems [99]. It also varies for the different observables of the same reaction [99]. A part of this reduction of the wall friction may be accounted for by considering the surface diffuseness as mentioned above. Another major part of this reduction can be explained as follows. It is assumed, in the derivation of wall formula, that the motion of particles inside the gas is fully chaotic. This is not completely true for a nuclear system where nucleon-nucleon collisions are rare for excitation energies much below the Fermi energy domain $(E/A \sim \epsilon_F)$. The dynamics of independent particles in time-dependent cavities has been extensively studied by Blocki and his coworkers [140, 141, 142, 143]. Considering classical particles in vibrating cavities of various shapes, a strong correlation between chaos in classical phase space and the efficiency of energy transfer from collective to intrinsic motion was numerically calculated [141]. It has been argued in [140, 141] that the wall friction in its original form should be applied only for systems for which the particle motion shows fully chaotic behavior. Hence the wall friction needs to be modified to make it applicable for those systems which are partially chaotic. The classical wall friction was originally derived for idealized systems employing a number of simplifying assumptions such as approximating the nuclear surface by a rigid wall and considering only adiabatic collective motions. On the other hand, Koonin

and Randrup [70] developed the theory of one body dissipation by using the linear response theory (LRT) approximation. Then, the validity of the classical wall friction was scrutinized in the framework of LRT damping and it was shown that in the limiting situation LRT damping coincides with the wall friction [144, 145]. Pal and Mukhopadhyay [146] introduced a measure of chaos into the classical linear response theory for one body dissipation, developed in Ref. [70], and a scaled version of the wall friction, was thus obtained [146, 147]. The chaos weighted wall friction was applied successfully in the one-dimensional Langevin dynamical calculations to explain the experimental prescission neutron multiplicity [98] and evaporation residue cross section [148].

(3) **_Window friction:_**

This collective energy dissipation is caused by the transfer of momentum through the neck of a dinuclear system. Following the work of Blocki _et al._ [67], let us consider the one-body dissipative drag between two systems (nascent fragments in case of fission), 1 and 2, in relative motion and communicating through a small window of area $\triangle\sigma$ (Fig. 2.5). Both of these systems are assumed to contain ideal gasses of similar particles. Now, the force on system 1 due to presence of 2 is given by

$$\overrightarrow{F}_{21} = \overrightarrow{\mathbb{P}}_{21}\triangle\sigma - \overrightarrow{\mathbb{P}}_{12}\triangle\sigma, \tag{2.24}$$

where $\overrightarrow{\mathbb{P}}_{21}$ is the momentum-flux from system 1 into system 2 and similar interpretation exists for $\overrightarrow{\mathbb{P}}_{12}$. If the collective velocities of the two systems are small compared to the speed of nucleons then according to Ref. [67], we get

$$\overrightarrow{\mathbb{P}}_{21} = \frac{1}{4}\rho_m\overline{v}\left(2\overrightarrow{U}_{\parallel} + \overrightarrow{U}_{\perp}\right) + \text{other terms}, \tag{2.25}$$

where $\overrightarrow{U}$ is the relative drift velocity of the gas particles, about to cross the window from system 1 to system 2, with respect to the velocity of the window. $\overrightarrow{U}_{\parallel}$ and $\overrightarrow{U}_{\perp}$ are the components of $\overrightarrow{U}$ along and right angle to the normal through the window, respectively. Putting the above expression, and similar expression for $\overrightarrow{\mathbb{P}}_{12}$, in Eq. (2.24), we get

$$\overrightarrow{F}_{21} = \frac{1}{4}\rho_m\overline{v}\triangle\sigma(2\overrightarrow{u}_{\parallel} + \overrightarrow{u}_{\perp}), \tag{2.26}$$

where $\overrightarrow{u}$ is the relative velocity between the two systems, and $\overrightarrow{u}_{\parallel}$ and $\overrightarrow{u}_{\perp}$ are the components of this velocity along and right angle to the normal through the window $\triangle\sigma$. Equation (2.26)

is the window formula for the velocity dependent dissipative drag calculated to the first order in the relative velocity $\overrightarrow{u}$. As can be seen from Eq. (2.26), this force is not in general parallel to $\overrightarrow{u}$. However, in case of fission, it is assumed that the axial symmetry is always maintained and hence $\overrightarrow{u}_\perp = 0$, which leads to the formula for the rate of energy dissipation:

$$-\dot{E}^{window} = \frac{1}{2}\rho_m \overline{v} \triangle \sigma u^2. \tag{2.27}$$

If R is the relative separation between the two future fragments then, $u = \dot{R} = \sum(\partial R/\partial q_i)\dot{q}_i$ and, therefore, by comparing Eq. (2.27) with Eq. (2.19) we get

$$\eta_{ij}^{window}(\overrightarrow{q}) = \frac{1}{2}\rho_m \overline{v} \triangle \sigma \frac{\partial R}{\partial q_i}\frac{\partial R}{\partial q_j}. \tag{2.28}$$

(4) *Dissipation due to mass-asymmetry current:*

The wall and window formula, describing the macroscopic energy dissipation for a dinuclear system undergoing shape evolution, do not include the dissipation associated with a time rate of change of the mass asymmetry of the system. The corresponding dissipation coefficient, which is shown [99] to be essential in order to reproduce the experimental results on fission fragment mass distribution, was first calculated by Randrup and Swiatecki [149] using the simple Fermi gas model. To describe their work let us assume the nucleus as a gas of fermions in a container consisting of two pieces with volumes V_1 and V_2 containing A_1 and A_2 particles, respectively,
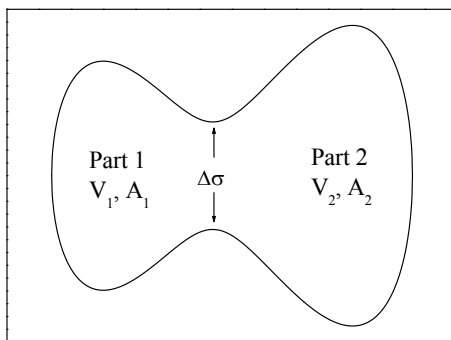

Figure 2.5: A schematic diagram of dinuclear shape.

and communicating through a small window of area $\triangle \sigma$ (see Fig. 2.5). The total volume is considered to be constant but the part V_1 is imagined to be changing at a rate $\dot{V}_1$ so that there is

a net current of particles, say $\dot{A}_1$, through the window. Associated with the given configuration and state of motion of the system, there is a macroscopic potential energy E_{asym} which is a explicit function of the mass partition (A_1 or A_2, as $A = A_1 + A_2$ is constant) only. Now, consider the following identity:

$$-\dot{E}^{asym} = \left(-\frac{dE^{asym}}{dA_1}\right)\dot{A}_1, \tag{2.29}$$

where $(-dE^{asym}/dA_1)$ is the force associated with the mass asymmetry degree of freedom. Similar to general conditions like the ordinary viscous hydrodynamics and the flow of electric current through a resistor, the current of particles between two systems induced by some driving force is expected to be proportional to this driving force. As a result, we anticipate a proportionality relation of the form

$$\dot{A}_1 = k\left(-\frac{dE}{dA_1}\right), \tag{2.30}$$

where k is a constant. Substituting Eq. (2.30) in Eq. (2.29) we get $-\dot{E}^{asym} = (1/k)\dot{A}_1^2$. Now, the constant k can be calculated [149] by considering infinitesimal difference in the properties of the Fermi gasses adjacent to the two sides of the window $\triangle\sigma$ and eventually, by putting the value of k in the expression for $-\dot{E}^{asym}$, we get

$$-\dot{E}^{asym} = \frac{16}{9}\frac{\rho_m\overline{v}}{\triangle\sigma}\dot{V}_1^2. \tag{2.31}$$

In a similar manner as in the case of window formula one can derive the formula for dissipation coefficient which is given by

$$\eta_{ij}^{asym}(\overrightarrow{q}) = \frac{16}{9}\rho_m\overline{v}\frac{1}{\triangle\sigma}\frac{\partial V_1}{\partial q_i}\frac{\partial V_1}{\partial q_j}. \tag{2.32}$$

Now, we are in a position to sum up all the different contributions to get the total one-body dissipation coefficient η_{ij}. For neck-less nuclear shapes, η_{ij} is calculated from the wall formula. As the neck starts to develop, i.e., when Eq. (2.5) is just satisfied, η_{ij} changes abruptly due to the appearance of η_{ij}^{window} and η_{ij}^{asym}. Following the work of Adeev $et\ al.$ [101], we introduce a function $f(\overrightarrow{q})$ to get a smooth variation of η_{ij} from the mononuclear shapes to the dinuclear shapes. Then, in general, η_{ij} can be expressed as

$$\eta_{ij}(\overrightarrow{q}) = \eta_{ij}^{mono}(\overrightarrow{q})f(\overrightarrow{q}) + \eta_{ij}^{di}(\overrightarrow{q})\left(1 - f(\overrightarrow{q})\right), \tag{2.33}$$

49

where

$$\eta_{ij}^{mono}(\overrightarrow{q}) = \kappa \eta_{ij}^{wall}(\overrightarrow{q}), \tag{2.34}$$

and

$$\eta_{ij}^{di}(\overrightarrow{q}) = \kappa \eta_{ij}^{wall}(\overrightarrow{q}) + \eta_{ij}^{window}(\overrightarrow{q}) + \eta_{ij}^{asym}(\overrightarrow{q}), \tag{2.35}$$

where κ is the reduction factor in the wall formula. The choice of the function $f(\overrightarrow{q})$ is however not unique [101]. It is chosen in such a way that it varies smoothly from 1 for neck-less shape to 0 for shapes with well-defined neck. For the two-dimensional calculation with c and α', we have defined $f(\overrightarrow{q})$ as

$$
\begin{aligned}
f(c, \alpha') &= 0 && \text{if } c \leq c_N(\alpha'), \\
&= \left(\frac{c - c_N(\alpha')}{c_1 - c_N(\alpha')} \right)^2 && \text{if } c_N(\alpha') < c \leq c_1, \\
&= 1 && \text{if } c > c_1,
\end{aligned} \tag{2.36}
$$

where $c_N(\alpha')$ is the locus of the neck-formation line in (c, α') space and c_1 is the value of c from where the $\eta_{ij}^{mono}(\overrightarrow{q})$ is completely switched over to the $\eta_{ij}^{di}(\overrightarrow{q})$. The value of c_1 is judiciously
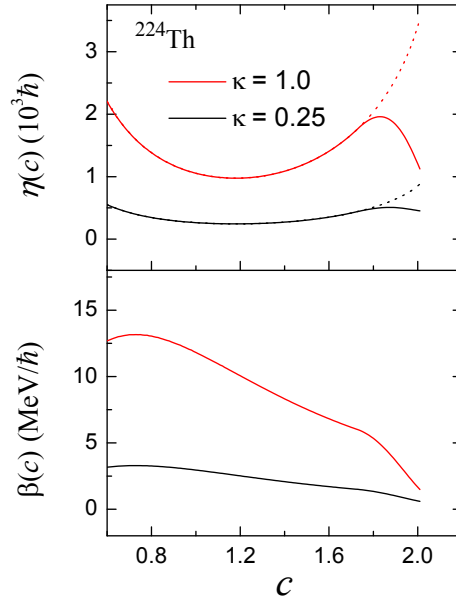

Figure 2.6: The dissipation coefficient ($\eta(c)$) and the reduced dissipation coefficient ($\beta(c)$) as functions of c. The dotted lines in the upper panel indicate η^{wall}.

50

chosen such that the results are not sensitive to this choice.

As discussed earlier, a constant value for κ is often used in Eq. (2.34) and Eq. (2.35) [99, 100, 101, 103]. It is mentioned in Ref. [100] that the value of $\kappa = 0.25$ is a good choice to fit the experimental data. For the one-dimensional calculations, $\eta_{ij}(\overrightarrow{q})$ has only one component $\eta(c)$ which is plotted in Fig. 2.6 (upper panel) for two different values of κ. In accordance with the expressions of Eq. (2.34) and Eq. (2.35), $\eta(c)$ is equal to the $\eta^{wall}(c)$ before the neck appears in the nuclear shape and then for dinuclear shapes $\eta(c)$ starts deviating from $\eta^{wall}(c)$ which is indicated by dotted lines in Fig. 2.6. However, instead of η, the reduced dissipation coefficient $\beta = \eta/m$ is often used as a free parameter to fit the experimental data [108]. For completeness, β is also plotted in Fig. 2.6 (lower panel).

2.4   Langevin dynamics in one dimension

In one dimension, with c as the collective coordinate, the Langevin equations can be written as

$$
\begin{aligned}
\frac{dc}{dt} &= \frac{p}{m}, \\
\frac{dp}{dt} &= -\frac{p^2}{2}\frac{d}{dc}\left(\frac{1}{m}\right) - \frac{dV}{dc} - \frac{\eta}{m}p + g\Gamma(t),
\end{aligned}
\tag{2.37}
$$

where p is the momentum conjugate to c. The different inputs to the Langevin dynamics, namely the shape dependent collective inertia m, the friction coefficient η and the potential energy of the system V are described in detail in the previous section. The random force is given by $g\Gamma(t)$, where the diffusion coefficient $D(= g^2)$ is related to the friction coefficient η through the Einstein relation $D(c) = \eta(c)T$. In this framework the temperature T is simply a measure of the non-collective part of the nuclear excitation energy E^* and related to the later by the usual Fermi gas relation $E^* = a(c)T^2$, where $a(c)$ is the level density parameter of the considered nucleus at a nuclear deformation characterized by c. The excitation energy itself is determined by the conservation of the total energy as will be discussed afterwards.

2.4.1   Method of solving Langevin equation

The Langevin equations are used extensively in different branches of physics and chemistry. The analytical solutions of these equations can be derived only for parabolic potentials [84, 150]. A

general analytical scheme to solve multi-dimensional Langevin equations near the saddle point was given in Ref. [151]. However, for practical applications, the solutions of Langevin equations are mostly attempted with numerical simulations. In a direct simulation method [82], the stochastic equations of motion are formulated first and subsequently, these equations are integrated directly for a given initial condition. Random number generator is used to perform this integration and, by repeating the simulation, independent realizations of the relevant process are obtained for different sequences of random numbers. It is obvious that the number of desired realizations will be small compared to the total number of events if the probability of the corresponding process is small. However, this difficulty does not arise in the study of fission dynamics of hot and heavy nuclei for which the fission probabilities are considerably high. We use the direct integration method in the present work and it is described as follows.

The Langevin equations in Eq. (2.37) can be written as

$$
\begin{aligned}
\frac{dc}{dt} &= \frac{p}{m} = v(p, c; t), \\
\frac{dp}{dt} &= H(p, c; t) + g(c; t)\Gamma(t),
\end{aligned}
\tag{2.38}
$$

where

$$
H(p, c; t) = -\frac{p^2}{2}\frac{\partial}{\partial c}\left(\frac{1}{m}\right) - \frac{\partial V}{\partial c} - \frac{\eta}{m}p.
\tag{2.39}
$$

Integrating Eq. (2.38) from t to $t + \Delta t$, we get

$$
\begin{aligned}
c(t + \Delta t) &= c(t) + \int_t^{t+\Delta t} dt'\, v(p, c; t'), \\
p(t + \Delta t) &= p(t) + \int_t^{t+\Delta t} dt'\, H(p, c; t') + \int_t^{t+\Delta t} dt'\, g(c; t')\Gamma(t').
\end{aligned}
\tag{2.40}
$$

Here, Δt is large compared to the average period of fluctuations in $\Gamma(t)$, but it is small enough so that the dynamical variables do not change much during this time interval. Therefore, to perform the above integrations, we can expand $H(p, c; t')$, $g(c; t')$ and $v(p, c; t')$ in Taylor series around their values at time t, i.e.,

$$
\begin{aligned}
H(p, c; t') &\approx H + \frac{\partial H}{\partial p}\left\{(t' - t)H + g\int_t^{t'} dt''\Gamma(t'')\right\} + \frac{\partial H}{\partial c}(t' - t)v, \\
v(p, c; t') &\approx v + \frac{\partial v}{\partial p}\left\{(t' - t)H + g\int_t^{t'} dt''\Gamma(t'')\right\} + \frac{\partial v}{\partial c}(t' - t)v,
\end{aligned}
$$

$$g(c;t') \approx g + \frac{dg}{dc}(t'-t)v, \tag{2.41}$$

where the terms up to linear in $(t'-t)$ are retained and $H \equiv H(p,c;t)$, $v \equiv v(p,c;t)$ and $g \equiv g(c;t)$. Now, putting the above expansions in Eq. (2.40) and then carrying out the integrations, we obtain

$$c(t+\Delta t) = c(t) + \Delta t v + \frac{(\Delta t)^2}{2}\left[\frac{\partial v}{\partial c}v + \frac{\partial v}{\partial p}H\right] + \frac{\partial v}{\partial p}g\widetilde{\Gamma}_2,$$

$$p(t+\Delta t) = p(t) + \Delta t H + \frac{(\Delta t)^2}{2}\left[\frac{\partial H}{\partial c}v + \frac{\partial H}{\partial p}H\right] + g\widetilde{\Gamma}_1 + \frac{\partial H}{\partial p}g\widetilde{\Gamma}_2 + \frac{dg}{dc}v\widehat{\Gamma}_2, \tag{2.42}$$

where the terms involving the Gaussian random numbers, $\Gamma(t)$, are defined as follows:

$$\widetilde{\Gamma}_1 = \int_t^{t+\Delta t} dt'\Gamma(t') = (\Delta t)^{1/2}\omega_1(t),$$

$$\widetilde{\Gamma}_2 = \int_t^{t+\Delta t} dt' \int_t^{t'} dt''\Gamma(t'') = (\Delta t)^{3/2}\left[\frac{1}{2}\omega_1(t) + \frac{1}{2\sqrt{3}}\omega_2(t)\right],$$

$$\widehat{\Gamma}_2 = \int_t^{t+\Delta t} dt'(t'-t)\Gamma(t') = (\Delta t)^{3/2}\left[\frac{1}{2}\omega_1(t) - \frac{1}{2\sqrt{3}}\omega_2(t)\right]. \tag{2.43}$$

Here, $\omega_n(t)$ ($n = 1, 2$) are the new set of Gaussian random numbers with time-correlation properties: $\langle\omega_n(t)\rangle = 0$ and $\langle\omega_1(t_1)\omega_2(t_2)\rangle = 2\delta_{12}\delta(t_1 - t_2)$. Starting at $t = 0$, we can obtain $p(t)$ and $c(t)$ at any later time by repeating the above procedure. In the present work, a very small time step of $\Delta t = 0.0005\hbar/\text{MeV}$ is used for the numerical integration. With this value of Δt, the validity of the algorithm and the numerical stability of the results are checked earlier [66].

2.4.2 Initial condition and the scission criteria

For an ensemble of events, the initial distribution of coordinates and momenta of the Brownian particles are assumed to be close to equilibrium and hence, the initial values of (c, p) are chosen from sampling random numbers which follow the Maxwell-Boltzmann distribution. Starting with a given total excitation energy (E_{ex}) and angular momentum (ℓ) of the CN, the energy conservation is obeyed in the following form,

$$E_{ex} = E^* + V(c) + p^2/2m. \tag{2.44}$$

The foregoing equation gives the intrinsic excitation energy E^* and the corresponding nuclear temperature $T = (E^*/a)^{1/2}$ at each time-step of the fission process (each integration step).

The scission criterion is an essential input in the dynamical calculations of fission It defines the boundary surface (for example a point and a line for one- and two-dimensional cases, respectively) on which a Langevin dynamical trajectory ends up as a fission event. In practice, different prescriptions are used to determine the scission condition. As described earlier, the condition of zero neck radius is impractical because we can not apply LDM to model the nuclear potential when the neck radius becomes comparable to the inter-nucleonic distance. Therefore, it is often assumed [113, 118, 152] that scission occurs with a relatively thick neck. From physical arguments, the scission surface can be defined as the locus of points at which a nucleus becomes unstable against the variation of neck thickness [91, 113, 153]. It can be shown [113, 118] that this scission condition corresponds to the shapes of the fissioning nucleus with a finite neck radius of $0.3R_0$ on the average , where R_0 is the radius associated with the spherical shape. In another criterion, the Coulomb repulsion between the future fragments is equated with the corresponding nuclear attraction at scission. This scission condition, in fact, leads to scission configurations with approximately the same neck radius of $0.3R_0$ for the actinide nuclei [154]. A probabilistic criterion is also proposed [155] for the scission of a fissile nucleus, where the probability is estimated by considering scission as a fluctuation. The reproduction of different experimental osservables with the probabilistic criterion indicates that the earlier criterion [118], according to which nuclear scission occurs at a finite neck radius of $0.3R_0$, is a good approximation to the probabilistic scission criterion in Langevin dynamical calculations. Therefore, for the present purpose, we shall consider the neck radius of $0.3R_0$ as the scission condition.

2.4.3 Calculation of fission width

Here, we discuss how the fission width is extracted from a one-dimensional Langevin dynamical calculation with c as the collective variable. Starting from the initial condition, the time evolution of a Langevin trajectory is followed with the numerical technique described above. Then, according to the scission criterion adopted in the present thesis, a Langevin trajectory is considered as a fission event if it reaches the scission point c_{sci} where the neck radius becomes $0.3R_0$. The calculations are repeated for a large number (typically 100,000 or more) of trajectories and the number of fission events are recorded as a function of time. At each iteration step, we calculate the probability of the system remaining as CN, P_{CN}, i.e, number of samples

with $c < c_{sci}$ divided by the total number of samples, and then calculate the fission rate $R(t)$ as [82],

$$R(t) = -\frac{1}{P_{CN}}\frac{dP_{CN}}{dt}. \tag{2.45}$$

There will be a large fluctuation in $R(t)$ if it is calculated at each time step and, therefore, a time averaging is done over time Δt as

$$R(t) = \frac{1}{\Delta t}\int_{t-\Delta t/2}^{t+\Delta t/2} R(t)dt = \frac{1}{\Delta t}\ln(P_{CN}(t-\Delta t/2)/P_{CN}(t+\Delta t/2)). \tag{2.46}$$

Finally, we get the Langevin dynamical fission width as $\Gamma_L(t) = \hbar R(t)$.
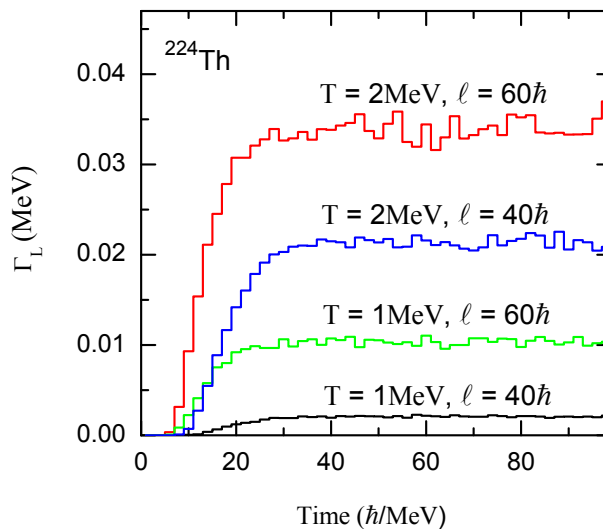

Figure 2.7: The Langevin fission width (Γ_L) for different combinations of ℓ and T. Calculations are done with $\kappa = 0.25$ in the equation for one body dissipation.

In Fig. 2.7, $\Gamma_L(t)$ values are plotted which we have calculated for different combinations of ℓ and T. As shown in this figure, we can divide the whole time scale of Γ_L into three parts. Initially, it remains zero for a few units of $\hbar$/MeV and the corresponding time period is called the "formation time". It signifies the time during which the 'first' CN reaches the scission configuration from the ground-state configuration. Then, Γ_L starts to increase and becomes stationary within a few tens of $\hbar$/MeV. This growth period is called the "transient time" [45]. After that, for an ensemble of CN formed near the ground-state configuration, Γ_L remains stationary as there is sufficient supply of CN to the diffusion current over the fission barrier.

Chapter 3

Spin dependence of the modified Kramers' width of fission

3.1   Introduction

Fission of a compound nuclei formed in heavy ion induced fusion reactions at energies above the Coulomb barrier has been investigated quite extensively, both experimentally and theoretically, during the last two decades. The multiplicities of pre-scission neutrons, light charged particles and statistical γ-rays have been measured [46, 47, 48, 49, 50, 51, 52, 53, 54, 55, 56, 57, 58, 59, 60] and compared with the predictions of the statistical model of nuclear fission [24, 55, 59, 60]. These investigations have revealed that the statistical model of nuclear fission based on the transition-state method [Eq. (1.3)], where effects due to nuclear dissipation are not considered, is inadequate to describe fission of a highly excited heavy nuclei, and consequently dissipative dynamical models [72, 78, 99] are found to be essential to account for the experimental data. Similar conclusion are also reached while analyzing the evaporation residue cross sections of highly fissile compound nuclei [24, 61]. Consequently, fission has become a useful probe to study the dissipative properties of the nuclear bulk. The dynamical calculations are performed either by employing the Langevin equations in a dynamical model of nuclear fission [72, 78, 99] or by using the statistical modal where the fission width includes the effect of dissipation [Eq. (1.46)]. The Langevin dynamical model for fission width, without incorporating the particle and γ evaporations, is explained in the previous chapter. The computations are quite involved

and demands a great deal of computer time. On the other hand, the statistical model approach is used more frequently since it is rather straightforward to implement.

As discussed in the first chapter, Kramers solved the Fokker-Planck equation considering fission as a diffusive process of a Brownian particle across the fission barrier in a viscous medium. He imposed a few simplifying approximations which finally yielded the so-called Kramers' expression for fission width as [Eq. (1.46)]

$$\Gamma_K = \frac{\hbar\omega_g}{2\pi} \exp(-V_B/T) \left\{ \sqrt{1 + \left(\frac{\beta}{2\omega_s}\right)^2} - \frac{\beta}{2\omega_s} \right\},$$ (3.1)

where β is the reduced dissipation strength defined in terms of the dissipation strength η as $\beta = \eta/m$, m being the collective inertia associated with the nuclear deformation parameter. T is the compound nuclear temperature, V_B is the fission barrier hight and ω_g and ω_s are the frequencies of the harmonic oscillators, as described in the first chapter, representing approximately the nuclear potentials at the ground state and at the saddle configurations. The harmonic oscillator frequencies ω_g and ω_s are usually assumed to be constant for all spin values of the compound nucleus (CN) while applying the Kramers' formula in statistical model calculations. The centrifugal barrier however changes the potential profile at higher values of spin of a CN (see Fig. 2.2), which consequently results in a spin dependence of ω_g and ω_s [107]. In this chapter, we discuss the effect of this spin dependence using a statistical model calculation for fission [108].

In the next section, we explain how the harmonic oscillator frequencies are defined suitably from the finite range liquid drop model (FRLDM) potential and calculated as a function of compound nuclear spin. Also, the possible effect of these spin-dependent frequencies in the Kramers' fission width is illustrated in this section. Then, a brief description of the statistical model calculation of fission is given in Sec. 3.3. One can found an elaborate description of the statistical model code in Appendix B. Subsequently, in Sec. 3.4, we analyze the results of statistical model calculations and, finally, we summarize those results in Sec. 3.5.

3.2 Calculation of ω_g and ω_s and modified Kramers' width

The FRLDM potential energies at and about the ground-state configuration (c_g) and the saddle point (c_s) are approximated with harmonic oscillator potentials in order to use the analytical expression of Eq. (3.1) in the statistical model of compound nuclear decay. Then the expression for the potential becomes

$$
\begin{aligned}
V &= \frac{1}{2}m\omega_g^2 (c - c_g)^2 && \text{near} \;\; c = c_g, \\
&= V_B - \frac{1}{2}m\omega_s^2 (c - c_s)^2 && \text{near} \;\; c = c_s,
\end{aligned}
\tag{3.2}
$$

where m is the collective inertia associated with c and V_B is the fission barrier. Since the Kramers' formula is originally obtained for a constant inertia, we first use the shape-independent collective inertia m calculated at the ground-state deformation. Later, in the generalization of the Kramers' formula for variable inertia, we will see how the frequencies change for a shape-dependent inertia. The frequencies of these harmonic oscillators can be given in terms of the curvatures of the FRLDM potential as

$$
\omega_g = \left(\frac{1}{m}\frac{d^2 V}{dc^2} \right)_g^{1/2}, \qquad \omega_s = \left| \frac{1}{m}\frac{d^2 V}{dc^2} \right|_s^{1/2}.
\tag{3.3}
$$

To calculate these frequencies numerically, we need to discretize the potential energy V along the deformation axis. Then the curvature on either side of a turning point (c_g or c_s) can be written as

$$
\omega_{g,s}^{+,-} = \left[\frac{2}{m}\frac{\triangle V}{\triangle(c^2)} \right]^{1/2},
\tag{3.4}
$$

where $\triangle V$ and $\triangle(c^2)$ are corresponding shifts in V and c^2 away from the turning point and the super-script $+$ $(-)$ denotes the direction of the shift to the right (left) of a turning point. If $\triangle V$ is made too small, then the curvatures obtained will not reproduce the actual (FRLDM) potential very well. If $\triangle V$ is made too large, then the curvatures obtained will not reflect the curvatures around the turning points. An appropriate balance between these two extremes is obtained by Lestone [107] using $\triangle V = 1$ MeV if the fission barrier V_B is larger than 2 MeV and, for V_B less than 2 MeV, $\triangle V = V_B/2$ is used. The curvature at the turning points is then determined using the following relations:

$$
\omega_g = 2 \left(\frac{1}{\omega_g^+} + \frac{1}{\omega_g^-} \right)^{-1}, \qquad \omega_s = 2 \left(\frac{1}{\omega_s^+} + \frac{1}{\omega_s^-} \right)^{-1}.
\tag{3.5}
$$

We extend the idea of Lestone and fit the numerically obtained FRLDM potentials with har-
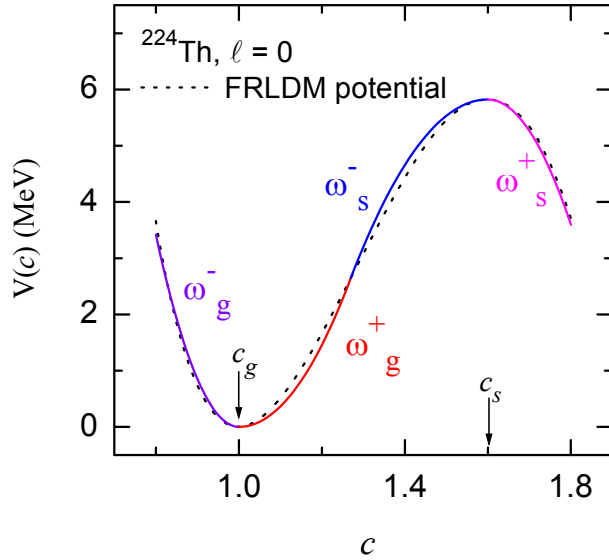

Figure 3.1: Different parts of a FRLDM potential fitted with harmonic oscillators of different frequencies.

monic oscillator potentials in such a way that the latter satisfies $\triangle V = V_B/2$ for all the values of V_B [108]. The corresponding fit for the ^{224}Th nucleus with spin $\ell = 0$ is plotted in the Fig. 3.1. It can be seen that the oscillator potentials are now connected smoothly between c_g and c_s, thereby providing a better approximation to the FRLDM potential. Similar plots obtained for non-zero values of ℓ are shown in Fig. 3.2, where the corresponding frequencies are also given. The resulting spin dependence of the harmonic oscillator frequencies are shown in Fig. 3.4 (top panel). On the other hand, if the second derivatives of the potential at the turning points are used to obtain the harmonic oscillator frequencies then, as shown in Fig. 3.3, the resulting potential becomes disjoint between c_g and c_s, and hence the scenario of dynamical diffusion over the fission barrier turns out to be unfeasible. Therefore, in the present thesis, we adopt the prescription where the approximated harmonic oscillator potentials are connected at the mid-point between the ground-state and the saddle configurations.

In practice, the dimensionless quantity $\gamma = \eta/2m\omega_s$ is often used as a free parameter in order to fit experimental data. According to the definition of γ, it becomes a function of compound nuclear spin (ℓ) when the spin dependence of ω_s is considered. The variation of γ is
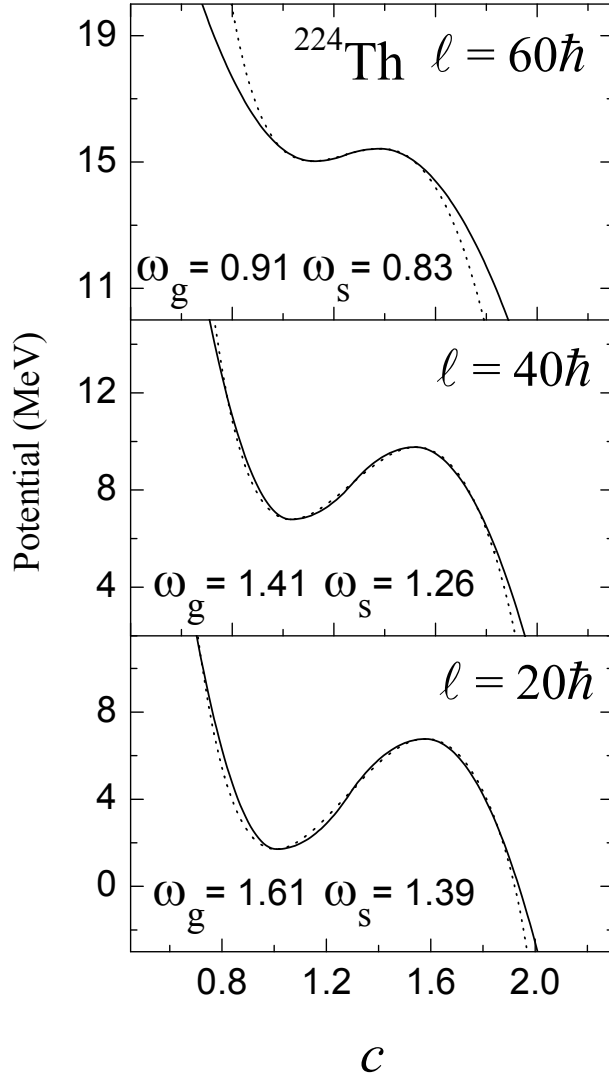
Figure 3.2: The approximated potentials (solid lines) obtained in the present work for different values of ℓ. Corresponding LDM potentials are indicated by dotted lines.

shown in the middle panel of Fig. 3.4 for a constant value of $\beta = 5 \times 10^{21} s^{-1}$. This form of γ affects in the spin dependence of Γ_K in the following way. We have shown earlier (see Fig. 2.3) that the fission barrier V_B decreases rapidly as the spin of a CN increases. As a result, there will be a strong spin dependence in Γ_K if the harmonic oscillator frequencies are assumed to be constant. It is demonstrated by the dotted line in the lower panel of Fig. 3.4, where the Γ_K, given by Eq. (3.1), is obtained for the constant values of ω_g and ω_s corresponding to $\ell = 0$. On the other hand, as shown in Fig. 3.4, the spin dependence of Γ_K is reduced substantially for
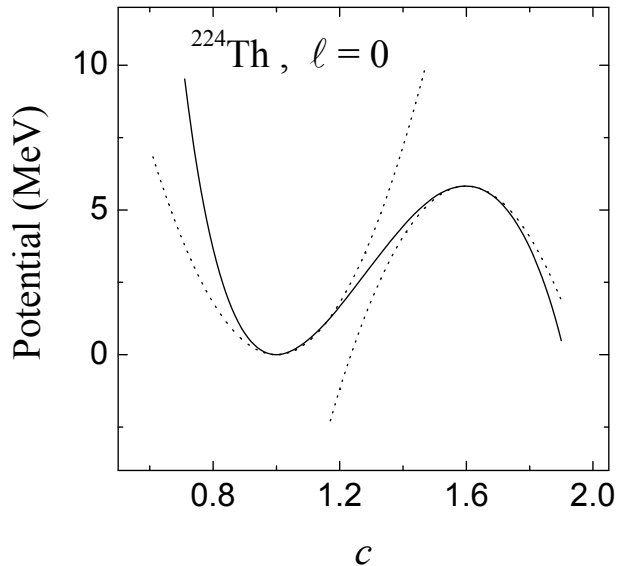
Figure 3.3: The harmonic oscillator potentials (dotted lines) which are obtained from the curvatures at the ground state and the saddle point of the corresponding LDM potential (solid line).

the higher values of ℓ, when the variations of ω_g and ω_s are taken into account.

Since higher values of angular momentum states are populated at higher excitation energies of a CN formed in a heavy-ion induced fusion reaction, the above observation indicates that larger value of γ would be required at higher excitation energies. In fact, a strong energy dependence of γ had been observed earlier [55, 60] in a number of statistical model analysis of experimental data. This immediately suggests that the observed energy dependence of γ, or at least a part of it, can be accounted for by the above spin dependence of ω_g and ω_s. To address this issue we perform the statistical model calculations for pre-scission neutron multiplicities n_{pre} and evaporation residue (ER) cross sections using the fission width as given by Eq. (3.1) along with the spin dependent values of ω_g and ω_s.

3.3   Statistical model calculation

In the statistical model calculation, we consider evaporation of neutrons, protons, α particles and statistical giant dipole resonance (GDR) γ rays as the decay channels of an excited CN in
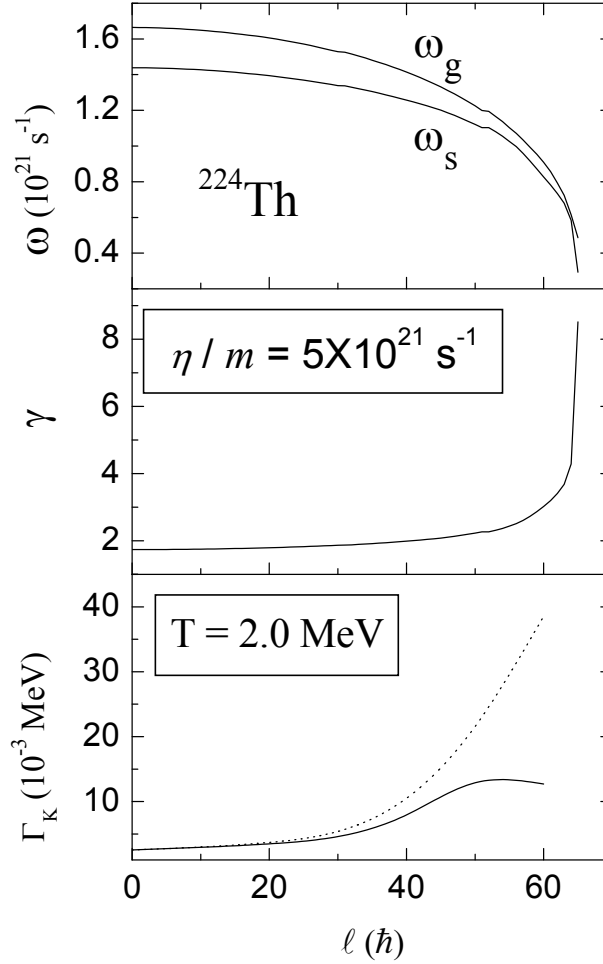
Figure 3.4: The ω_g and ω_s (top panel), γ (middle panel) for a constant η/m, and the corresponding Kramers' fission width Γ_K (bottom panel) as functions of ℓ. Γ_K is also indicated for a constant $\gamma(\ell = 0)$ by dotted line where the sharp spin dependence is coming due to the decrease in V_B with ℓ.

addition to fission. The particle and GDR γ partial decay widths are obtained from the standard Weisskopf formula [78] as described in Appendix B. A time-dependent fission width is used in order to account for the transient time, as explained in the previous chapter, which elapses before the stationary value of the Kramers' modified width is reached [45]. A parametrized form of the dynamical fission width is given as [156]

$$\Gamma_f(t) = \Gamma_K \left[1 - exp(-2.3t/\tau_f) \right], \tag{3.6}$$

where

$$\tau_f = \frac{\beta}{2\omega_g^2} \ln \left(\frac{10V_B}{T} \right)$$

is the transient time period and V_B is the spin dependent fission barrier. Though a recent work [157] provides a more accurate description of time-dependent fission widths, we have used Eq. (3.6) in the present work in order to compare our results with the earlier works. In the above definition of the fission width, fission is considered to have taken place when the CN crosses the saddle point deformation. During transition from saddle to scission, the CN can emit further neutrons, which would contribute to the pre-scission multiplicity. The saddle-to-scission time is given as [158]

$$\tau_{ss} = \tau_{ss}^0 \left\{ \sqrt{1 + \left(\frac{\beta}{2\omega_s} \right)^2} + \frac{\beta}{2\omega_s} \right\}, \tag{3.7}$$

where τ_{ss}^0 is the non-dissipative saddle-to-scission time interval and its value is taken from Ref. [159]. We also calculate the multiplicity of neutrons emitted from the fission fragments (n_{post}) assuming symmetric fission.

3.4   Results and discussions

We chose the system ^{16}O+^{208}Pb for our calculations. It is mainly because of two reasons. Firstly, experimental data on n_{pre} (prescission neutron multiplicity) and ER cross section over a wide range of beam energy are available for this system [24, 61] and, secondly, it has been theoretically investigated extensively in the past [60, 148]. We first show the calculated values of neutron multiplicities along with the experimental spin-dependent data in Fig. 3.5 for different values of the reduced dissipation coefficient β. We perform two sets of calculations. In one set, the fission widths are calculated using the spin-dependent frequency values while they are obtained with spin-independent frequency values (set equal to the $\ell = 0$ values) in the other set of calculation. It is observed that n_{pre} calculated with spin-dependent frequencies for a given β has larger dependence on the initial beam energy than those calculated with constant ωs. In fact, a reasonable agreement with the experimental values can be obtained with $\beta = 6$ (in $10^{21}s^{-1}$) in the former calculation. In what follows, we study the dependence of β on the initial excitation energy of the CN and not on its instantaneous values which decreases with time due to successive particle and γ emissions. Though the later would have
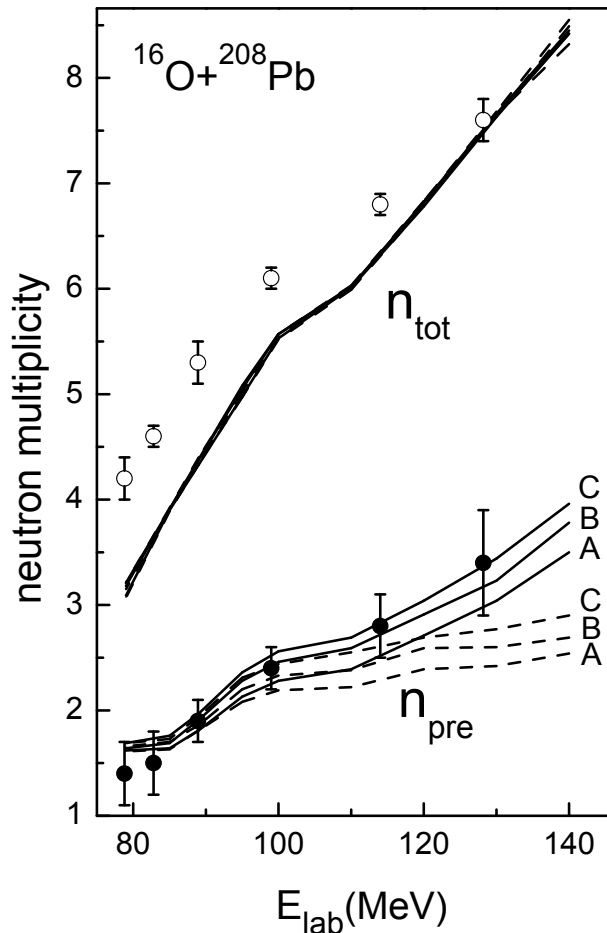
Figure 3.5: Pre-scission (n_{pre}) and total (n_{tot}) neutron multiplicities. The experimental values (filled circles) are taken from [54]. The solid and dashed lines are statistical model calculations with and without spin dependence of frequencies, respectively. A, B, and C denote results with $\beta =4$, 5, and 6 (in 10^{21} s^{-1}), respectively. The n_{tot} values obtained with different βs from the two sets of calculations are almost indistinguishable [108].

been more desirable, the former can still provide us the gross features of energy dependence which is adequate for our present purpose. We subsequently extract the values by fitting the experimental multiplicity separately at each value of incident energy in order to compare the initial excitation energy dependence of β from the two sets of calculations. Figure 3.6 shows the results. The initial excitation energy dependence of β obtained with frequencies is much weaker compared to that obtained with constant values of the frequencies. The total neutron multiplicity $(n_{tot} = n_{pre} + n_{post})$ is also plotted in Fig. 3.5 . Since the initial excitation energy
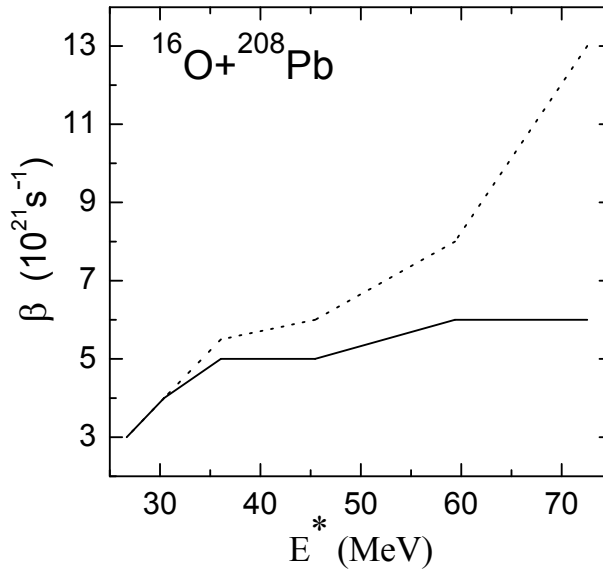
Figure 3.6: Initial excitation energy (E^*) dependence of β. The solid and dashed lines correspond to fitted values obtained with and without spin dependence of frequencies, respectively [108].

of the nuclear system (CN plus fission fragments) is essentially carried away by the pre-scission and fission-fragment neutrons, n_{tot} values are not sensitive to β as can be seen from this figure.

We next show in Fig. 3.7 the ER excitation functions calculated with different values of β along with the experimental cross sections. In addition to the total ER cross sections, the ER cross sections with ($\sigma(\alpha, xn, yp)$) and without ($\sigma(xn, yp)$) α emission are also plotted in this figure. It is observed that unlike the results for n_{pre}, the difference between the ER cross sections from the two sets of calculations, with and without the spin dependence of the frequencies, is small. This can be explained as follows. Since evaporation residues are preferably formed from compound nuclei with lower spin values while a CN with a higher spin is more likely to undergo fission, the spin dependence of frequencies (see Fig. 3.4) will affect the fission probability more strongly than the ER cross section. In particular, this feature is expected to be more prominent for highly fissile systems like ^{224}Th where residues are mostly formed from CN with very small values of angular momentum, which results in a marginal spin dependence of residue formation as shown in Fig. 3.7 . On the other hand, fission probabilities and particularly those at higher excitation energies where high spin states are populated are expected to be more sensitive to
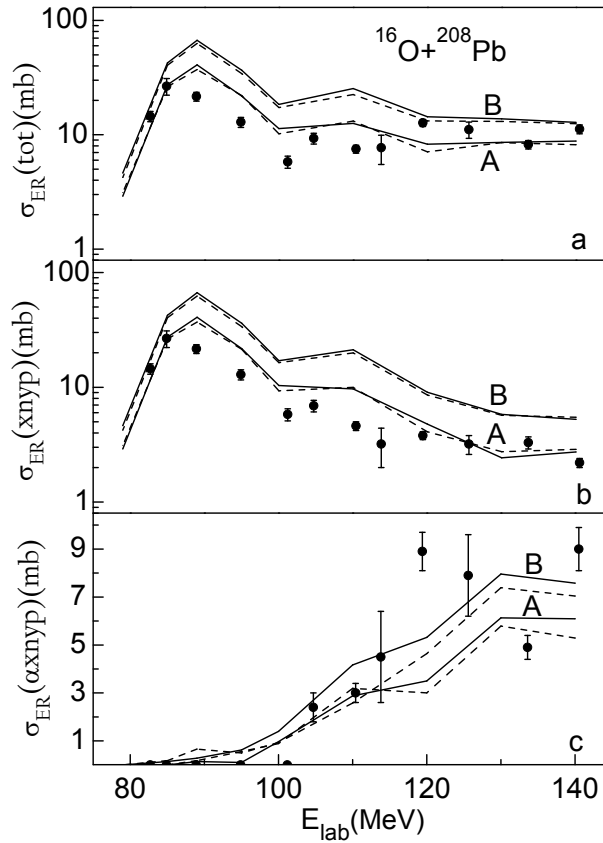
65

Figure 3.7: Evaporation residue cross sections. The total ER cross sections are plotted in the top (a) panel. The middle (b) and the lower (c) panels show the cross sections of evaporation residues formed in ($xnyp$) and ($\alpha xnyp$) channels, respectively. The experimental values (filled circles) are taken from [24]. The solid and dashed lines are statistical model calculations with and without spin dependence of frequencies, respectively. A and B denote results with $\beta = 1$ and 2 (both in $10^{21}s^{-1}$), respectively [108].

the spin dependence of frequencies as we find in the calculated values of pre-scission neutrons in Fig. 3.5 in the above. We further calculate the average number of α particles emitted by the evaporation residues. The experimental and the statistical model predictions are given in Fig. 3.8. From Fig. 3.7 and Fig. 3.8, we find that a value of 1 (in $10^{21}s^{-1}$) for β can account for all the ER related processes in a satisfactory manner.

We thus arrive at two values for β, both energy independent, in order to separately fit the neutron multiplicities and ER cross sections. Similar observations have been made earlier
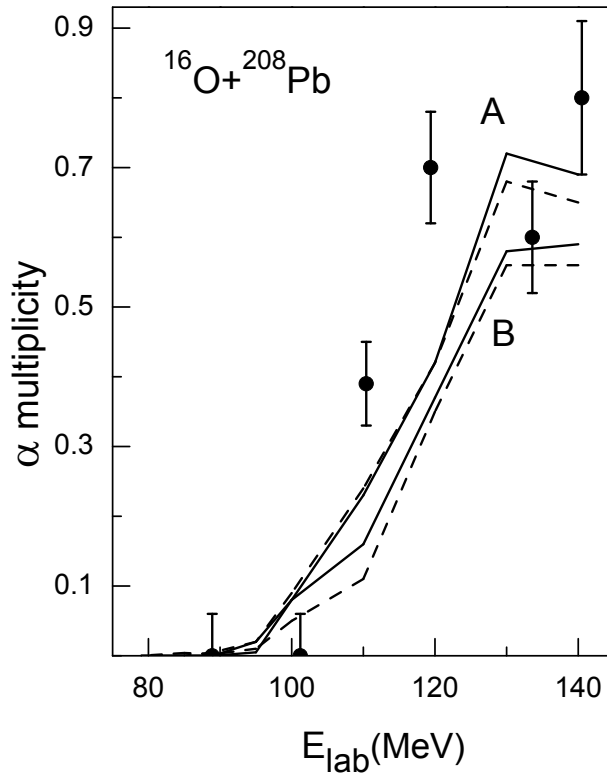
Figure 3.8: α multiplicities from evaporation residues. Experimental values are taken from [24] and the solid and dashed lines are statistical model calculations with and without spin dependence of frequencies, respectively. 'A' and 'B' denote results with $\beta = 1$ and 2 (both in $10^{21}s^{-1}$), respectively [108].

in both dynamical [160] and statistical [60] model calculations. In order to reproduce both n_{pre} multiplicities and ER cross sections, phenomenological form factors for the dissipation strength have been suggested where dissipation is weak at small deformations of the CN and becomes many times larger at large deformations [160]. Such choices are motivated by the facts that the ER cross sections essentially portray the pre-saddle fission dynamics whereas additional neutrons can be emitted during transition of the CN from the saddle configuration to the scission. It is however also possible that one of the reasons for a strong dissipation at large deformations is to account for the enhanced neutron emission from the neutron-rich neck region. This aspect however requires further investigations [161]. A shape-dependent dissipation has also been obtained in a microscopic derivation of one-body dissipation where

the chaotic nature of the single particle motion was considered [146] giving rise to a suppression of dissipation strength for small CN deformations.

3.5   Summary

In summary, we have investigated a specific aspect of the fission width due to Kramers, namely its spin dependence arising out of the change in the shape of the liquid drop model potential with angular momentum. The present work shows that the energy dependence of the dissipation strength extracted from fitting experimental data is substantially reduced when the change in shape of the fission barrier with increasing spin of a CN is properly taken into account. We thus conclude that this spin-dependent effect should be included in a statistical model analysis employing Kramers' modified fission width in order to deduce the correct strength and energy dependence of the phenomenological dissipation.

Chapter 4

Kramers' fission width for variable inertia

4.1 Introduction

As described in the first chapter, a dynamical model for fission of a hot compound nucleus was first proposed by Kramers [63] based on its analogy to the motion of a Brownian particle in a heat bath. In this model, the collective fission degrees of freedom represent the Brownian particle while the rest of the intrinsic degrees of freedom of the compound nucleus (CN) correspond to the heat bath. The dynamics of such a system is governed by the appropriate Langevin equations or equivalently by the corresponding Fokker-Planck equation. Kramers analytically solved the Fokker-Planck equation with a few simplifying assumptions and obtained the stationary width of fission. The detail derivation is given in the first chapter where, following the work of Kramers, parabolic shapes are considered for the nuclear potential at the ground state and at the saddle region and the inertia of the fissioning system is assumed to be shape independent and constant. The stationary width predicted by Kramers was found to be in reasonable agreement with the asymptotic fission width obtained from numerical solutions of the Fokker-Planck [45, 156, 157, 162, 163, 164, 165] and Langevin [105, 166, 167, 168, 169] equations in which harmonic oscillator potentials and constant inertia were used.

In the present chapter, we examine the applicability of Kramers' expression for stationary fission width for more realistic systems. Specifically, we use the finite range liquid drop model (FRLDM) potential [128, 129] and shape-dependent inertia. To this end, we first approximate the FRLDM potential with suitably defined harmonic oscillator potentials, as we have done in the previous chapter also, in order to make use of Kramers' expression for fission width. Since the centrifugal barrier changes the potential profile as the nuclear spin increases, the frequencies of the harmonic oscillator potentials approximating the FRLDM potential also develop a spin dependence [107, 108, 170]. Though the oscillator potentials are fitted to closely resemble the FRLDM potential, it is instructive to compare Kramers' fission width with that obtained from the numerical solution of Langevin equations where the full FRLDM potential is employed. Considering the width from the Langevin equations to represent the true fission width, this comparison enables us to confirm the validity of Kramers' expression for systems described by realistic potentials over the entire range of compound nuclear spin populated in a heavy ion induced fusion reaction. We next extend Kramers' formulation of stationary width in order to include the slow variation of the collective inertia with deformation. The Kramers' formula was generalized earlier [171] for variable inertia where a factor $\sqrt{m_g/m_s}$ was introduced in the expression for the fission width. The inertias at the ground state and at the saddle point are denoted respectively by m_g and m_s here. In a Langevin calculation with variable inertia, Karpov *et al.* [167], however, reported that Kramers' width (without the above mentioned factor) predicts the asymptotic fission width very accurately. We therefore address this issue here in some detail and show that the difference lies in different matching conditions. We draw our conclusions by comparing Kramers' predicted widths with the widths calculated from the Langevin equations.

Further, in the present chapter, we examine the applicability of Kramers' fission width when the variation of collective inertia is made very sharp but continuous. In the stochastic dynamical models of nuclear fission described by Langevin or Fokker-Planck equations, the collective kinetic energy of the CN expressed in terms of the speeds of the relevant collective coordinates contains an inertia term, which also depends on the collective coordinates. This collective inertia can be evaluated under suitable assumptions regarding the intrinsic nuclear motion. By considering the intrinsic nuclear motion as that of a classical irrotational and incompressible

fluid, the inertia can be calculated in the Werner-Wheeler approximation [71, 172] as described in Chapter 2. The inertia against slow shape distortion can also be obtained from the cranking model where nuclear single-particle states are considered [137]. Both these approaches predict a substantial increase of the collective inertia of a fissioning heavy nucleus as its shape evolves from the ground state to the saddle configuration. Inertia parameters in a dinuclear system have also been evaluated using linear response theory [69, 173]. In general, the inertia associated with a collective coordinate depends on the choice of the collective coordinate and the underlying microscopic motion.

The dissipation coefficient η is usually obtained by considering one- or two-body mechanisms of dissipation [67, 68, 70, 71, 138]. The shape dependencies of inertia and the dissipation coefficient from different models are found to be similar. As an illustration, the shape dependencies of the one-body dissipation coefficient (η) and the irrotational fluid inertia (m) are given in Chapter 2. Similar plots of η and m are shown in Fig. 4.1(top and middle panels, respectively) for the ^{224}Th nucleus; the bottom panel shows the reduced dissipation coefficient $\beta = \eta/m$. Evidently, both the dissipation coefficient and the inertia have strong shape dependencies of similar nature whereas their ratio, the reduced dissipation coefficient β, has a weaker shape dependence. A similar observation is also made for the reduced two-body dissipation coefficient (see Fig. 4 of Ref. [72]) where the ratio of two-body viscosity divided by the hydrodynamical inertia is found to be almost shape independent. As a first approximation, we therefore consider in the subsequent discussion the reduced dissipation coefficient β to be shape independent while allowing both the collective inertia m and the dissipation coefficient η to assume similar shape-dependent forms.

In the next section, we present the necessary steps taken to include the effect of slowly varying inertia in Kramers' expression for the stationary fission width. A comparison between the results from the Langevin calculation and Kramers' prediction is made in Sec. 4.3. Subsequently in Sec. 4.5, the necessary steps to include the effects of steeply varying inertia in the stationary fission width are given. The comparison between the Kramers' predicted widths thus obtained and the corresponding stationary widths from the Langevin simulations is given in Sec. 4.6. A summary of all the results is presented in the last section.
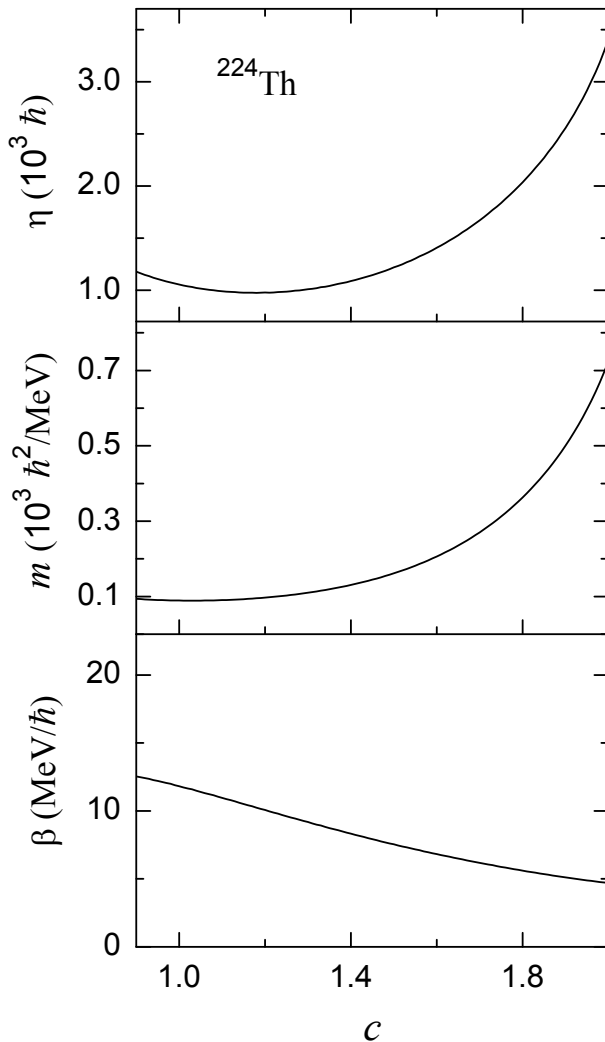
Figure 4.1: One-body dissipation coefficient η (top), irrotational fluid inertia m (middle), and reduced dissipation coefficient $\beta = \eta/m$ (bottom) as a function of dimensionless elongation parameter c for ^{2}24Th. The spherical shape and the scission configuration with zero neck radius correspond to $c = 1$ and $c = 2.09$, respectively [109].

4.2 Kramers' width for slowly varying inertia

To introduce a shape-dependent collective inertia in the analytical formulation of stationary fission width, we follow the work of Kramers [63] (discussed in Chapter 1) very closely. The Liouville equation describing the fission dynamics in one-dimensional classical phase space is

$$\frac{\partial \rho}{\partial t} + \frac{p}{m}\frac{\partial \rho}{\partial c} + \left\{ K - \frac{p^2}{2}\frac{\partial}{\partial c}\left(\frac{1}{m}\right) \right\}\frac{\partial \rho}{\partial p} = \beta p \frac{\partial \rho}{\partial p} + \beta \rho + m\beta T \frac{\partial^2 \rho}{\partial p^2}, \tag{4.1}$$

where ρ denotes the phase space density, c is the collective coordinate with p as its conjugate momentum and m is the collective inertia. The conservative and dissipative forces are given as, $K = -\partial V/\partial c$ and $-\beta p$ respectively where V is the collective potential and β is the dissipation coefficient. T represents the temperature of the CN. In what follows, we consider fission as a slow diffusion of Brownian particles across the fission barrier. When quasi-equilibrium is reached and a steady diffusion rate across the fission barrier has been established, Eq. (4.1) becomes

$$\frac{p}{m}\frac{\partial \rho}{\partial c} + \left\{ K - \frac{p^2}{2}\frac{\partial}{\partial c}\left(\frac{1}{m}\right) \right\}\frac{\partial \rho}{\partial p} = \beta p\frac{\partial \rho}{\partial p} + \beta \rho + m\beta T\frac{\partial^2 \rho}{\partial p^2}. \tag{4.2}$$

The calculations of potential and inertia are explained and plotted for ^{224}Th in the previous chapter. We make the Werner-Wheeler approximation [71] for incompressible and irrotational flow to calculate the collective inertia (Fig. 2.4). The FRLDM potential is obtained by double folding a Yukawa-plus-exponential potential with the nuclear density distribution using the parameters given by Sierk [128]. For convenience, the potential and inertia are shown again in Fig. 4.2.

In nuclear fission, a CN that is at a temperature significantly less than the height of the fission barrier mostly stays close to its ground-state configuration except for occasional excursions toward the saddle region when it has picked up sufficient kinetic energy from the thermal motion and which may eventually result in fission. Evidently, we do not consider transients that are fast nonequilibrium processes and happen for nuclei with vanishing fission barriers. Therefore, in the present picture, the Brownian particles are initially confined in the potential pocket at the ground-state configuration with a fission barrier V_B and for $V_B \gg T$, they can be assumed to be in a state of thermal equilibrium described by the Maxwell-Boltzmann distribution,

$$\rho = Ae^{-\left(\frac{p^2}{2m}+V\right)/T}, \tag{4.3}$$

where A is a normalization constant. We next seek a stationary solution of the Liouville equation which corresponds to a steady flow of the Brownian particles across the fission barrier. The desired solution should be of the form
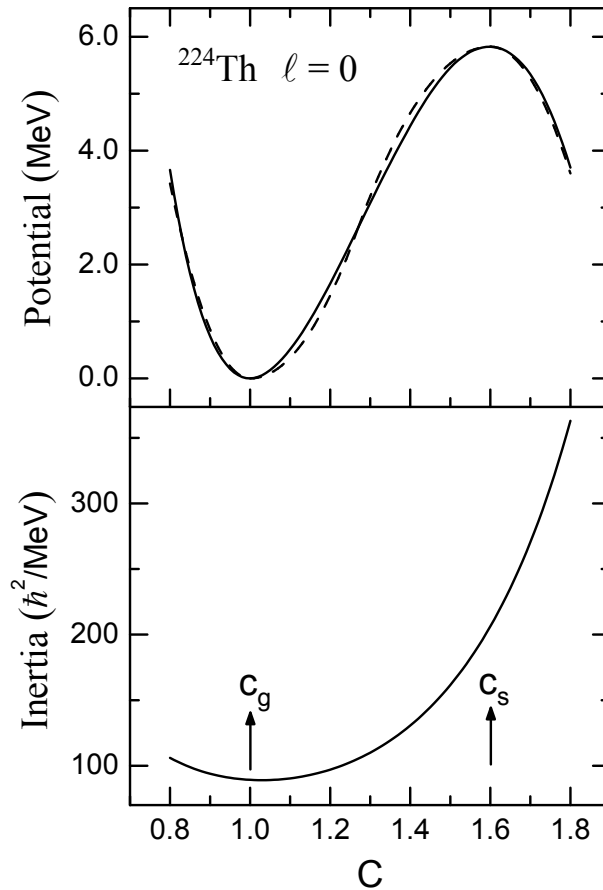
$$\rho = AF(c,p)e^{-\left(\frac{p^2}{2m}+V\right)/T} \tag{4.4}$$

Figure 4.2: FRLDM potential (gray-colored line) and the collective inertia (black line) of ^{2}24Th. The dotted line is obtained by fitting the FRLDM potential with two harmonic oscillator potentials (see section 3.1). The ground-state (c_g) and saddle (c_s) configurations are also marked [27].

such that $F(c, p)$ satisfies the boundary conditions

$$
\begin{aligned}
F(c, p) &\simeq 1 \quad \text{at} \quad c = c_g, \\
&\simeq 0 \quad \text{at} \quad c \gg c_s,
\end{aligned}
\tag{4.5}
$$

where c_g and c_s define the ground-state and the saddle deformations. The first boundary condition corresponds to a continuous change of both the potential and the inertia values with deformation. In this context, it may be pointed out that Hofmann *et al.* [171] considered discrete values of inertia for the saddle and ground-state configurations which resulted in the factor $\sqrt{m_g/m_s}$ in the stationary fission width expression. This factor, however, does not ap-

pear in the present work, since we consider a continuous variation of the inertia value.

Substituting Eq. (4.4) in the stationary Liouville equation we obtain

$$m\beta T\frac{\partial^2 F}{\partial p^2} = \frac{p}{m}\frac{\partial F}{\partial c} + \frac{\partial F}{\partial p}\left\{-\frac{\partial V}{\partial c} + \beta p - \frac{p^2}{2}\frac{\partial}{\partial c}\left(\frac{1}{m}\right)\right\}. \tag{4.6}$$

To assess the importance of the inertia derivative term in this equation, we estimate the magnitude of the term $\left|\frac{p^2}{2}\frac{\partial}{\partial c}\left(\frac{1}{m}\right)\right|$ with respect to βp in the neighborhood of the fission barrier. Considering the inertia values as given in Fig. 4.2 for ^{224}Th and a temperature of 2MeV, which gives the most probable momentum values, we find $\beta p > \left|\frac{p^2}{2}\frac{\partial}{\partial c}\left(\frac{1}{m}\right)\right|$ for $\beta > 0.1\text{MeV}/\hbar$. Since a conservative estimate of the magnitude of nuclear dissipation β is about 2MeV$/\hbar$ [105], we can neglect the inertia derivative term in Eq. (4.6). It may be pointed out here that though we neglect the inertia derivative term in Eq. (4.6) for F, the Boltzmann factor $\exp\left[-\left(p^2/2m + V\right)/T\right]$ of the density in Eq. (4.4) fully satisfies Eq. (4.2). This is the reason for not neglecting the inertia derivative term earlier in Eq. (4.2) for the full density function $\rho(c,p)$. In fact, we also retain the inertia derivative term in the Langevin equations, which we discuss in the next section.

Since we require the solution for F in the vicinity of the saddle point, we approximate the FRLDM potential in this region with a harmonic oscillator potential

$$V = V_B - \frac{1}{2}m_s\omega_s{}^2(c - c_s)^2, \tag{4.7}$$

where the frequency ω_s is obtained by fitting the FRLDM potential. Introduction of $X = c - c_s$ further reduces Eq. (4.6) to

$$m_s\beta T\frac{\partial^2 F}{\partial p^2} = \frac{p}{m_s}\frac{\partial F}{\partial X} + \frac{\partial F}{\partial p}\left(m_s\omega_s^2 X + \beta p\right). \tag{4.8}$$

Following Kramers [63], we next assume for F the form

$$F\left(X, p\right) = F\left(\zeta\right), \tag{4.9}$$

where $\zeta = p - aX$ and a is a constant. The value of a is subsequently fixed as follows. Substituting Eq. (4.9) for F in Eq. (4.8), we obtain

$$m_s\beta T\frac{d^2 F}{d\zeta^2} = -\left(\frac{a}{m_s} - \beta\right)\left\{p - \frac{m_s\omega_s{}^2}{\frac{a}{m_s} - \beta}X\right\}\frac{dF}{d\zeta}. \tag{4.10}$$

75

To have consistency between Eq. (4.10) and Eq. (4.9), we require

$$\frac{m_s \omega_s{}^2}{\frac{a}{m_s} - \beta} = a, \qquad (4.11)$$

which leads to

$$\frac{a}{m_s} - \beta = -\frac{\beta}{2} + \sqrt{\omega_s{}^2 + \frac{\beta^2}{4}}, \qquad (4.12)$$

where the positive root of a is chosen in order to satisfy the following boundary conditions: $F(X,p) \to 1$ for $X \to -\infty$ (assuming the ground state to be far on the left of the saddle point) and $F(X,p) \to 0$ for $X \to +\infty$. Equation (4.10) then becomes

$$m_s \beta T \frac{d^2 F}{d\zeta^2} = -\left(\frac{a}{m_s} - \beta\right)\zeta \frac{dF}{d\zeta}. \qquad (4.13)$$

The solution of Eq. (4.13) satisfying the above boundary conditions is

$$F(\zeta) = \frac{1}{m_s}\sqrt{\frac{(a - m_s\beta)}{2\pi\beta T}} \int_{-\infty}^{\zeta} e^{-\left(\frac{a}{m_s} - \beta\right)\zeta^2 / 2m_s\beta T} d\zeta. \qquad (4.14)$$

Substituting for F according to this equation in Eq. (4.4), the stationary density in the saddle region is finally obtained.

We next obtain the net flux or current across the saddle as

$$
\begin{aligned}
j &= \int_{-\infty}^{+\infty} \rho(X = 0, p)\frac{p}{m_s} dp \\
&= AT e^{-V_B/T}\sqrt{\frac{a - m_s\beta}{a}} \\
&= AT e^{-V_B/T}\left\{\sqrt{1 + \left(\frac{\beta}{2\omega_s}\right)^2} - \frac{\beta}{2\omega_s}\right\}. \qquad (4.15)
\end{aligned}
$$

The total number of particles in the potential pocket at the ground-state deformation is

$$n_g = \int_{-\infty}^{+\infty}\int_{-\infty}^{+\infty} \rho \, dc \, dp = \frac{2\pi AT}{\omega_g}, \qquad (4.16)$$

where we have approximated the FRLDM potential with the following harmonic oscillator potential near ground state,

$$V = \frac{1}{2}m_g \omega_g{}^2 (c - c_g)^2 \qquad (4.17)$$

76

in which the frequency ω_g is again obtained by fitting the FRLDM potential. The probability P of a Brownian particle crossing the fission barrier per unit time is then

$$P = \frac{j}{n_g} = \frac{\omega_g}{2\pi} e^{-V_B/T} \left\{ \sqrt{1 + \left(\frac{\beta}{2\omega_s}\right)^2} - \frac{\beta}{2\omega_s} \right\}. \tag{4.18}$$

It is immediately noticed that this expression is exactly the same as the one obtained by Kramers using a shape-independent collective inertia. Eq. (4.18), however, is obtained with different inertia values at the ground-state and saddle configurations, which consequently define the frequencies (ω_g and ω_s) in this equation. The fission width from Eq. (4.18) is

$$\Gamma = \hbar P = \frac{\hbar \omega_g}{2\pi} e^{-V_B/T} \left\{ \sqrt{1 + \left(\frac{\beta}{2\omega_s}\right)^2} - \frac{\beta}{2\omega_s} \right\}, \tag{4.19}$$

which we compare with the stationary width from Langevin equations in the following subsection.

4.3 Comparison with Langevin width for slowly varying inertia

Before we proceed to compare the fission widths from Langevin dynamics and Kramers' formula, we point out that the net flux leaving the potential pocket is calculated at different points in the two approaches, though both of them represent the time rate of fission. In a stochastic process such as nuclear fission, a fission trajectory can return to a more compact shape even after it crosses the saddle configuration due to the presence of the random force in the equations of motion. This back streaming is typical of Brownian motion and has been noted earlier by several authors [78, 97, 174]. The back streaming is described by the phase-space density for negative momentum values at the saddle point in Kramers' solution [Eq. (4.15)]. If one considers outward trajectories passing a larger coordinate value, the probability of returning approaches zero as the potential becomes steeper beyond the saddle point. In numerical simulations of the Langevin dynamics, the scission point is usually so chosen such that the strong Coulomb repulsion beyond the scission point makes the return of a trajectory highly unlikely after it crosses the scission point. The calculated outgoing flux of the Langevin trajectories

at the scission point then represents the net flux and hence corresponds to the net flux as defined in Kramers' approach. This feature is illustrated in Fig. 4.3, where fission trajectories
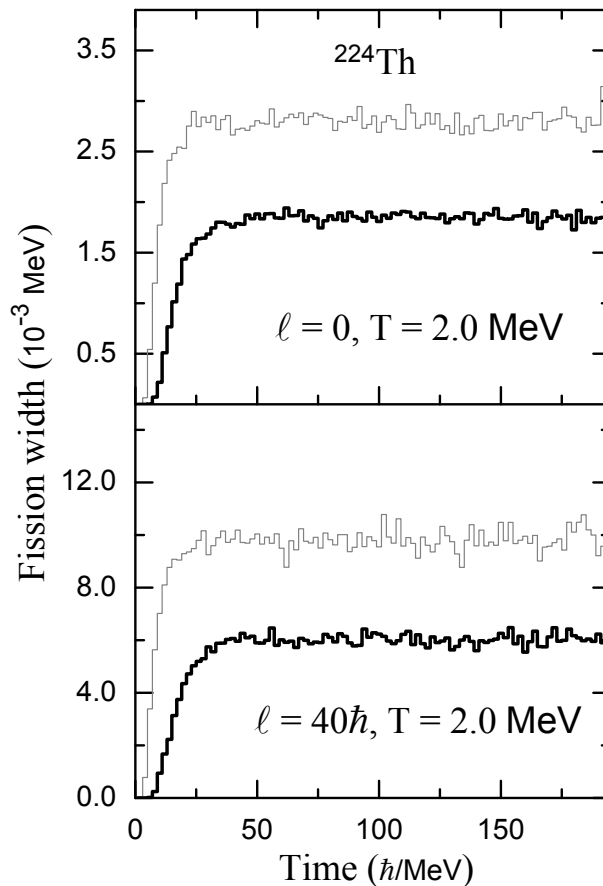

Figure 4.3: Time-dependent fission widths from Langevin equations. The thick black and thin gray lines represent the fission rates obtained at the scission point and at the saddle point, respectively [27].

crossing the saddle and the scission points are considered separately in order to obtain the time-dependent fission rates from the Langevin equations. Clearly, the stationary width calculated at the saddle point is higher than that obtained at the scission point, since the former does not include the back-streaming effects. In what follows, we therefore compare Kramers' width with the stationary widths from Langevin equations obtained at the scission configuration.

The fitted values of ω_g and ω_s are obtained both for a constant value of the collective inertia [108] (shown earlier in Fig. 3.4) as well as for its different values at c_g and c_s. Fig. 4.4
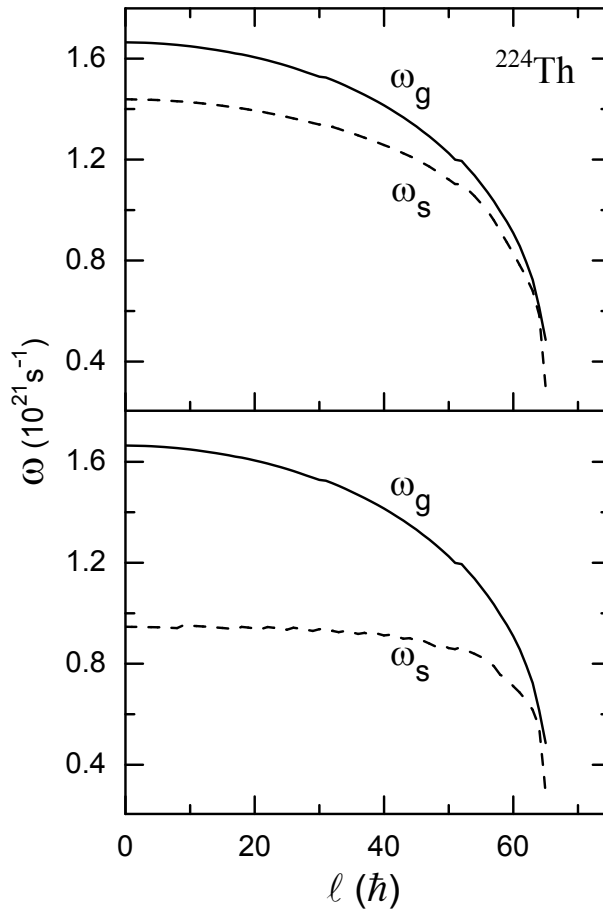
Figure 4.4: Compound nuclear spin (ℓ) dependence of the frequencies of the harmonic oscillator potentials approximating the rotating FRLDM potential at the ground state (ω_g) and at the saddle point (ω_s). In the upper panel, the values of inertia at the ground state and at the saddle are taken to be the same, while the Werner-Wheeler approximation to the inertia is used in the lower panel [27].

shows the compound nuclear spin dependence of the frequencies thus obtained. The Langevin equations [Eq. (2.37)] are next solved with a constant value of the inertia at all deformations. A constant value of $\beta = 5\text{MeV}/\hbar$ is used in all the calculations. The time-dependent fission widths from the Langevin dynamics are displayed in Fig. 4.5 for different values of spin of the CN ^{224}Th. The corresponding Kramers' widths are also shown in this figure. A close agreement between the stationary widths from Langevin dynamics and those from the Kramers' formula is observed for compound nuclear spin (ℓ) of 0 and $25\hbar$ while for $\ell = 50\hbar$, the Kramer' limit

Figure 4.5: Time-dependent fission widths (solid lines) from Langevin equations with no shape dependence of collective inertia. Results for different values of compound nuclear spin (ℓ) at a temperature (T) of 2 MeV are shown. The corresponding values of Kramers' width are indicated by the dashed lines [27].

underestimates the fission width by about 20%. The last discrepancy possibly reflects the fact that the condition $V_B \gg T$ required for validity of Kramers' limit is not met in this case, since the fission barrier is 1.64 MeV for $\ell = 50\hbar$, while the temperature of the CN is 2 MeV.

The Langevin equations are subsequently solved using shape-dependent values of the collective inertia, and the calculated time-dependent fission widths are shown in Fig. 4.6. Kramers' widths are calculated using the frequencies ω_g and ω_s, which are obtained using the local values
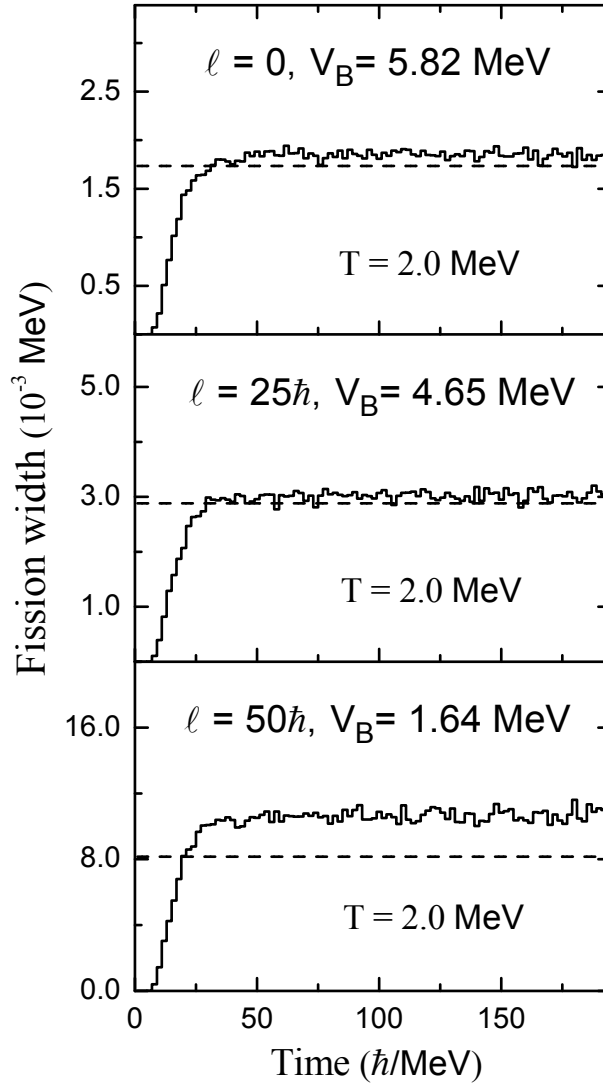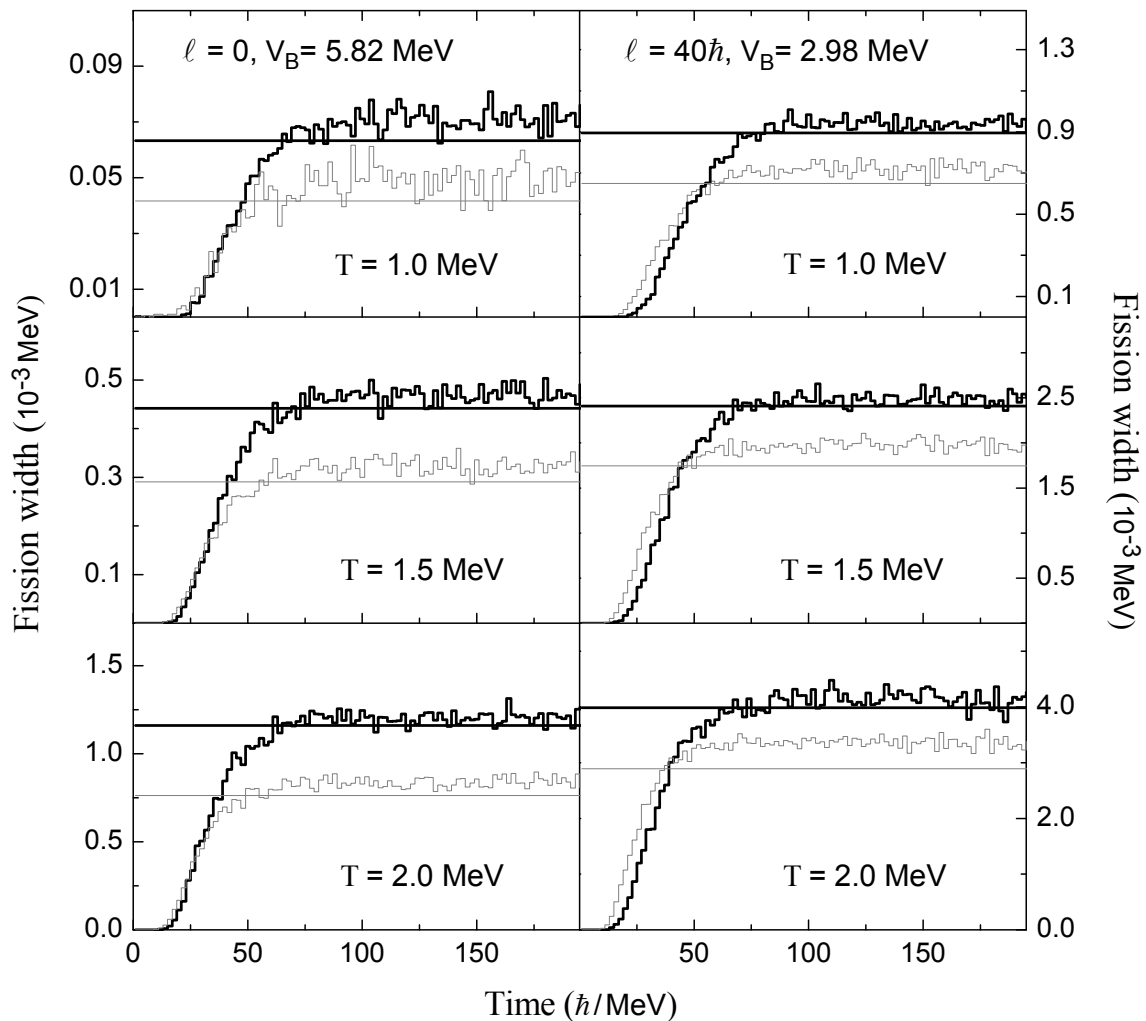

Figure 4.6: Time-dependent fission widths from Langevin equations with shape-dependent collective inertia. Results for different values of compound nuclear spin (ℓ) and temperatures (T) are shown. The shape dependence is continuous for the histograms in thick black lines. The corresponding values of Kramers' width [Eq. (4.19)] are indicated by the horizontal thick black lines. The histograms in thin gray lines are obtained with discrete values of inertia in the ground-state and saddle regions (see text) and the horizontal thin gray lines represent the corresponding stationary limits [Eq. (4.20)] [27].

of the collective inertia at c_g and c_s, respectively. Kramers' widths, also shown in Fig. 4.6, are found to be in excellent agreement with the stationary widths from the Langevin equations. It is thus demonstrated that Kramers' formula [Eq. (4.19)] gives the correct stationary fission width even when the collective inertia of the system has a shape dependence.

We now study the stationary fission rate with a different type of shape dependence of collective inertia. We assume that the value of the inertia remains constant at m_g for all deformations around the ground state and at an intermediate deformation between the ground state and the saddle point, its value abruptly increases to m_s and remains so for all deformations in the saddle region. Such a system was considered by Hofmann *et al.* [171] and a modified version of the Kramers' fission width was obtained as

$$\Gamma = \sqrt{\frac{m_g}{m_s}} \frac{\hbar\omega_g}{2\pi} e^{-V_B/T} \left\{ \sqrt{1 + \left(\frac{\beta}{2\omega_s}\right)^2} - \frac{\beta}{2\omega_s} \right\}. \tag{4.20}$$

We have solved the Langevin equations with the inertia defined as in the above and the calculated fission widths are also plotted in Fig. 4.6. The modified Kramers' width from Eq. (4.20) is also shown for each case. The modified Kramers' width is found to predict satisfactorily the stationary fission width from dynamic calculations. This result shows that the Kramers' width and the stationary width from Langevin dynamical calculation remain in close agreement even under very distinct prescriptions of shape dependence of inertia. We, however, consider the Kramers' width as given by Eq. (4.19) to be more appropriate for nuclear fission since it is obtained for realistic and smooth dependence of inertia on deformation. Therefore, a system with a deformation dependent slowly-varying collective inertia, the stationary fission width retains the form as was originally obtained by Kramers for constant inertia.

4.4 Connection between Kramers' and Bohr-Wheeler fission widths

In this section, we discuss the following expression for Kramers' width

$$\Gamma = \frac{\hbar\omega_g}{T} \Gamma_{BW} \left\{ \sqrt{1 + \left(\frac{\beta}{2\omega_s}\right)^2} - \frac{\beta}{2\omega_s} \right\}, \tag{4.21}$$

which is often used in the literature [60, 108, 166, 168]. Γ_{BW} in this equation is the transition-state fission width due to Bohr and Wheeler [8], and it is introduced in Eq. 4.21 in the following manner. According to Bohr and Wheeler, the transition-state fission width is given as (the detailed derivation can be found in Chapter 1)

$$\Gamma_{BW} = \frac{1}{2\pi\rho_g\left(E_i\right)} \int_0^{E_i-V_B} \rho_s\left(E_i - V_B - \epsilon\right) d\epsilon, \tag{4.22}$$

where ρ_g is the level density at the initial state (E_i, ℓ_i) and ρ_s is the level density at the saddle point. Under the condition $V_B/E_i << 1$ and assuming the level density parameter for the ground state and at the saddle point to be the same and further assuming a simplified form of the level density as $\rho(E) \sim \exp\left(2\sqrt{aE}\right)$, the Bohr-Wheeler width reduces to

$$\Gamma_{BW} = \frac{T}{2\pi}e^{-V_B/T}. \tag{4.23}$$

Substituting for Γ_{BW} from Eq. (4.23) in Eq. (4.21), the Kramers' width as given in Eq. (4.20) is obtained. In other words, Eq.(4.21) represents the fission width which was originally obtained by Kramers only when the approximate expression for Γ_{BW} is used. Consequently, it is not appropriate to obtain Kramers' width from Eq. (4.21) where the transition-state fission width Γ_{BW} is calculated from Eq. (4.22) using a shape-dependent level-density parameter. This observation follows from the fact that while the density of quantum mechanical microscopic states are explicitly taken into account in the work of Bohr and Wheeler [8], Kramers' work [63] essentially concerns the classical phase space of the collective motion. Since there is no scope of introducing any detailed information regarding density of states apart from the nuclear temperature in dissipative dynamical models of nuclear fission, Kramers' fission width cannot be connected to the Bohr-Wheeler expression where detailed density of states are employed. In fact, as shown in Fig. 1.3, the magnitude of the fission width obtained from the simplified version of the Bohr-Wheeler expression [Eq. (4.23)] differs substantially from that calculated using Eq. (4.22), particularly at high excitation energies where the dissipative effects are important, when the standard form of the shape-dependent level-density formula [see Eq. (1.5)] is used [27]. Therefore, the use of the Bohr-Wheeler fission width obtained with a shape-dependent level density in Eq. (4.21) does not correspond to dissipative dynamics, as envisaged in Kramers' formula. Further, it can introduce an energy dependence in the dissipation coefficient when Eq. (4.21) is employed to fit experimental data. This can be one of the contributing factors

leading to the inference of very large values of nuclear dissipation [105].

It may be worthwhile to discuss at this point the distinguishing features of the transition-state fission width Γ_K^{tr} which was obtained by Kramers (see Chapter 1) and is given as

$$\Gamma_K^{tr} = \frac{\hbar\omega_g}{2\pi} e^{-V_B/T}. \tag{4.24}$$

This width differs by a factor of $\hbar\omega_g/T$ from the approximate form of the Bohr-Wheeler fission width as given by Eq. (4.23). As described earlier, this difference arises because the accessible phase spaces are considered differently in the two approaches as we pointed out earlier. Strutinsky [85] introduced a phase-space factor in the Bohr-Wheeler transition-state fission width to account for the collective vibrations around the ground-state shape and obtained the same width as given in Eq. (4.24). It is important to recognize here that while the Bohr-Wheeler expressions [Eqs. (4.22) and (4.23)] represent the low-temperature limit ($T \ll \hbar\omega_g$) of fission width, Kramers' width [Eq. (4.20)] corresponds to fission at higher temperatures ($T \gg \hbar\omega_g$). At low temperatures of a CN, quantal treatment of the collective motion is required, since the energy available to the collective motion is also very small [172]. Consequently, in the low-temperature limit, the collective motion is restricted to one state, namely, the zero-point vibration. Therefore, the Bohr-Wheeler width based upon density of quantum mechanical intrinsic nuclear states alone represents the low temperature limit of nuclear fission width. On the other hand, the phase space for collective vibrations increases with increasing temperature, and the Strutinsky-corrected width thus becomes the high-temperature limit of transition-state fission width. At higher temperatures, however, the nuclear collective motion also turns out to be dissipative in nature. Thus Kramers' expression [Eq. (4.20)] should be considered as the high-temperature limit of the width of nuclear fission.

4.5   Kramers' fission width for sharply varying inertia

As discussed in the introduction of this chapter, the collective inertia associated with fission dynamics depends on the collective coordinates and different different microscopic models for inertia suggest a strong coordinate dependence. It is also shown in Sec. 4.3 that the Kramers' width remains valid when a slow variation of collective inertia is considered. The frequencies ω_g and ω_s in the Kramers' width for this case are defined in terms of m_g and m_s, the inertia values

at ground-state and saddle configurations respectively. The question therefore arises as to how the Kramers' expression for fission width is affected when the inertia value changes steeply but continuously from m_g to m_s and when the inertia derivative term in the Fokker-Planck equation is retained. We address this issue in some detail in the present subsection and investigate the limiting factors in extending the Kramers' approach to systems with a sharp increase of collective inertia between the ground state and the saddle. We draw our conclusions by comparing Kramers' predicted widths with the widths obtained from the Langevin equations, which represent the true fission width.

To study the effect of a sharp variation of inertia with deformation in the solution of the Liouville equation [Eq. (4.2)], we consider a model shape-dependent inertia where its value rises steeply at the deformation c_t , as illustrated in Fig. 4.7 (bottom panel) [109]. The inertia has a constant value m_g in the ground-state region up to a deformation of c_1. Beyond c_1, the inertia rises fast and attains a value m_s at c_2, which remains constant in the saddle region. The variation of inertia over the entire range is considered to be smooth and continuous. The potential V is given by two harmonic oscillator potentials defined by Eq. (4.17) and Eq. (4.7) near c_g and c_s, respectively. Now we proceed in a similar way as described for slowly varying inertia and seek a solution of Eq. (4.2) in the form

$$\rho = AF\left(c,p\right)e^{-\left(\frac{p^2}{2m(c)}+V\right)/T} \tag{4.25}$$

such that $F\left(c,p\right)$ satisfies the boundary conditions

$$
\begin{aligned}
F\left(c,p\right) &\simeq 1 && \text{at} \ \ c = c_g, \\
&\simeq 0 && \text{at} \ \ c \gg c_s.
\end{aligned} \tag{4.26}
$$

For a shape-dependent inertia of the type shown in Fig. 4.7 where the inertia increases fast at a deformation c_t, the change of inertia value takes place over a limited region of deformation space between c_1 and c_2. Consequently the inertia values are constant at the ground-state and at the saddle regions. The inertia derivative term in Eq. (4.6) is thus zero beyond c_2 and the solution for $F(c,p)$ in the saddle region is given by

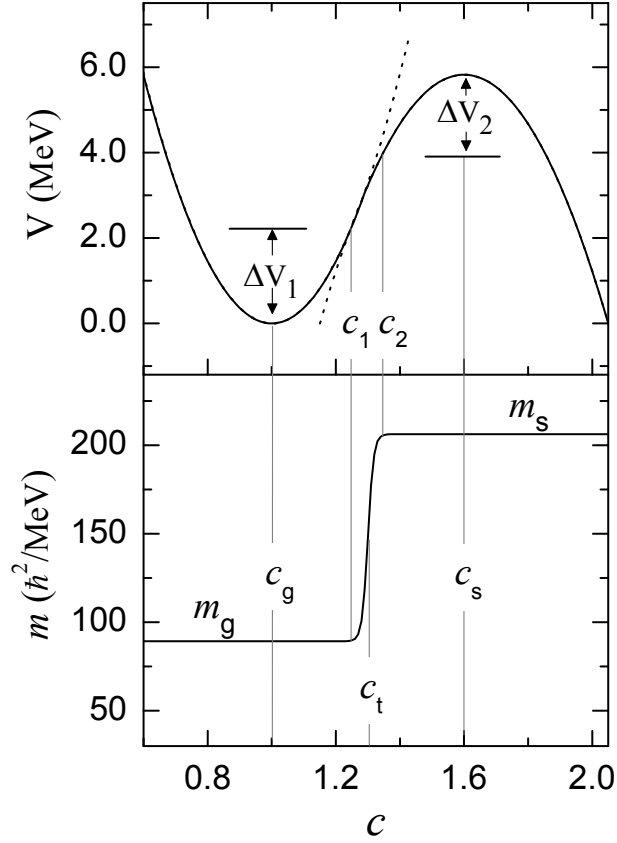$$F(c,p) = \sqrt{\frac{B}{\pi}} \int_{-\infty}^{\zeta_{max}} e^{-B\zeta^2} d\zeta, \tag{4.27}$$

Figure 4.7: Collective potential (top) for ^{224}Th and the sharply varying model inertia (bottom) where the sharp variation takes place at c_t between c_1 and c_2. $\triangle V_1$ is the potential difference between c_1 and c_g and $\triangle V_2$ is the same between c_2 and c_s [109].

where

$$B = \frac{1}{2m_s\beta T}\left(\frac{a}{m_s} - \beta\right) \tag{4.28}$$

with

$$\frac{a}{m_s} = \frac{\beta}{2} + \sqrt{\omega_s{}^2 + \frac{\beta^2}{4}} \tag{4.29}$$

and

$$\zeta_{max}(c, p) = p - a(c - c_s). \tag{4.30}$$

We first notice that for $c \gg c_s$, $F \to 0$ and the second boundary condition in Eq. (4.26) is satisfied. It can be further seen that the upper limit ζ_{max} of the integral in Eq. (4.27) evaluated

at $(c_2, \tilde{p})$, where $\tilde{p}$ is the magnitude of the most probable momentum $(\sqrt{2m_s T})$, is given as

$$\zeta_{max}(c_2, \tilde{p}) = \sqrt{2m_s T} \left\{ \sqrt{\frac{\triangle V_2}{T}(\gamma + \sqrt{1 + \gamma^2})} - 1 \right\}, \tag{4.31}$$

where $\triangle V_2$ is the potential difference between c_2 and c_s (Fig. 4.7). Consequently, the leading term in $B\zeta_{max}^2$ becomes $\frac{\triangle V_2}{2T}(1 + \sqrt{1 + 1/\gamma^2})$. Hence for $\triangle V_2/T > 1$, the integrand becomes much smaller than unity. This implies $F(c, p) \simeq 1$ even at $c = c_2$. Since the Maxwell-Boltzmann distribution

$$\rho = A e^{-\left(\frac{p^2}{2m(c)} + V\right)/T} \tag{4.32}$$

satisfies the full Liouville equation Eq. (4.2) including the inertia derivative term and it represents the density of particles confined in the potential pocket at the ground-state configuration, we find in the above that the Maxwell-Boltzmann distribution also remains a solution at $c = c_2$. The required solution for ρ thus takes the form,

$$\begin{aligned} \rho &= A e^{-\left(\frac{p^2}{2m(c)} + V\right)/T} & \text{up to} \quad c_2, \\ &= A F(c, p) e^{-\left(\frac{p^2}{2m(c)} + V\right)/T} & \text{beyond} \quad c_2. \end{aligned} \tag{4.33}$$

The above scenario essentially implies that the diffusion process affects the density distribution only beyond c_2. As obtained previously, the net flux or current across the saddle [Eq. (4.15)] and the total number of particles in the potential pocket at the ground-state deformation [Eq. (4.16)] are given respectively by

$$j = A T e^{-V_B/T} \left\{ \sqrt{1 + \left(\frac{\beta}{2\omega_s}\right)^2} - \frac{\beta}{2\omega_s} \right\} \tag{4.34}$$

and

$$n_g = \frac{2\pi A T}{\omega_g}, \tag{4.35}$$

where we make use of the fact that the inertia has a constant value of m_g near the ground-state deformations and it is also assumed that $\frac{\triangle V_1}{T} > 1$ where $\triangle V_1$ is the potential difference between c_g and c_1 (see Fig. 4.7). The fission width is obtained subsequently from the probability of a Brownian particle crossing the fission barrier per unit time and is given as,

$$\Gamma = \frac{\hbar \omega_g}{2\pi} e^{-V_B/T} \left\{ \sqrt{1 + \left(\frac{\beta}{2\omega_s}\right)^2} - \frac{\beta}{2\omega_s} \right\}. \tag{4.36}$$

87

It is immediately noticed that this expression is similar to the one that was obtained by Kramers using a shape-independent collective inertia. This equation however is obtained [109] with a strong shape dependence in the collective inertia resulting in different inertia values at the ground-state and saddle configurations and which, in turn, define the frequencies (ω_g and ω_s) in this equation.

4.6 Comparison with Langevin width for sharply varying inertia

We now compare the Kramers' fission width obtained for sharply varying inertia with the corresponding stationary fission width from Langevin dynamical calculations. ^{224}Th is considered as the CN to perform the calculations for both underdamped ($\beta/2\omega_s = 0.38 < 1$) and overdamped ($\beta/2\omega_s = 7.55 > 1$) motions with $\beta = 0.4\text{MeV}/\hbar$ and $8\text{MeV}/\hbar$, respectively. The β values thus chosen cover the range of dissipation strengths obtained from fitting experimental data [72]. We first compare the dynamical fission widths from Langevin equations with the Kramers' width as given by Eq. (4.36). Figure 4.8 shows the comparison where results for both underdamped and overdamped motions are plotted. The transition point c_t is chosen as the mid-point between c_g and c_s for the Langevin dynamical calculations. Γ_{gs} represents the Kramers' fission width when the inertia values at c_g and c_s are different as considered in Eq. (4.36). A close agreement between the stationary widths from Langevin equations and Γ_{gs} is observed in Fig. 4.8 for both the underdamped and overdamped fission. Since the assumptions regarding potential variation ($\triangle V_{1,2} > T$) are reasonably met for the cases considered here, the agreement demonstrates that Eq. (4.36) gives the fission width correctly when extended for a steep shape dependence of inertia.

It is of interest to note here that, in the limit of strong dissipation when $\beta/2\omega_s \gg 1$, Kramers' fission width [Eq. (4.36)] for systems with shape-dependent inertia and dissipation coefficient becomes

$$\Gamma = \frac{\hbar}{2\pi} \frac{1}{\sqrt{\beta_g \beta_s}} \sqrt{\left| \frac{\partial^2 V}{\partial c^2} \right|_g} \sqrt{\left| \frac{\partial^2 V}{\partial c^2} \right|_s} e^{-V_B/T}, \qquad (4.37)$$
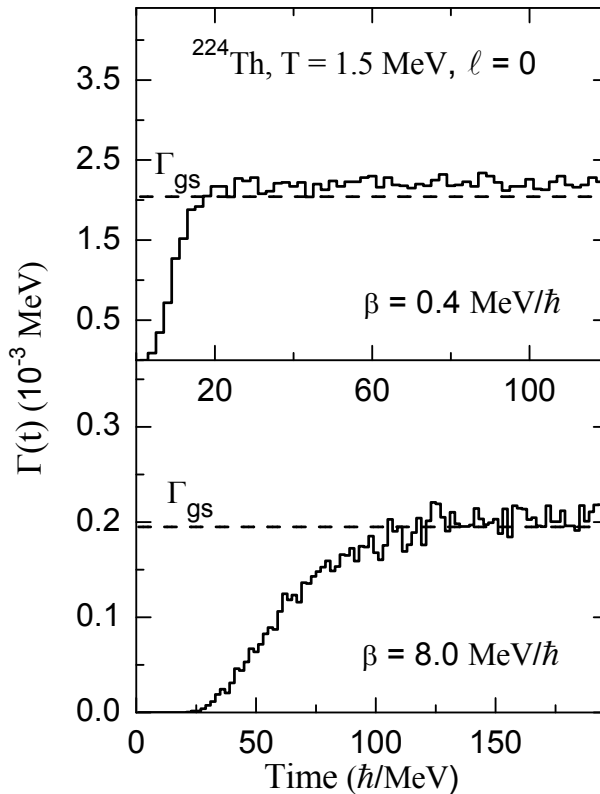
Figure 4.8: Time-dependent Langevin width (solid line) for sharply varying inertia with $c_t =$ 1.3. Γ_{gs} (dashed line) represents the fission width with different values of inertia at c_g and c_s as considered in Eq. (4.36). The top and bottom panels, respectively, show results for underdamped and overdamped fission [109].

where $(\frac{\partial^2 V}{\partial c^2})_g$ and $(\frac{\partial^2 V}{\partial c^2})_s$ are the potential curvatures at the ground-state and at the saddle configurations, respectively. The dissipation coefficients at the ground state and at the saddle are denoted by β_g and β_s, respectively. Equation 4.37 is similar to the expression for fission width [72] that one obtains in the strong friction limit from the Smoluchowski equation. The shape-independent dissipation coefficient β that appears in the fission width from the Smoluchowski equation is however replaced by $\sqrt{\beta_g \beta_s}$, the geometric mean of β_g and β_s, in Eq. (4.36).

We next perform Langevin dynamical calculations with shape-dependent inertias in which the steep rise in the inertia value takes place at different points. Figure 4.9 shows the dependence of the stationary fission width (Γ_L) from Langevin equations on the location of the transition
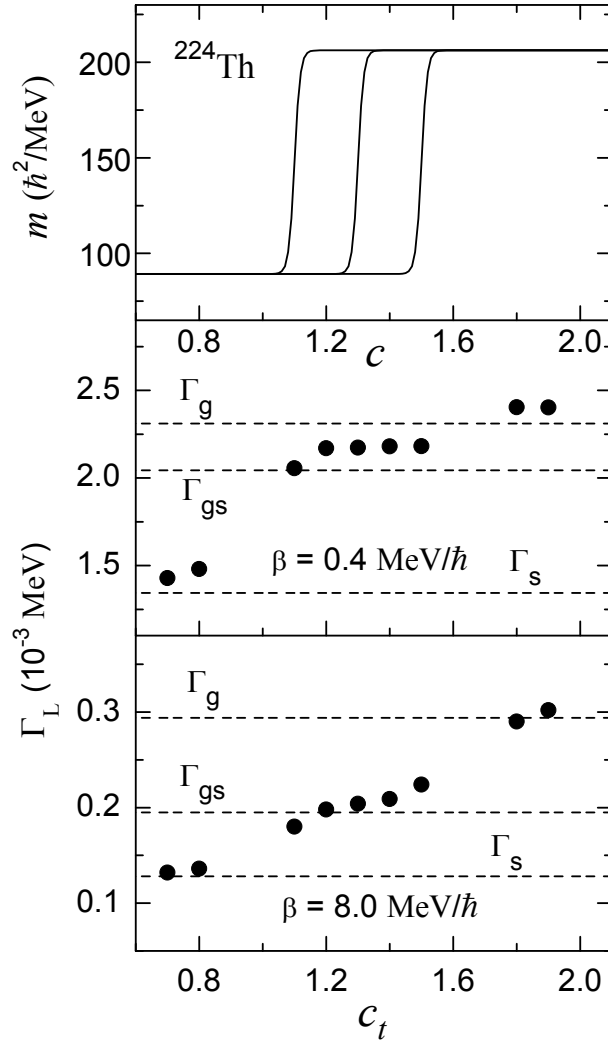
Figure 4.9: Sharply varying inertia for different values of c_t (top panel). Middle and bottom panels, respectively, show results for underdamped and overdamped fission. In the lower two panels, solid circles represent stationary Langevin width (Γ_L) plotted as a function of c_t . Γ_{gs} represents the fission width with different values of inertia at c_g and c_s as considered in Eq. (4.36). Γ_g and Γ_s denote the widths obtained from Eq. (3.1) with shape-independent constant values of inertia, m_g and m_s, respectively [109].

point c_t. Results for both underdamped and overdamped fission widths are shown in this figure. The Kramers' widths obtained with shape-independent inertia values are also shown in this figure. Here Γ_g is obtained with a shape-independent constant value of m_g while Γ_s is similarly defined with m_s. We first observe in Fig. 4.9 that Γ_L is very close to Γgs for

c_t values near the mid-point between ground-state and saddle configurations, confirming the applicability of Eq. (4.36) in this region. However, as the transition point moves closer to the ground-state deformation, Eq. (4.16) for n_g increasingly starts losing its validity. Similarly, when c_t is shifted toward c_s, the solution for ρ as given by Eq. (4.33) does not remain accurate. This essentially reflects the fact that most part of the Langevin dynamics takes place with inertia value at the saddle when $c_t < c_g$ and therefore Γ_L approaches Γ_s here. Similarly, the Browninan particles move mostly with ground-state inertia for $c_t > c_s$ and Γ_L is close to Γ_g in this region. Therefore, we have expanded the domain of validity of Kramers' fission width formula by including a steep variation of collective inertia with deformation.

4.7 Summary

In the preceding sections, we considered the applicability of Kramers' formula to the stationary fission width of a CN that is described by a realistic collective potential and a shape-dependent collective inertia. It is shown that for a system with a deformation-dependent collective inertia, the stationary fission width retains the form as originally obtained by Kramers for constant inertia. The accuracy of the various approximations in deriving the above fission width is tested by comparing its values with the stationary fission widths obtained by solving the Langevin equations. Both approaches are found to be in excellent agreement with each other. The present work thus extends the applicability of Kramers' formula for stationary fission width to more realistic systems.

Further, we have expanded the domain of validity of Kramers' fission width formula by including a steep variation of collective inertia with deformation in the Brownian motion. Comparison with numerical simulations from the corresponding Langevin equations confirms the adequacy of the extended formula and also demonstrates its region of validity and the consequences of the limiting conditions.

We also compare the strength of the statistical-model fission width obtained under different simplifying assumptions and point out the constraints in interpreting Kramers' width in terms of the statistical-model fission width of Bohr and Wheeler.

Chapter 5

Role of shape dependent dissipation

5.1 Introduction

Experimental and theoretical studies of heavy-ion-induced fusion-fission reactions at beam energies above Coulomb barriers have made significant contributions to the understanding of nuclear collective dynamics at high excitation energies in recent years. In particular, careful analysis of experimental data have established that the fission dynamics of a hot compound nucleus (CN) is dissipative in nature. Consequently, fission has become a useful probe to study the dissipative properties of the nuclear bulk. The detailed discussion on this topic is given in Chapter 1.

As described earlier in many occasions, Kramers' fission width can be obtained as

$$\Gamma = \frac{\hbar\omega_g}{2\pi}e^{-V_B/T}\left\{\sqrt{1+\left(\frac{\beta}{2\omega_s}\right)^2} - \frac{\beta}{2\omega_s}\right\}, \tag{5.1}$$

considering fission as diffusion of a Brownian particle across the fission barrier (V_B) placed in a hot and viscous fluid bath of temperature T and reduced dissipation coefficient β. The frequencies of the harmonic oscillator potentials describing the nuclear potential at the ground-state and the saddle configurations are ω_g and ω_s, respectively. Equation (5.1) was obtained [27] assuming the reduced dissipation coefficient β to be shape independent and constant for all deformations of the nucleus. Subsequently, the aforementioned stationary fission width predicted by Kramers was found to be in reasonable agreement with the asymptotic fission width

obtained from numerical solutions of the Fokker-Planck [45, 156, 157, 162, 163, 164, 165] and Langevin [105, 166, 167, 168, 169] equations where shape-independent and constant values of dissipation were used. Kramers' fission width is extensively used in statistical model calculation for decay of CN. The coefficient β is often treated as a free parameter to fit experimental data. Efforts are also continuing to improve the modeling of the fission process to extract more reliable values of the dissipation coefficient [27, 105, 106].

It was first reported by Fröbrich *et al.* [160] that the experimental data on pre-scission neutron multiplicity and fission cross section cannot be fitted by the same strength of the reduced dissipation in Langevin dynamical calculations. While a smaller value of β can account for fission excitation function, a larger value of β is required to describe the pre-scission multiplicity data. A shape-dependent nuclear dissipation was found necessary to simultaneously fit the pre-scission neutron multiplicity and fission cross-section data [78, 160]. From considerations of chaos in single-particle motion within the nuclear volume, shape dependence of a similar nature is also predicted for one-body dissipation, considered to be mainly responsible for damping of nuclear motion [98, 147]. A smaller dissipation strength in the presaddle region and a larger dissipation strength in the postsaddle region is found necessary in subsequent applications of Langevin equations for dynamics of fission [175, 176].

Shape-dependent dissipation is also introduced in statistical model calculation for the decay of a CN, in the following manner [59, 60, 108, 177]. One considers two dissipation strengths here: a smaller one (β_{in}) operating within the saddlepoint region and a larger one (β_{out}) effective outside the saddle point. In a statistical model calculation of nuclear fission, it is assumed that the fission width is given by Γ_K^{in} [Γ_K in Eq. (5.1) with β_{in}]. For a fission event, β_{out} is subsequently used to calculate the saddle-to-scission transition time during which further neutron evaporation can take place. However, the assumption that the fission width is given by Γ_K^{in} requires close scrutiny, as we are considering a shape-dependent dissipation here, while Kramers' width was originally obtained assuming a shape-independent dissipation.

In the present chapter, we examine [110] the validity of determining the fission width from β_{in} alone when a shape-dependent dissipation is considered. To this end, we compare Γ_K^{in}

93

with stationary widths from Langevin dynamical model calculations, considering the latter to represent the true fission width. We also compare the prescission neutron multiplicities (n_{pre}) and evaporation residue (ER) cross sections obtained from the statistical model with a shape-dependent dissipation with those obtained from the corresponding Langevin equations. In the next section, comparison between the Kramers' fission width and the corresponding Langevin dynamical width is described for the shape-dependent dissipation. For the present purpose, dynamical model calculations are done by including particle and γ evaporation channels. A brief account of this calculation procedure is given in Sec. 5.3. The results of the dynamical model calculations are compared with the corresponding statistical model results in Sec. 5.4. Finally, we summarize the results in Sec. 5.5.
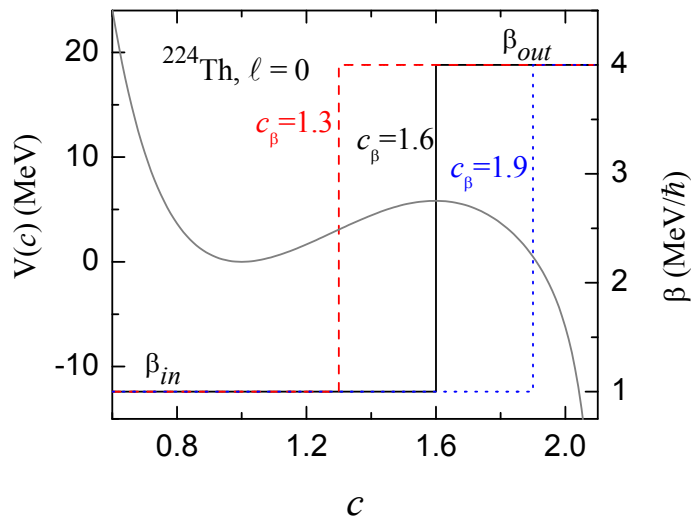

Figure 5.1: Collective potential and shape-dependent reduced dissipation (β) for ^{224}Th. Different forms of β corresponding to different values of c_β are shown [110].

5.2 Comparison between Kramers' and Langevin dynamical fission widths

We choose the CN ^{224}Th for the present calculation and solve the one-dimensional Langevin equations [110]. Figure 5.1 shows the collective potential for ^{224}Th along with the shape-dependent dissipation coefficients used in the Langevin calculations. Denoting the elongation

at which the dissipation changes its strength from β_{in} to β_{out} by c_β, the Langevin equations are solved for different values of c_β. Figure 5.2 shows the time-dependent fission widths from the
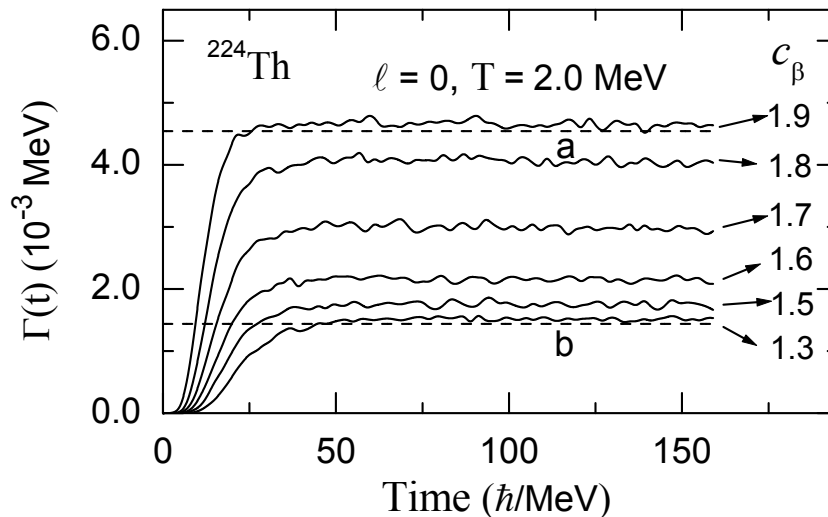

Figure 5.2: Time-dependent fission rates from Langevin equations for different values of c_β. Values of Kramers' fission width (dashed lines) Γ_K^{in} and Γ_K^{out} are also labeled a and b, respectively [110].

Langevin equations for different values of c_β. The values of Kramers' fission widths Γ_K^{in} and Γ_K^{out} obtained with β_{in} and β_{out}, respectively, in Eq. (3.1) are also shown in this figure. The values of stationary fission widths Γ_L from Langevin dynamics are subsequently plotted as a function of c_β in Fig. 5.3 . It is immediately noted from Fig. 5.3 that for $c_\beta = 1.6$, which corresponds to the elongation at saddle, the stationary fission width (Γ_L) from Langevin equations is substantially smaller than the Γ_K^{in} obtained with a constant value of β_{in}. This observation is contrary to the interpretation made in statistical model calculations employing shape-dependent dissipations, that Γ_K^{in} accounts for the fission rate. We further note in Fig. 5.3 that as c_β is shifted outward beyond the saddle point, Γ_L approaches Γ_K^{in}. When c_β is moved inward, Γ_L approaches Γ_K^{out}.

The preceding observations are made when we choose $\beta_{out} \gg \beta_{in}$ in accordance with the applications of shape-dependent dissipation in statistical model calculations [59, 60, 108, 177]. However, when the value of β_{out} is reduced toward β_{in}, Fig. 5.4 shows that the stationary fission width from Langevin dynamics gets closer to Kramers' width for β_{in}, as expected.
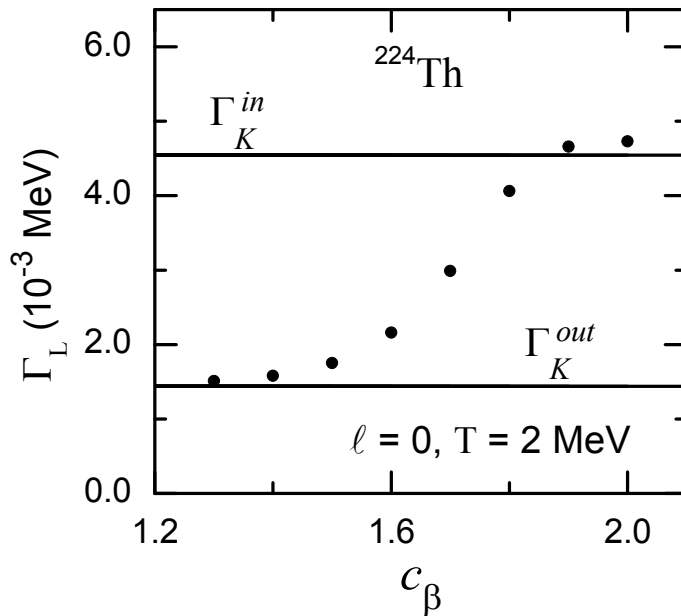
Figure 5.3: Stationary values (Γ_L) of fission rate from Langevin equations as a function of c_β (filled circles). Kramers' widths Γ_K^{in} and Γ_K^{out} are shown by horizontal lines [110].

To understand the foregoing observations qualitatively, we proceed as follows. Kramers' width (Γ_K) [Eq. (3.1)] represents the steady-state diffusion rate of phase-space density (ρ) of Brownian particles across the fission barrier satisfying the appropriate Liouville equation, and the net flux or current across the saddle is [Eq. (4.15)]

$$j = \int_{-\infty}^{+\infty} \rho(c = c_s, p) \frac{p}{m_s} dp,$$

where both the outward (positive-p) and the inward (negative-p) fluxes are considered to obtain the net flux [63]. In terms of Langevin fission trajectories, while the outward flux is controlled by the dissipation within the saddle, the inward flux (from outside to inside the saddle) or the back-streaming trajectories experience the dissipation outside the saddle. Hence the net flux (j) depends on both the "pre-saddle" and the "post-saddle" dissipation strengths, and the fission width is no longer determined by the pre-saddle dynamics alone. The stochastic nature of nuclear fission makes it dependent on the fission dynamics around the saddle, the extent of which is illustrated in Fig. 5.3.
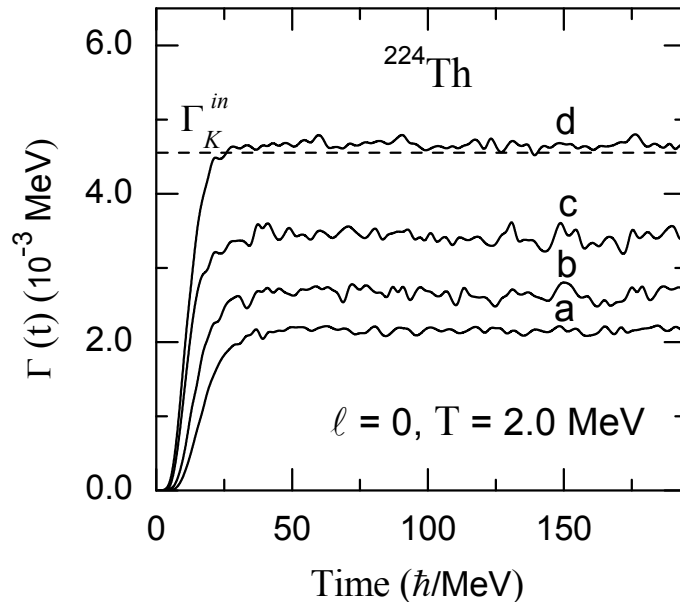
96

Figure 5.4: Time-dependent Langevin fission widths, $a-d$, with $c_\beta = 1.6$, $\beta_{in} = 1.0$ MeV/$\hbar$, and $\beta_{out} = 4.0$, 3.0, 2.0, and 1.0 MeV/$\hbar$, respectively. Γ_K^{in} is shown by the horizontal dashed line [110].

5.3 Langevin dynamical model including evaporation channels

The one-dimensional Langevin dynamical calculation for the fission width is demonstrated in Chapter 2. For the present purpose, we need to include the evaporations of neutrons, protons, α particles, and statistical γ-rays along with the fission channel. Earlier, the statistical model calculation including the evaporation channels is described in Sec. 3.3, where the fission width can be calculated either from the Bohr-Wheeler formula [Eq. (1.4)] or the Kramers' formula [Eq. 5.1]. A Monte-Carlo sampling is then performed at each time step to decide over the all possible decay modes. On the other hand, in a dynamical trajectory calculation, the shape evolution of an CN nuclear is followed with time and the evaporation channels are sampled at the end of each time step of this dynamical evolution. More specifically, two Monte-Carlo samplings have been performed, first, to decide whether any evaporation is happening or not and if it occurs then a second one to select a particular decay mode out of neutrons, protons, α particles, and γ evaporation channels. During the dynamical evolution, if fission does not
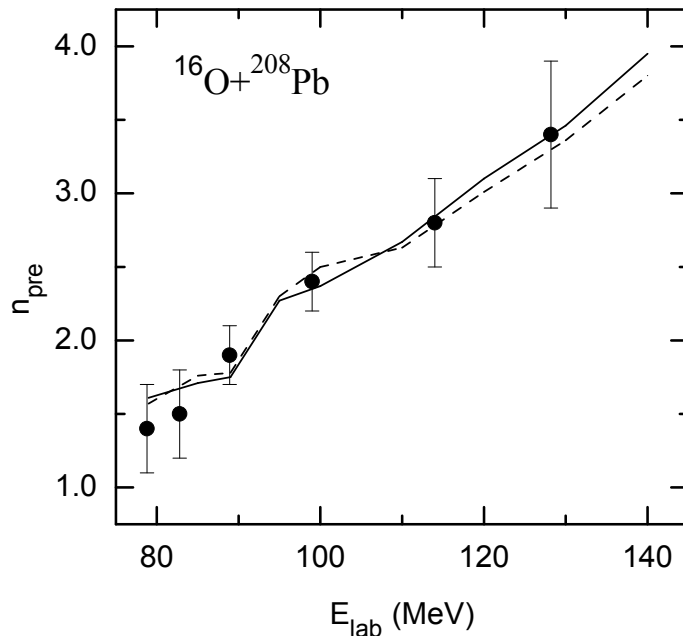
Figure 5.5: Pre-scission neutron multiplicities from statistical (dashed line) and dynamical (solid line) model calculations with a shape-independent dissipation $\beta = 3.5$ MeV/$\hbar$. Experimental points are from Ref. [54]

occur within a time which is sufficiently long so that the fission width reaches a stationary value, then the decay process is shifted to a statistical model calculation where the fission width is now either calculated from the Kramers' formula or interpolated from pre-calculated Langevin dynamical widths. This type of calculation is known as combined dynamical and statistical model (CDSM). The dynamical trajectory calculations including particle and γ evaporations are very much time consuming. Therefore, in CDSM the decay algorithm is followed with the statistical model code as soon as the fission width reaches the stationary value. Usually, the Kramers' fission width is used in the statistical model part [78, 99]. However, the applicability of Kramers' width is the main issue in the present calculation and hence we use the interpolated values of Langevin fission width computed initially for different combinations of compound nuclear spin and temperature [110]. An elaborate discussion on the CDSM code is given in Appendix B.

5.4 Comparison between statistical and dynamical model results

We now compare the pre-scission neutron multiplicities (n_{pre}) and ER cross sections obtained from statistical model calculation of compound nuclear decay with those from Langevin dy-
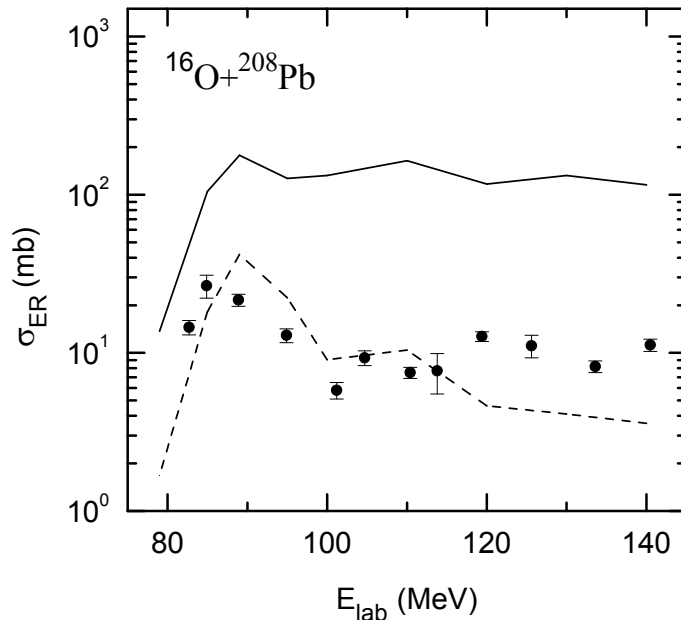

Figure 5.6: Evaporation residue cross sections from statistical (dashed line) and dynamical (solid line) model calculations for a shape-dependent dissipation with $\beta_{in} = 1.5$ MeV/$\hbar$ and $\beta_{out} = 15$ MeV/$\hbar$. Experimental points are from Ref. [24].

namical model calculation. Evaporation of neutrons, protons, α particles, and statistical γ-rays are considered along with the fission channel in both the calculations. While the particle and the γ emission widths used in both approaches are obtained from the Weisskopf formula [78], the fission width for the statistical model calculation is taken as Γ_K^{in}. We first consider the results obtained with a shape-independent strength of dissipation. Figure 5.5 shows the statistical and dynamical model predictions of n_{pre} excitation function calculated for the system ^{16}O+^{208}Pb along with the experimental data [54]. The dissipation strength is obtained here by fitting the data. A close agreement between the results from the two calculations is observed here, which reflects the validity of Kramers' width for shape-independent dissipation as demonstrated in
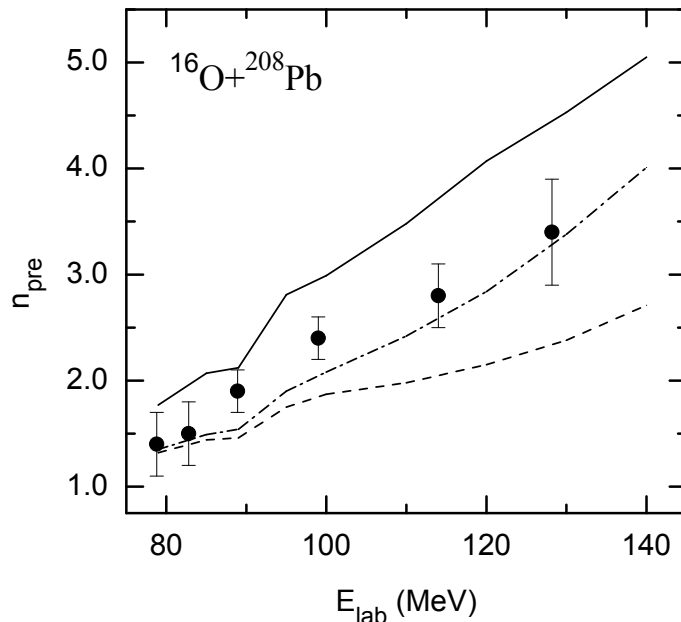
Figure 5.7: Pre-scission neutron multiplicities from statistical and dynamical model calculations for a shape-dependent dissipation with $\beta_{in} = 1.5$ MeV/$\hbar$ and $\beta_{out} = 15$ MeV/$\hbar$. Dash-dotted and dashed lines represent statistical model calculation results with and without the saddle-to-scission neutrons, respectively. Langevin dynamical results are shown by the solid line. Experimental points are from Ref. [54].

Fig. 5.4.

We next perform statistical and Langevin dynamical model calculations where a shape-dependent dissipation is used. In the statistical model calculation, Γ_K^{in} is used as the fission width, while β_{out} is used to calculate the saddle-to-scission transition time given by Eq. (3.7). Additional neutrons are allowed to evaporate during this period [60]. The pre-saddle dissipation strength β_{in} and hence Γ_K^{in} are first obtained by fitting the experimental ER excitation function. The strength of β_{out} is subsequently adjusted to reproduce the experimental n_{pre} excitation function. Excitation functions for n_{pre} and ER are also obtained from the Langevin dynamical calculation using a shape-dependent dissipation given by the preceding values of β_{in} and β_{out}. Figure 5.6 shows the calculated ER cross sections along with the experimental data. The dynamical model results are considerably larger than the statistical model predictions. This shows that the post-saddle dynamics controlled by β_{out} plays an important role in determining

100

the fission probability of a CN, which in turn demonstrates the inadequacy of using only the β_{in} value in Eq. (3.1) to obtain the fission width. Figure 5.7 shows the calculated n_{pre} multiplicities and the experimental values. The statistical model results without including the additional saddle-to-scission neutrons are also given in this figure. The dynamical model predictions, however, turn out to be much higher than the statistical model results. Because the Langevin equations give the true description of dynamics of fission, the preceding differences between statistical and dynamical model results show that for shape-dependent dissipation, the assumptions of β_{in} accounting for the fission width and β_{out} controlling the saddle-to-scission neutrons are not consistent with the dynamical model results. Consequently, the fitted values of β_{in} and β_{out} from statistical model calculations when used in dynamical model calculations give rise to substantially different values of n_{pre} and ER cross sections.

5.5 Summary

We therefore conclude that due caution should be exercised when using Kramers' expression for fission width for systems with shape-dependent dissipation. In such cases, the Kramers' width obtained with a pre-saddle dissipation strength does not represent the true fission width, and consequently, the "pre-saddle dissipation strength" fitted to reproduce the experimental data in statistical model calculations does not represent the true strength of pre-saddle dissipation.

Chapter 6

Two-dimensional (2D) Langevin dynamical model for fission fragment mass distribution (FFMD)

6.1   Introduction

Nuclear fission is a unique process in which the shape of a nearly equilibrated system evolves continuously till it splits into two fragments. The probability of finding a compound nucleus (CN) separating into fragments with given masses depends upon both the statistical and the dynamical properties of the fissioning system. As described in Chapter 1, Fong [31, 35] first developed a statistical theory for the FFMD where it was assumed that a complete equilibration among all the degrees of freedom is established in the fissioning nucleus at every instant and the relative probability of a given mass partition is proportional to the density of quantum states at the scission point. The statistical theory successfully explained the mass yield in thermal-neutron-induced fission. Nix and Swiatecki [42] subsequently pointed out that the saddle configuration is a better static point than the scission one since the latter cannot be defined in a unique manner. They assumed an equilibrated distribution at the saddle configuration and the transition from the saddle to the scission was treated dynamically without considering any dissipation. This approach gave a reasonable agreement with experimentally measured fission fragment mass variances for α-particle-induced fission of CN up to mass number A=213

[178]. A dissipative force was subsequently included in the saddle-to-scission motion [71, 154]. In order to explain the mass variances observed in the fission of heavier CN, the importance of stochastic dynamics during the saddle-to-scission transition was latter established by Adeev and Pashkevich [153]. In recent years, fission fragment mass and kinetic energy distributions have been calculated by several authors from full stochastic dynamical treatments of the evolution of a hot CN from ground state to scission configuration [72, 99, 167, 114, 179, 180, 181].

A suitable model to describe the stochastic dynamics of a hot compound nucleus is that of a Brownian particle in a heat bath. In this model, the collective motion involving the fission degrees of freedom is represented by a Brownian particle while the remaining intrinsic degrees of freedom of the CN correspond to the heat bath. In addition to the random force experienced by the Brownian particle in the heat bath, its motion is also controlled by the average nuclear potential. Fission occurs when the Brownian particle picks up sufficient kinetic energy from the heat bath in order to overcome the fission barrier. The dynamics of such a system is dissipative in nature and is governed by the appropriate Langevin equations or equivalently by the corresponding Fokker-Planck equation. As discussed earlier on several occasions, an analytical solution for the stationary diffusion rate of Brownian particles across the barrier was first obtained by Kramers from the Fokker-Planck equation [63]. The Fokker-Planck equation was subsequently used for extensive studies of nuclear fission [45, 156, 157, 162, 163, 164, 165]. The Langevin equations however found wider applications in recent years mainly because, unlike the Fokker-Planck equation, the Langevin equations do not require any approximation and it is easier to solve the latter for multidimensional cases by numerical simulations [82]. Fairly successful Langevin dynamical calculations for several observables such as fission and evaporation residue cross sections, pre-scission multiplicities of light particles and giant dipole resonance γ rays, and mass and kinetic energy distributions of the fission fragments have been reported [72, 99, 167, 114, 179, 180, 181].

In a stochastic dynamical model of nuclear fission, the FFMD essentially portrays the interplay between the conservative and the random forces acting along the mass asymmetry coordinate. Therefore, it will be of interest to find how the fluctuation in the mass asymmetry coordinate changes as the CN makes its journey from the saddle region to the scission config-

uration. This will essentially involve comparison of the asymmetry coordinate distribution at the saddle with that at the scission configuration. Such a comparison is expected to elucidate the role of the potential landscape vis-à-vis that of the random force in giving rise to the FFMD at scission [72, 99, 180]. The memory of the asymmetry coordinate fluctuation at the saddle that is retained at scission has also been discussed earlier on several occasions [153, 182].We address the above issues in the present chapter.

The fragment mass dispersions at the saddle and scission were compared in an earlier work of Gontchar *et al.* [180], where the mass variances at the saddle and scission were obtained from statistical and dynamical models, respectively. Though the mass variance at scission has been obtained from dynamical model calculations by a number of workers [182, 179, 180] in the past, the mass variance at the saddle has not been calculated from dynamical models so far. In the present calculation we obtain mass variances at both the saddle and scission from dynamical calculation since it is appropriate that both variances be obtained from the same model in order to compare them and investigate effects due to saddle-to-scission transition. In a Langevin dynamical calculation, a fission trajectory crosses the saddle ridge many times in a to-and-fro motion before it reaches the scission line. We obtain the mass asymmetry distribution along the saddle ridge by considering only those mass asymmetries which correspond to the last crossing of the saddle ridge by fission trajectories. The nature of the fission trajectories in the saddle region is further illustrated in the present work by comparing the distributions of the asymmetry coordinates corresponding to the first and last crossings of the saddle ridge by the fission trajectories.

The plan of our work is as follows. We perform Langevin dynamical calculations for fission in two dimensions using elongation and asymmetry as the relevant coordinates. We restrict the present calculation to the above two coordinates primarily because, while they bring out the essential features of the dynamics of the asymmetry coordinate, they also provide easy visualization of the fission process. For each fissioning Langevin trajectory, the asymmetry co-ordinates at which the trajectory crosses the saddle (for the last time) and scission regions are recorded. We thus directly obtain the asymmetry coordinate distributions at both the saddle and the scission. We make a detailed comparison of these two distributions for different nuclei

representing a broad range of distances between the saddle and the scission regions. Also, different aspects of the two-dimensional fission width are studied.

We describe the numerical technique to solve the Langevin equations in the next section. Then the various inputs for the two-dimensional calculations are illustrated in Sec. 6.3. Typical nature of the two-dimensional fission width and the FFMD are discussed in Sec. 6.4. Role of the saddle-to-scission dynamics in the FFMD is explained in Sec. 6.5. The last section contains a summary of the work.

6.2   How to solve 2D Langevin equations

In order to specify the collective coordinates for a dynamical description of nuclear fission, we use the shape parameters (c, h, α') as described in Chapter 2 [from Eq. (2.1) to Eq. (2.3)]. For the present calculation the value of h is fixed at zero. The two-dimensional Langevin equation in (c, α') coordinates has the following form [74],

$$
\begin{aligned}
\frac{dp_i}{dt} &= -\frac{p_j p_k}{2}\frac{\partial}{\partial q_i}(m^{-1})_{jk} - \frac{\partial V}{\partial q_i} - \eta_{ij}(m^{-1})_{jk}p_k + g_{ij}\Gamma_j(t), \\
\frac{dq_i}{dt} &= (m^{-1})_{ij}p_j,
\end{aligned}
\tag{6.1}
$$

where q_1 and q_2 stand for c and α', respectively, and p_i represents the respective momentum. V is the potential energy of the system and m_{ij} and η_{ij} are the shape-dependent collective inertia and dissipation tensors, respectively. The time-correlation property of the random force is assumed to follow the relation

$$
\langle \Gamma_k(t)\Gamma_l(t') \rangle = 2\delta_{kl}\delta(t - t'),
$$

and the strength of the random force is related to the dissipation coefficients through the fluctuation-dissipation theorem and is given as

$$
g_{ik}g_{jk} = \eta_{ij}T,
\tag{6.2}
$$

where the temperature T of the compound nucleus at any instant of its evolution is given as

$$
T = \sqrt{E_{int}/a(\overrightarrow{q})}.
$$

The intrinsic excitation energy E_{int} is calculated from the total excitation energy E^* of the compound nucleus using energy conservation,

$$E^* = E_{int} + E_{coll} + V(\overrightarrow{q}),$$

where E_{coll} is the collective translational kinetic energy and $V(\overrightarrow{q})$ is the potential energy including the rotational energy of the system. The level density parameter $a(\overrightarrow{q})$ depends on the collective coordinates and is taken from the works of Ignatyuk et $al.$ [20] as described in the Chapter 1.

To solve the Langevin differential equations numerically we proceed as follows [72]. As described for the one-dimensional case in Chapter 2, in this method, the coordinates and momenta given by Eq. (6.1) are first expressed as finite differences in time domain as

$$
\begin{aligned}
p_i(t + \Delta t) - p_i(t) &= \int_t^{t+\Delta t} dt' H_i(\overrightarrow{q}, \overrightarrow{p}; t') + \int_t^{t+\Delta t} dt' g_{ij}(\overrightarrow{q}; t') \Gamma_j(t'), \\
q_i(t + \Delta t) - q_i(t) &= \int_t^{t+\Delta t} dt' v_i(\overrightarrow{q}, \overrightarrow{p}; t'),
\end{aligned}
\tag{6.3}
$$

where

$$
\begin{aligned}
H_i(\overrightarrow{q}, \overrightarrow{p}; t) &= -\frac{\partial V}{\partial q_i} - \frac{1}{2} \frac{\partial (m^{-1})_{jk}}{\partial q_i} p_j p_k - \eta_{ij}(m^{-1})_{jk} p_k, \\
v_i(\overrightarrow{q}, \overrightarrow{p}; t) &= (m^{-1})_{jk} p_k.
\end{aligned}
\tag{6.4}
$$

Expanding $H_i(\overrightarrow{q}, \overrightarrow{p}; t')$, $v_i(\overrightarrow{q}, \overrightarrow{p}; t')$ and $g_{ij}(\overrightarrow{q}; t')$ as the Taylor series around the point $(\overrightarrow{q}, \overrightarrow{p}; t)$ and then inserting in Eq. (6.3), we get

$$
\begin{aligned}
p_i(t + \Delta t) &= p_i(t) + H_i \Delta t + \frac{(\Delta t)^2}{2} \left[v_j \frac{\partial H_i}{\partial q_j} + H_j \frac{\partial H_i}{\partial p_j} \right] + g_{ij} \widetilde{\Gamma}_{1j} + \frac{\partial H_i}{\partial p_j} g_{jk} \widetilde{\Gamma}_{2k} + \frac{\partial g_{ij}}{\partial q_k} v_k \widehat{\Gamma}_{2j}, \\
q_i(t + \Delta t) &= q_i(t) + v_i \Delta t + \frac{(\Delta t)^2}{2} \left[v_j \frac{\partial v_i}{\partial q_j} + H_j \frac{\partial v_i}{\partial p_j} \right] + \frac{\partial v_i}{\partial p_j} g_{jk} \widetilde{\Gamma}_{2k}.
\end{aligned}
\tag{6.5}
$$

As Δt is very small, we keep the terms up to quadratic in Δt. For a Markovian process, the terms involving $\Gamma(t)$ can be defined as follows [72]:

$$
\begin{aligned}
\widetilde{\Gamma}_{1j} &= \int_t^{t+\Delta t} dt' \Gamma_j(t') = (\Delta t)^{1/2} \omega_{1j}, \\
\widetilde{\Gamma}_{2k} &= \int_t^{t+\Delta t} dt' \int_t^{t'} dt'' \Gamma_k(t'') = (\Delta t)^{3/2} \left[\frac{1}{2} \omega_{1k}(t) + \frac{1}{2\sqrt{3}} \omega_{2k}(t) \right], \\
\widehat{\Gamma}_{2j} &= \int_t^{t+\Delta t} dt' (t' - t) \Gamma_j(t') = (\Delta t)^{3/2} \left[\frac{1}{2} \omega_{1j}(t) - \frac{1}{2\sqrt{3}} \omega_{2j}(t) \right].
\end{aligned}
\tag{6.6}
$$

In the above equations $\omega_{mn}(t)$ are the Gaussian random numbers with time-correlation properties: $\langle \omega_{mn}(t) \rangle = 0$ and $\langle \omega_{ni}(t_1)\omega_{mj}(t_2) \rangle = 2\delta_{nm}\delta_{ij}\delta(t_1 - t_2)$.

The strength of the fluctuating force is determined from Eq. (6.2) which can be decomposed into three simultaneous equations as

$$
\begin{aligned}
g_{cc}^2 + g_{c\alpha'}^2 &= \eta'_{cc}, \\
g_{cc}g_{c\alpha'} + g_{c\alpha'}g_{\alpha'\alpha'} &= \eta'_{c\alpha'}, \\
g_{\alpha'\alpha'}^2 + g_{c\alpha'}^2 &= \eta'_{\alpha'\alpha'},
\end{aligned}
\tag{6.7}
$$

where $\eta'_{ij} = T\eta_{ij}$ and g_{ij} is considered to be symmetric, i.e., $g_{c\alpha'} = g_{\alpha'c}$. Now the above equations are solved for the three components g_{ij} in the following manner. Let (x, y, z) be a trial solution of Eq. (6.7) and R be a number which is minimum of $\sqrt{\eta'_{cc}}$ and $\sqrt{\eta'_{\alpha'\alpha'}}$. First, we consider discrete values of z starting from $z = 0$ up to $z = R$ and, for each value of z, we calculate $x = \sqrt{\eta'_{cc} - z^2}, y = \sqrt{\eta'_{\alpha'\alpha'} - z^2}$ and $A = xz + yz$. In this iterative process, A will be ultimately equal to $\eta'_{c\alpha'}$ when (x, y, z) becomes a solution for Eq. (6.7). We then determine the value $z = z_0$ for which the foregoing equality condition is satisfied and obtain the solutions for g_{ij} as $g_{cc} = x_0$, $g_{\alpha'\alpha'} = y_0$ and $g_{c\alpha'} = z_0$. It is now possible to generate the time evolution of $(\overrightarrow{q}, \overrightarrow{p})$ by solving Eq. (6.5). In order to proceed further, we need to know the dynamical variables $V(c, \alpha')$, $(m^{-1})_{ij}(c, \alpha')$, $\eta_{ij}(c, \alpha')$ and $a_{ij}(c, \alpha')$, a brief description of which are given in the next section.

6.3   Collective properties in 2D

We make the Werner-Wheeler approximation [71] for incompressible irrotational flow to calculate the collective inertia tensor and its inverse $(m^{-1})_{ij}$ in Eq. (6.1). The potential energy $V(c, \alpha')$ is obtained from the finite-range liquid-drop model by a double folding procedure [128]. The rotational energy part of $V(c, \alpha')$ is calculated using the moment of inertia of a rigid rotator. For η_{ij}, we use the one-body model for nuclear dissipation in our calculations. The original wall-plus-window formula [67, 138], which was subsequently generalized to include the dissipation associated with the time rate of change of mass asymmetry degree of freedom [149],

is employed here and is given as

$$\eta_{ij} = \kappa \eta_{ij}^{wall} + \eta_{ij}^{window} + \eta_{ij}^{asym}, \tag{6.8}$$

where

$$\eta_{ij}^{wall} = \frac{1}{2}\pi\rho_m\bar{v}\left\{\int_{z_{min}}^{z_N}\left(\frac{\partial\rho^2}{\partial q_i}+\frac{\partial\rho^2}{\partial z}\frac{\partial D_1}{\partial q_i}\right)\left(\frac{\partial\rho^2}{\partial q_j}+\frac{\partial\rho^2}{\partial z}\frac{\partial D_1}{\partial q_j}\right)\left(\rho^2+\left(\frac{1}{2}\frac{\partial\rho^2}{\partial z}\right)^2\right)^{-\frac{1}{2}}dz\right.$$

$$\left.+\int_{z_N}^{z_{max}}\left(\frac{\partial\rho^2}{\partial q_i}+\frac{\partial\rho^2}{\partial z}\frac{\partial D_2}{\partial q_i}\right)\left(\frac{\partial\rho^2}{\partial q_j}+\frac{\partial\rho^2}{\partial z}\frac{\partial D_2}{\partial q_j}\right)\left(\rho^2+\left(\frac{1}{2}\frac{\partial\rho^2}{\partial z}\right)^2\right)^{-\frac{1}{2}}dz\right\}, \tag{6.9}$$

$$\eta_{ij}^{window} = \frac{1}{2}\rho_m\bar{v}\frac{\partial R}{\partial q_i}\frac{\partial R}{\partial q_j}\Delta\sigma, \tag{6.10}$$

and

$$\eta_{ij}^{asym} = \frac{16}{9}\rho_m\bar{v}\frac{1}{\Delta\sigma}\frac{\partial V_1}{\partial q_i}\frac{\partial V_1}{\partial q_j}. \tag{6.11}$$

The derivations of all these collective properties are discussed in Chapter 2. It has been established from earlier studies [99] that a smaller strength of the wall dissipation than that given by the wall formula is required in order to fit experimental data. κ represents the reduction factor for wall dissipation coefficient and a value of $\kappa = 0.25$ is used in the present work [99, 117, 183]. The coefficient for dissipative resistance against change in asymmetry degree of freedom is given by η_{ij}^{asym} [149]. This component of one-body dissipation strongly influences the FFMD, as we shall see in the subsequent studies.

It is of interest at this point to examine the two-dimensional landscapes of various input quantities in our calculation. We first show the potential energy contours in Fig. 6.1 for six rotating nuclei. The loci of the conditional saddle points or the saddle ridge and that of the scission configurations (scission line) are also shown in this figure for each nuclei. The scission configuration is determined following the criterion given in Ref. [99] and corresponds to a neck radius of $0.3R_0$, R_0 being the radius of a nucleus in spherical shape. The above nuclei and their spin values are so chosen that they represent a broad range of saddle-to-scission distances and also a reasonable range of fission barriers where Langevin dynamical calculations with good statistics can be performed. Table 6.1 gives the values of Z^2/A, the distance (c_{SS} in units of R_0) between the saddle ridge and the scission line along the c axis for $\alpha' = 0$, and the fission barrier of these nuclei. We also show in Fig. 6.1 the locus of the points (neck line) where neck
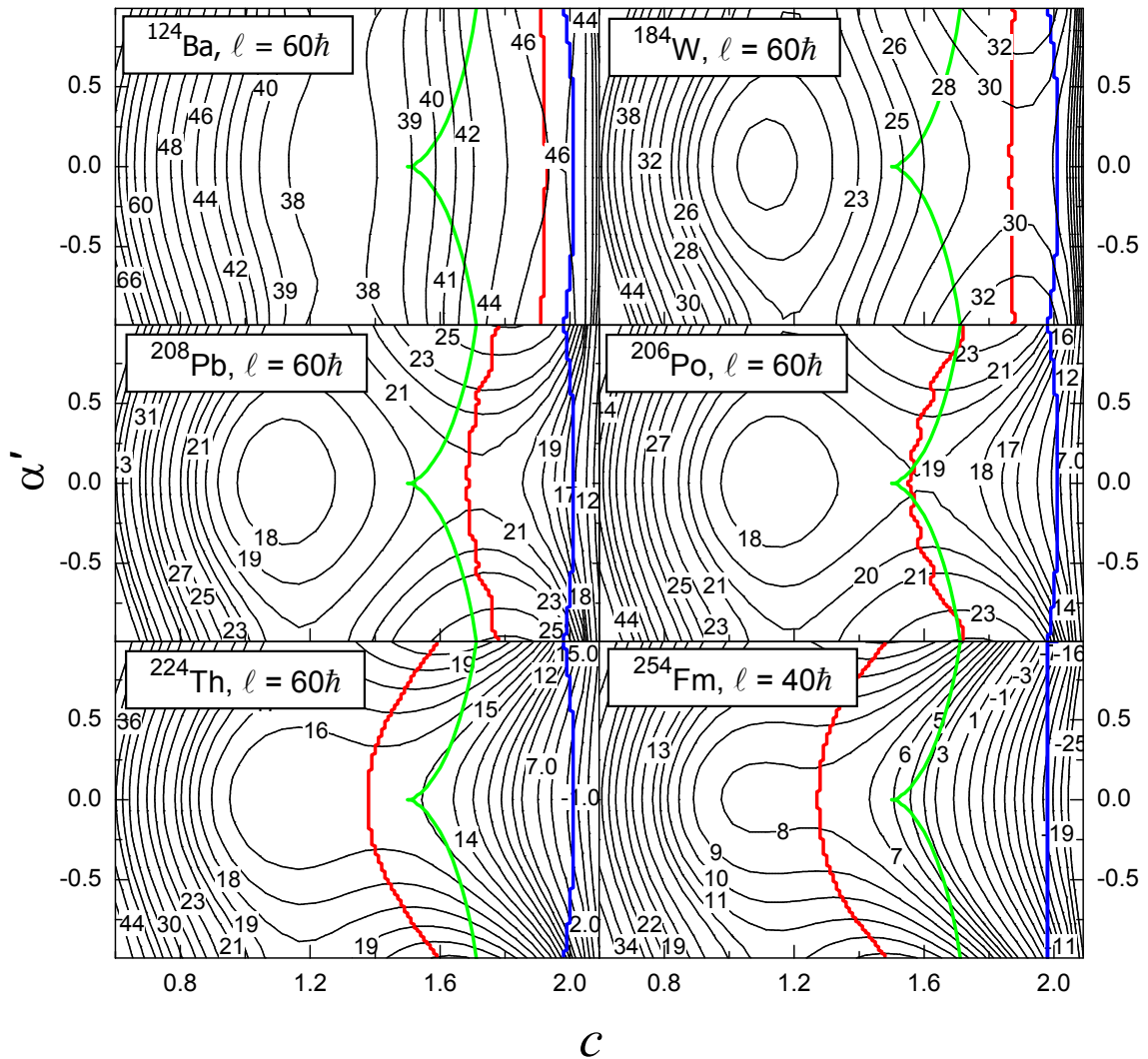
Figure 6.1: The finite-range liquid drop model potential contours (in MeV unit) for a number of compound nuclei. The saddle ridge and scission line are shown by red and blue lines respectively. The green line represents the neck line (see text) [103].

formation begins in (c, α') space. It is observed that while the saddle-to-scission transition is made through shapes with well-developed necks for lighter nuclei, a large fraction of the transition takes place in heavier nuclei before a neck is formed. Since the component of the stochastic force associated with the mass asymmetry degree of freedom becomes effective after the neck is formed, the above observation indicates that the relative roles of the conservative and stochastic forces are expected to be different for light and heavy nuclei. This aspect will be further explored in the following section. It is also of interest to note that the position of

Table 6.1: Z^2/A, saddle-to-scission distance c_{SS}(see text) and fission barrier (V_B) for symmetric fission of compound nuclei used in the work.

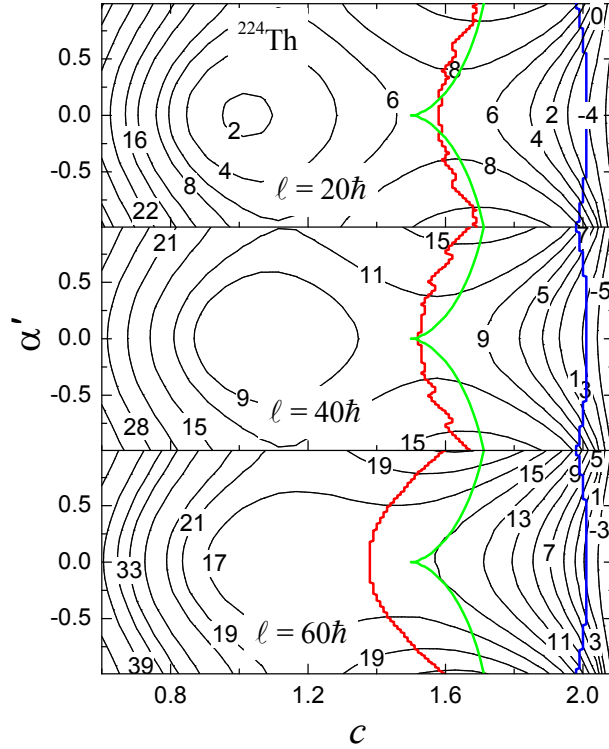|	^{124}Ba $\ell = 60\hbar$	^{184}W $\ell = 60\hbar$	^{208}Pb $\ell = 60\hbar$	^{206}Po $\ell = 60\hbar$	^{224}Th $\ell = 60\hbar$	^{254}Fm $\ell = 40\hbar$
Z^2/A	25.29	29.76	32.33	34.25	36.16	39.37
c_{SS}	0.08	0.14	0.32	0.46	0.63	0.74
V_B(MeV)	8.61	8.63	3.41	1.76	0.38	0.10

Figure 6.2: Potential contours (in MeV unit) for different spin of ^{224}Th. Red, blue and green lines have the same meaning as in the previous figure.

the saddle configuration becomes more compact along c axis with the increase of spin while the position of the scission line remains unchanged (Fig. 6.1). Therefore, it also gives us the opportunity to explore the role of saddle-to-scission dynamics by tuning the spin of a nucleus which effectively changes the value of c_{SS}. For this purpose, we chose the potential contours of

Table 6.2: Saddle-to-scission distance c_{SS} (see text) and fission barrier (V_B) for differen ℓ of ^{224}Th.

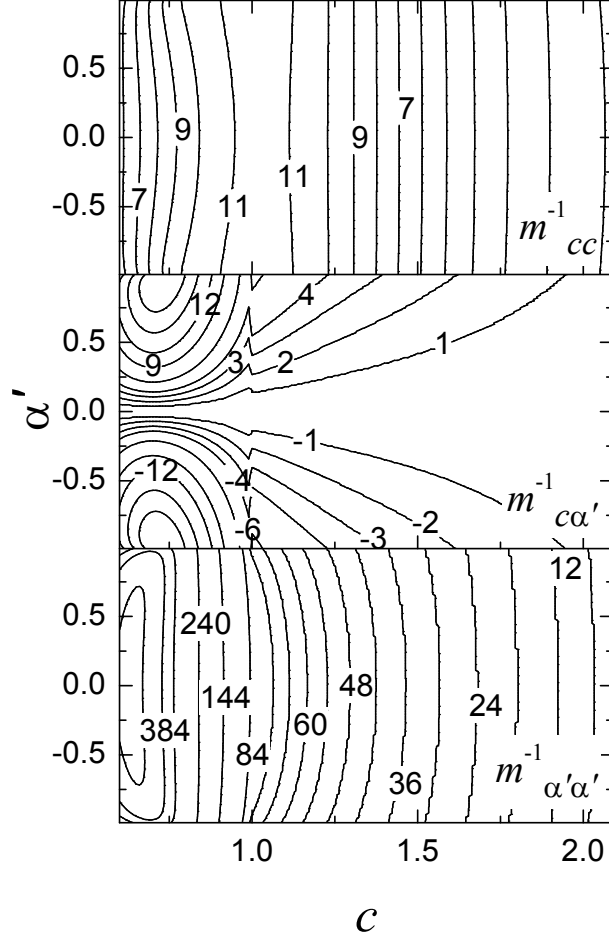|	$\ell = 20\hbar$	$\ell = 40\hbar$	$\ell = 60\hbar$
c_{SS}	0.43	0.49	0.63
V_B(MeV)	5.06	2.98	0.38

Figure 6.3: Different components of inverse inertia tensor (in MeV/$\hbar^2$ unit) of ^{224}Th [103].

^{224}Th as shown in Fig. 6.2. Corresponding values of the fission barrier and c_{SS} are indicated in Table 6.2.

We next show the contour plots of inverse inertia tensor components of ^{224}Th in Fig. 6.3. We observe that both the diagonal components m_{cc}^{-1} and $m_{\alpha'\alpha'}^{-1}$ have very weak α' dependence
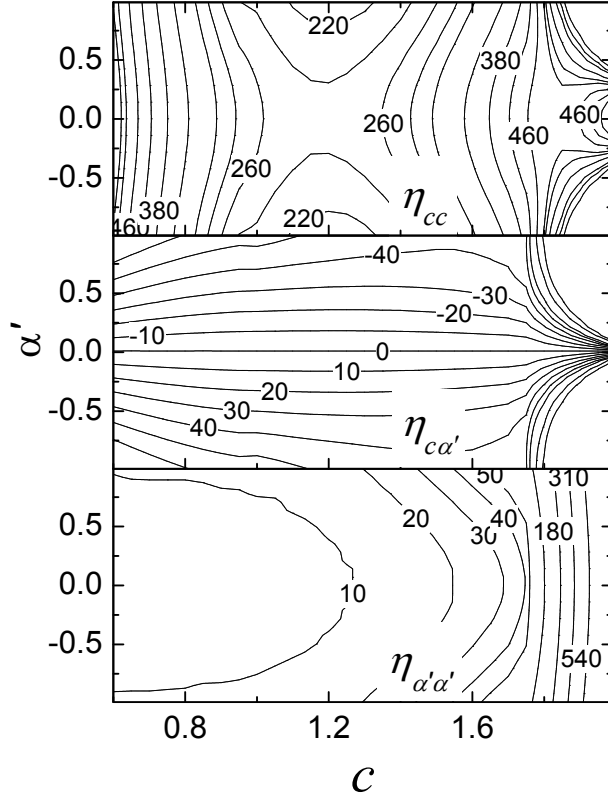

Figure 6.4: Different components of one-body dissipation tensor (in $\hbar$ unit) calculated for ^{224}Th using Eq. (2.32) with $\kappa = 0.25$ [103].

though their c dependence is quite strong. The nondiagonal component $m_{c\alpha'}^{-1}$ however has a stronger α' dependence and a weaker c dependence. This means that the contributions of the diagonal terms in the inertia derivative term in the Langevin equations [Eq. (6.1)] is much stronger in the c coordinate than that in the α' coordinate while it is the opposite for the nondiagonal term. It is also of interest to note that while the diagonal components m_{cc}^{-1} and $m_{\alpha'\alpha'}^{-1}$ have a symmetric α' dependence, it is antisymmetric for the non diagonal component $m_{c\alpha'}^{-1}$. The contour plots of the dissipation tensor shown in Fig. 6.4 also have features similar to those of inertia. The diagonal components are symmetric in α' though they have a somewhat stronger α' dependence compared to inverse inertia. The nondiagonal component $\eta_{c\alpha'}$ has a strong α' dependence and it is also antisymmetric in α'. The symmetry properties with respect
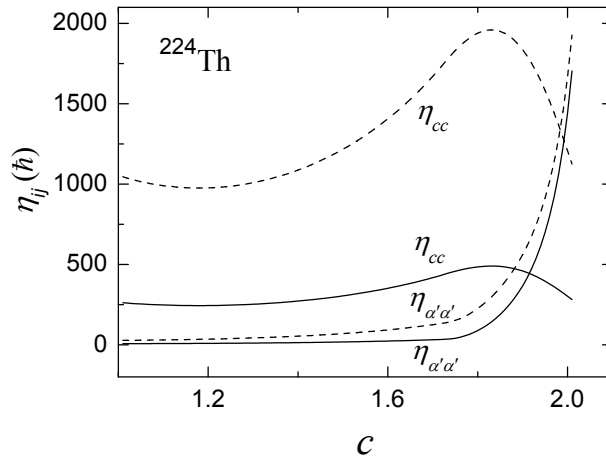
112

Figure 6.5: The diagonal components of one-body dissipation plotted against c for $\alpha' = 0$. The solid and dashed lines correspond to different dissipation strengths calculated with $\kappa=0.25$ and 1 respectively [103].

to α' of the inverse inertia and the dissipation coordinates taken together give rise to the correct symmetry of the Langevin dynamical equations. This essentially implies that the c component of force at c for $(\alpha', p_{\alpha'})$ is the same as that for $(-\alpha', -p_{\alpha'})$. However, the α' component of the force should change sign between $(\alpha', p_{\alpha'})$ and $(-\alpha', -p_{\alpha'})$. Both are realized when diagonal components are symmetric and non diagonal components antisymmetric with respect to reflection of α'. We also compare the magnitudes of η_{cc} and $\eta_{\alpha'\alpha'}$ in Fig. 6.5. $\eta_{\alpha'\alpha'}$ is much weaker than η_{cc} for most values of the elongation parameter c except at large deformations, where a neck has developed, due to the η^{asym} term.

6.4   Fission width and FFMD

With the input quantities defined as in the above, the Langevin equations are numerically integrated in second order using a small time step of $0.0005\hbar$/MeV. All the input quantities are first calculated on a uniform two-dimensional grid with 150×101 grid points covering the range of $c \in (0.6, 2.09)$ and $\alpha' \in (-1, 1)$. Calculations are performed for a compound nucleus at specified values of its spin and temperature. The initial collective coordinates are chosen as those of a spherical nucleus and the initial momentum distribution is assumed to follow that of a equilibrated thermal system. In the present calculation, we record the asymmetry

coordinate of the crossing point whenever a Langevin trajectory crosses the saddle ridge. If
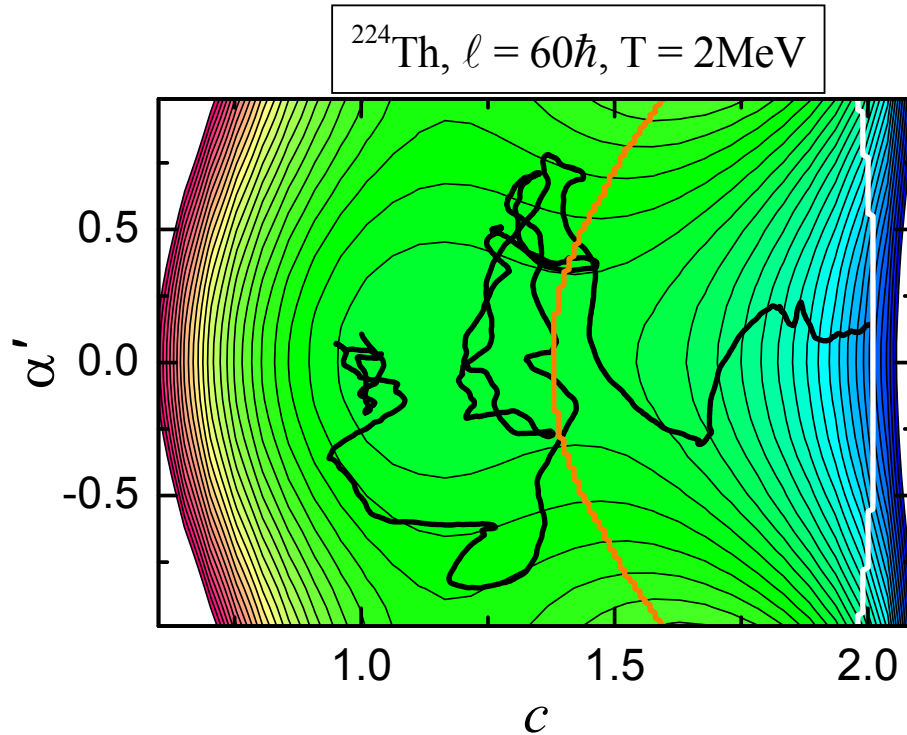

Figure 6.6: A typical Langevin trajectory going to fission.

the same trajectory subsequently reaches the scission line, it is identified as a fission event and the asymmetry coordinate at scission is also recorded. Such a trajectory is shown in Fig. 6.6. While the asymmetry coordinates corresponding to the last crossing of the saddle ridge by the fission trajectories are used to obtain the mass variance at the saddle, those corresponding to the crossing of the scission line give the mass variance at scission. The FFMD at the saddle thus corresponds to the distribution that would result if the asymmetry distribution at the saddle were transported to the scission configuration without any further modification. The calculations are performed for a large ensemble of Langevin trajectories such that the number of fission events are typically 10 000 or more. The fragment mass distributions at saddle and scission configurations are subsequently obtained from the asymmetry coordinate distributions by binning over the asymmetry coordinate. The fragment mass distributions at the saddle and scission are thus obtained from the same set of fission events. Before explaining the results on mass distribution, a systematic study of two-dimensional fission width is presented for ^{224}Th in the next subsection.
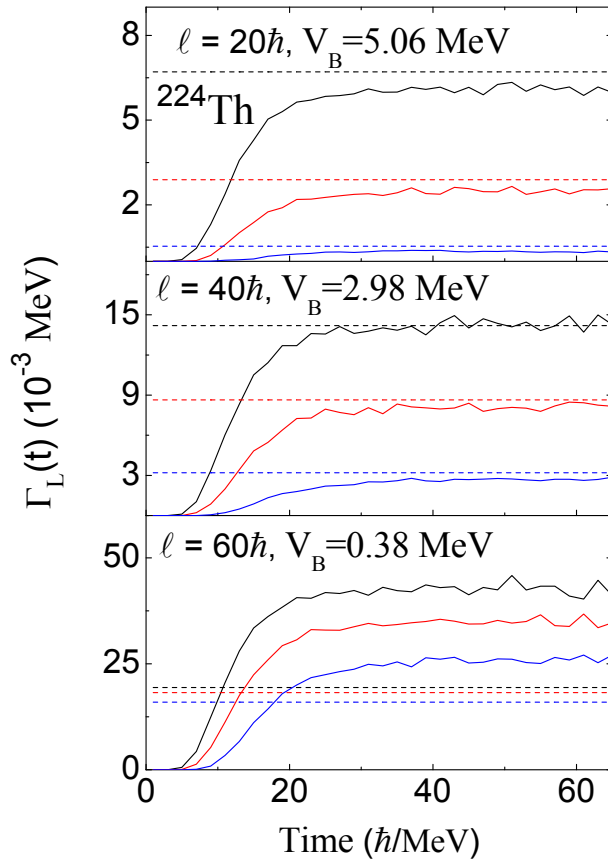
114

Figure 6.7: Two-dimensional Langevin dynamical fission width (solid lines) calculated for different values compound nuclear spin (mentioned in the panels). The blue, red and black lines correspond to $T = 1$, 1.5 and 2 MeV, respectively. Equivalent Kramers' widths are shown by dashed lines.

6.4.1 Fission width from 2D calculations

Starting from the initial condition, the time evolution of a Langevin trajectory is followed on the two-dimensional potential profile and it is considered as a fission event if it reaches the scission line where the neck radius becomes $0.3R_0$. For an ensemble of events, the number of fission events are recorded as a function of time. Subsequently, the fission width is calculated by pursuing the same procedure described in Subsec. 2.4.3 for the one-dimensional case. Alternatively, two-dimensional fission width can be calculated from the two-dimensional Kramers' formula given by Eq. (1.53). The Kramers' fission widths thus obtained are compared with the stationary values of Langevin dynamical fission width. Both of these widths are
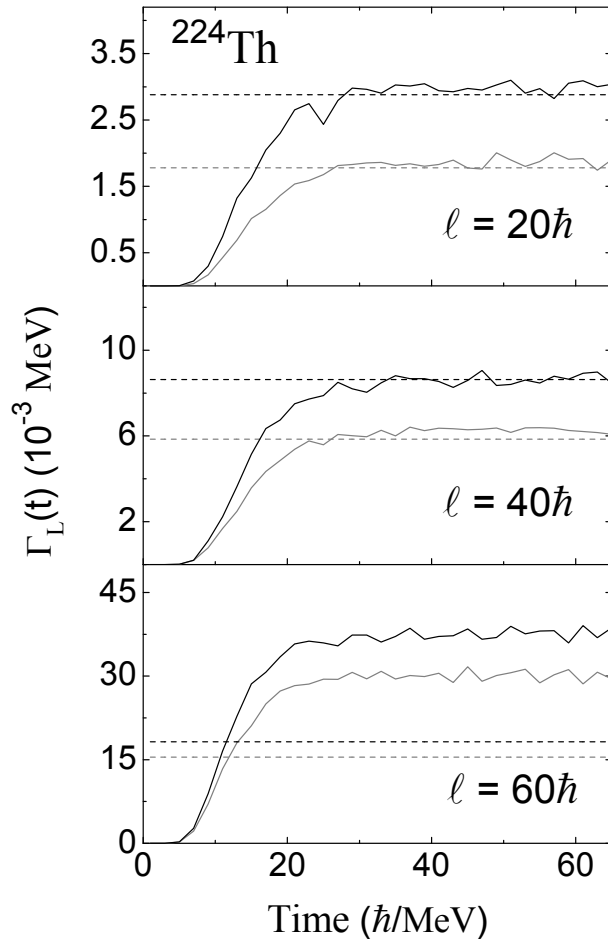
Figure 6.8: Two-dimensional Langevin dynamical fission widths (black lines) and correspond-
ing one-dimensional Langevin widths (gray lines) calculated at $T = 1.5 \text{MeV}$. Corresponding
Kramers' widths in one- and two-dimensions are indicated by dashed lines.

plotted for different combinations of compound nuclear spin and temperature of ^{224}Th in Fig.
6.7 and it is evident from this figure that the Langevin-dynamical fission width matches well
with the two-dimensional Kramers' fission width as long as the fission barrier (see Table 6.2)
is larger than the temperature. As Kramers' width is defined for a constant dissipation, we
have considered a constant dissipation strength in the above dynamical calculation. We next
compare the two-dimensional fission width with the corresponding one-dimensional width. It
is shown in Fig. 6.8 for the ^{224}Th nucleus and it explains that the inclusion of mass asymmetry
degree of freedom α' enhances the fission width substantially. We also examine the effect of
the shape dependent inertia, as given in Fig. 6.3, on the two-dimensional fission width. In Fig.
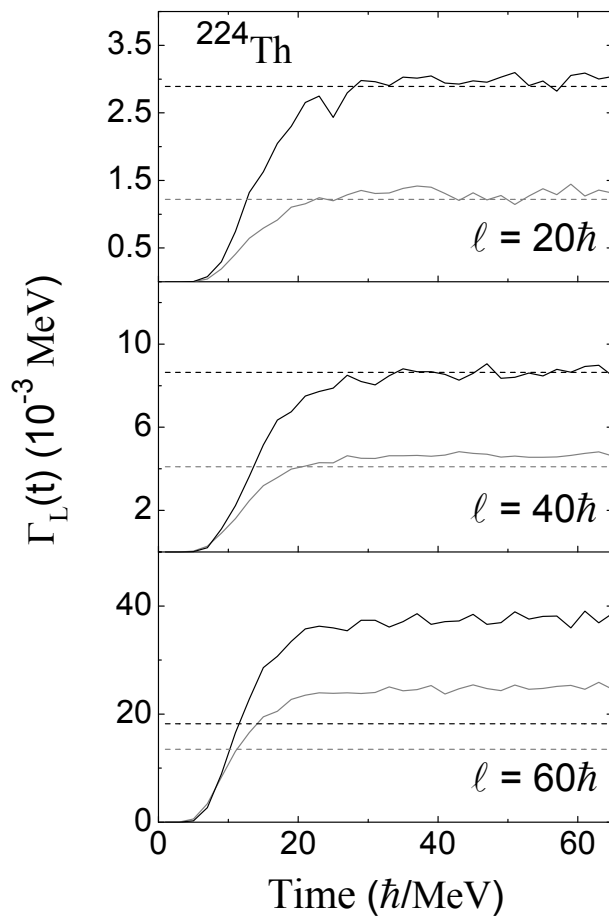
116

Figure 6.9: Two-dimensional Langevin dynamical fission widths for shape dependent (black lines) and shape independent (gray lines) inertia calculated at $T = 1.5$MeV. Kramers' widths are indicated by dashed lines.
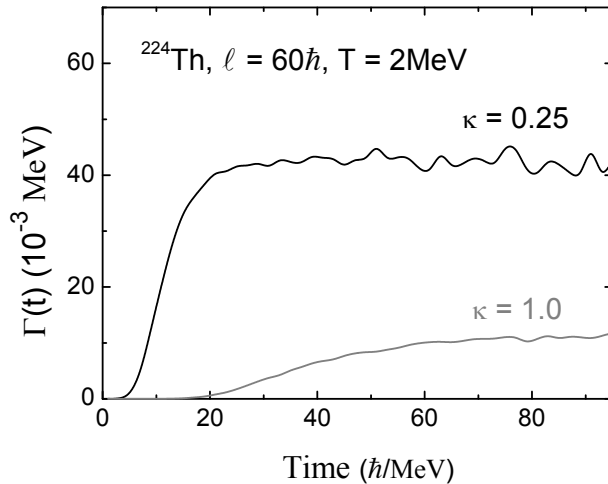
Figure 6.10: Two-dimensional Langevin dynamical fission widths for different values of κ.

6.9 Langevin fission widths are compared for constant and variable inertia and the equivalent Kramers' fission widths are shown by dashed lines. A significant increase in fission width is observed when the shape dependence of inertia is incorporated in the calculations. Also, similar to the one-dimensional case described in Chapter 4, the two-dimensional Kramers' fission width, as shown in Fig. 6.9, matches well with the Langevin dynamical results when the earlier one is modified to account for the shape dependence of inertia. This modification is done by proper estimation of potential curvature terms in Eq. (1.53).

Before concluding this subsection, in Fig. 6.10, we have illustrated the effect of the reduction factor κ [Eq. (6.8)] in the two-dimensional fission width. A considerable decrease in the stationary value of the fission width is observed as the value of κ changes from 0.25 to 1.0. This is expected as increase in κ increases the strength of η_{cc} which mainly hinders the motion towards fission, and thereby reduces the fission probability.

6.4.2   FFMD from 2D calculations

We obtain the fragment mass distribution by integrating the Langevin equations numerically for each trajectory, which was continued for a sufficiently long time interval such that a steady flow of fission trajectories across the saddle ridge is established. This is illustrated in Fig. 6.11 where the fragment mass distributions for ^{254}Fm, evaluated at the saddle after time intervals of
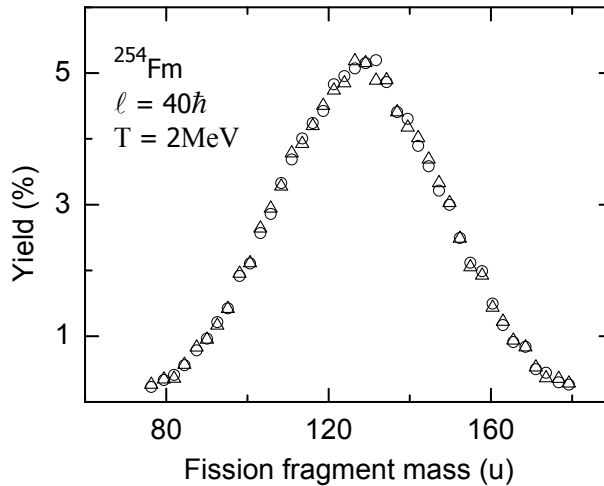
118

Figure 6.11: Fission fragment mass distributions of ^{254}Fm obtained at saddle ridge after time intervals of 50 $\hbar$/MeV (empty triangle) and 100 $\hbar$/MeV (empty circle), respectively.

50 and 100$\hbar$/MeV, are given. The distributions are practically indistinguishable which shows that a stationary flow is established within 50$\hbar$/MeV of time. In what follows, all the mass distributions are obtained after stationary state is established. We show in Fig. 6.12 the fragment mass distributions of nuclei listed in Table 6.1 and undergoing fission at a temperature of 2 MeV. This temperature defines the initial excitation energy of a nucleus in its ground-state configuration. The fragment mass distributions calculated at both saddle and scission configurations with the η^{asym} term in Eq. (6.8) are shown in this figure. A similar plot is given in Fig. 6.13 for different combinations of spin and temperature of the ^{224}Th nucleus. It can be observed that the fragment mass distribution becomes broader as the temperature (spin) increases at a particular value of spin (temperature). This feature of the mass distribution is quite obvious as the strength of fluctuating force increases with temperature which eventually drives the system toward more mass asymmetric shapes. On the other hand, increase of compound nuclear spin makes the potential landscape more flatter along mass asymmetry direction. As a result, the restoring force due to the potential is reduced along mass asymmetry.
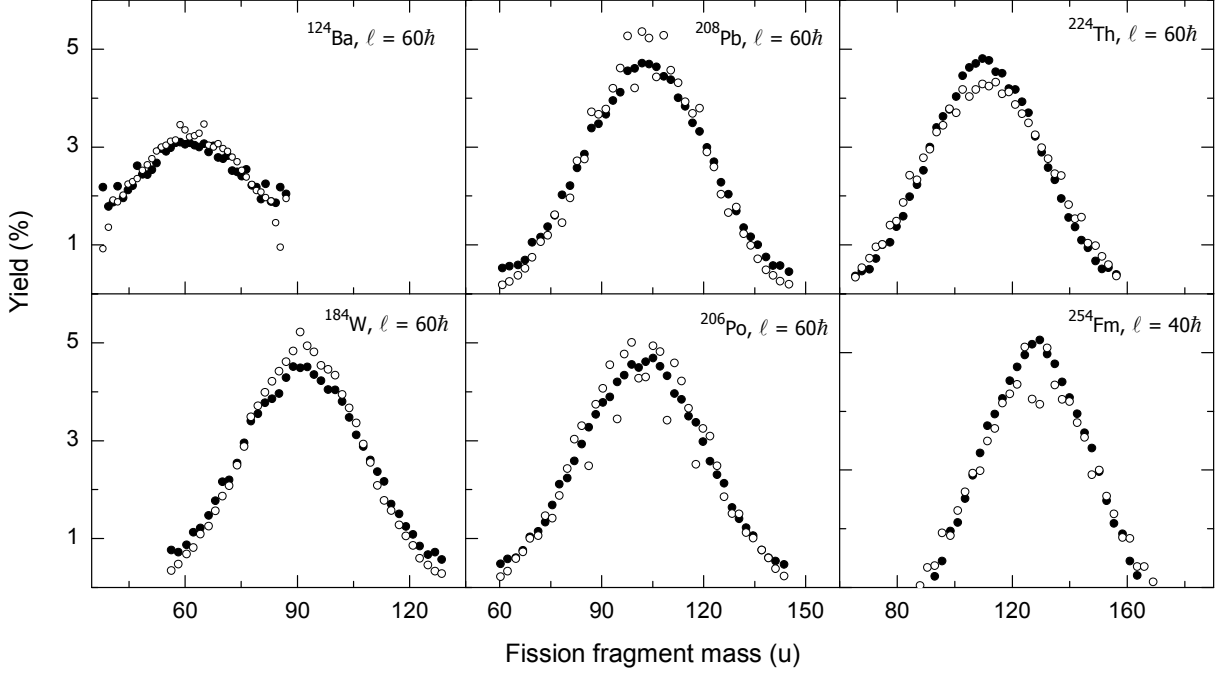
Figure 6.12: Fission fragment mass distributions (filled circles) at scission line for different nuclei obtained from dynamical model calculation with the η^{asym} term. The mass distributions on the saddle ridge, contributed by the trajectories which eventually reach the scission line, are shown by the empty circles.

6.5 Role of saddle-to-scission dynamics in FFMD

In a Langevin dynamical model of nuclear fission, the FFMD is effectively generated through the interplay between the conservative and the random forces acting along the mass asymmetry coordinate. To explore the role of dynamics in FFMD, it is therefore essential to find how the fluctuation in the mass asymmetry coordinate changes as the CN makes its journey from the saddle region to the scission configuration. This involves comparison of the asymmetry coordinate distribution at the saddle with that at the scission configuration. Such a comparison is expected to elucidate the relative role of the potential landscape and the dissipative forces in giving rise to the FFMD at scission [72, 99, 180]. The "memory" of the asymmetry coordinate fluctuation at the saddle that is retained at scission has also been discussed earlier on several occasions [153, 182]. We address the above issues in the present section.
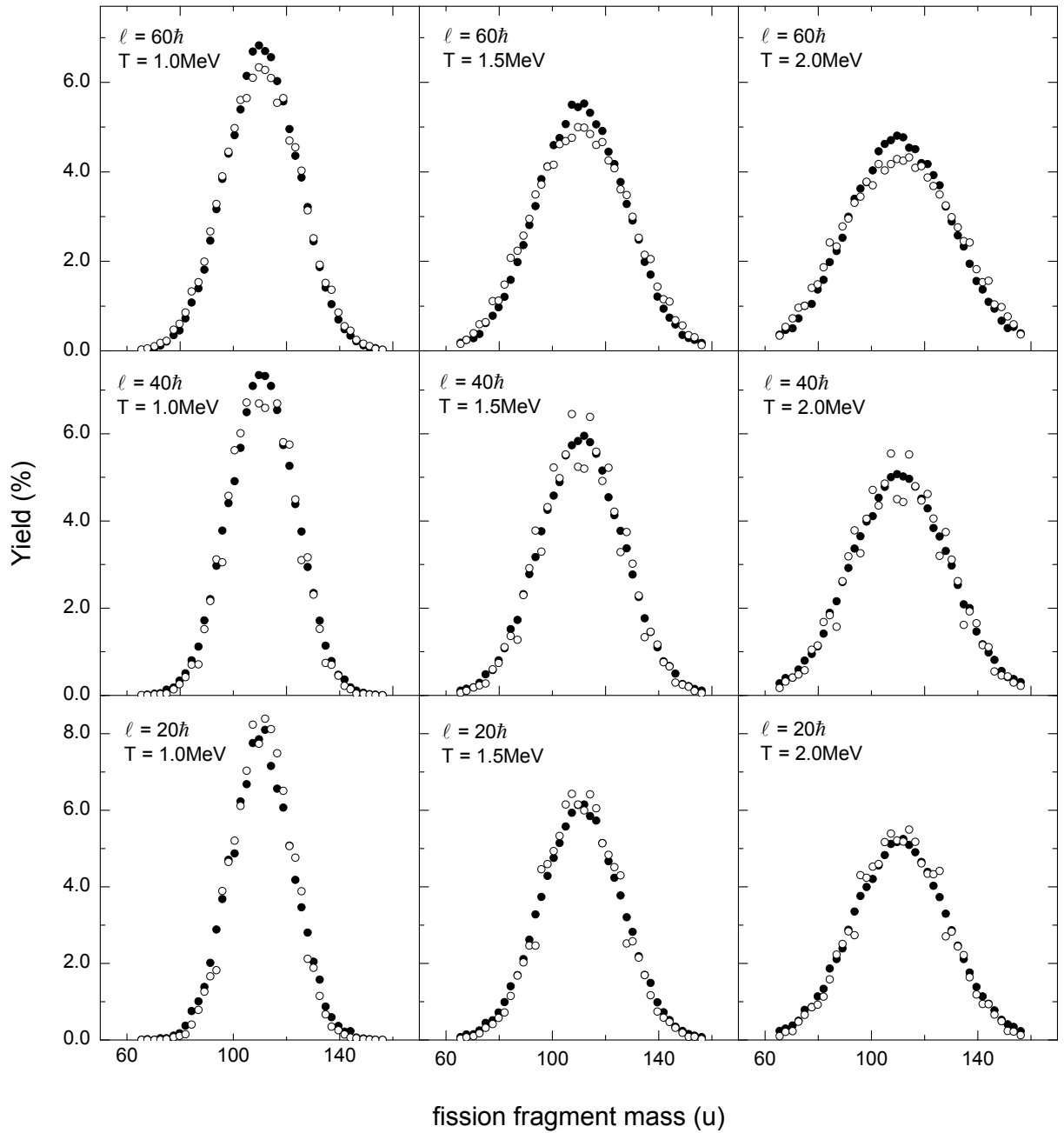
Figure 6.13: Fission fragment mass distributions (FFMD) for the fission of ^{224}Th at different combinations of ℓ and T. FFMD (filled circles) at scission line are obtained from dynamical model calculation with the η^{asym} term. The mass distributions on the saddle ridge, contributed by the trajectories which eventually reach the scission line, are shown by the empty circles.

At first, calculations are performed without η^{asym} and the corresponding mean-square deviations σ_m^2 for the different systems are plotted as a function of saddle-to-scission distances c_{SS} in Fig. 6.14. This figure provides a direct comparison between mass variances at saddle and scission when both are obtained from Langevin dynamical model calculation, in contrast with the results of [180], where the mass variances at saddle and scission were obtained from statistical and dynamical models, respectively. We find that the mass variance of a system de-
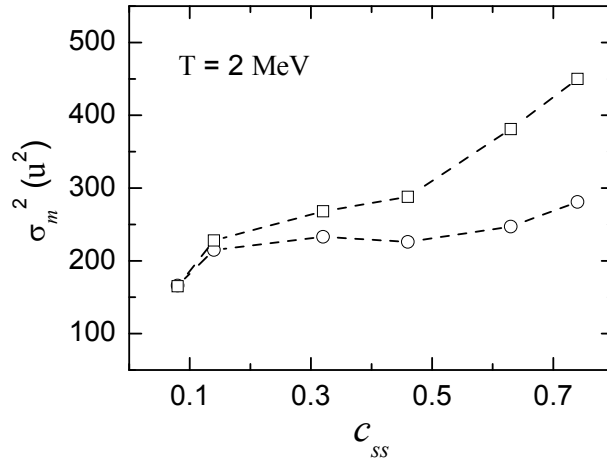

Figure 6.14: The variance of the FFMD(σ_m^2) at the saddle ridge (empty squares) and on the scission line (empty circles) as a function of the saddle-to-scission distance obtained from dynamical model calculations without the η^{asym} term [103]. Lines are drawn to guide the eyes.

creases as it moves from the saddle to the scission region. Though the magnitude of reduction is very small for small values of c_{SS}, it increases with increasing of saddle-to-scission distance. This feature clearly demonstrates the role of the potential landscape in developing the mass variance during saddle-to-scission transition. Since η^{asym} is not included in the calculation of mass variances in Fig. 6.14, a strong dissipative force is not present in the saddle-to-scission dynamics. Therefore, the funnel shape of the potential landscape in the saddle-to-scission region pushes the system toward a symmetric configuration and consequently the mass variance at scission decreases.

Mass variances obtained with η^{asym} in the Langevin dynamical calculation are next shown in Fig. 6.15. Dynamical model results without η^{asym} (as given in Fig. 6.14) are also shown in this figure for comparison. The variances at the saddle obtained with and without η^{asym} are

indistinguishable in this figure, which is expected since η^{asym} becomes effective only beyond the neck line. We make two observations from this figure. First, the variances at scission are enhanced (with respect to values obtained without η^{asym}) with inclusion of η^{asym} in the calcula-
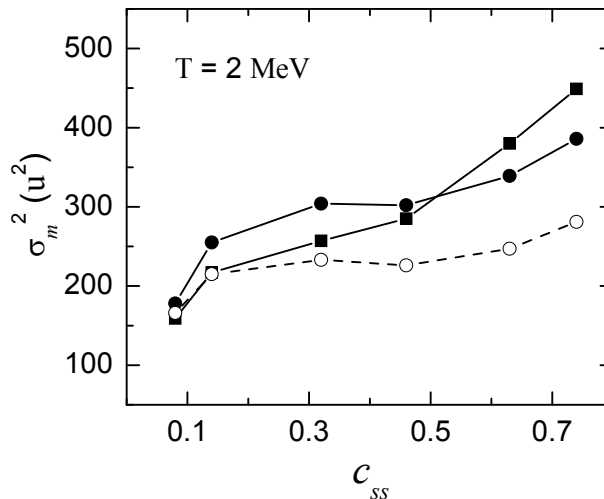

Figure 6.15: The mass variances σ_m^2 calculated with (filled symbols) and without (empty symbols) the η^{asym} term for different systems. The circles represent the variances at scission while the squares represent the variances at the saddle. The variances at the saddle for both cases (with and without η^{asym}) are nearly the same and are indistinguishable in the plot [103]. Lines are drawn to guide the eyes.

tion. This is a consequence of the random force associated with η^{asym}, which operates between the neck line and the scission line and drives the system toward larger asymmetry. This also demonstrates the importance of the asymmetry term η^{asym} in the generalized one-body dissipation [149]. Our next observation concerns a comparison of variances at saddle and scission when both are obtained with the η^{asym} term in the calculation. The variance at scission is found to be larger than that at the saddle for smaller values of c_{SS} while the reverse is the case for higher values of c_{SS}. In order to make a qualitative understanding of this observation, we proceed as follows. From the potential landscape of the different systems given in Fig. 6.1, we have observed in the earlier section that necks are already developed in the saddle-to-scission region for lighter nuclei (small c_{SS}) while a neck is formed only during the latter stage of saddle-to-scission transition in heavier nuclei (large c_{SS}). Therefore, the random force due to η^{asym} operates over the entire stretch of the saddle-to-scission region for lighter nuclei while

123

it is effective only for a part of the saddle-to-scission region for heavier nuclei. On the other hand, the funneling effect of the potential landscape is present for all nuclei over the entire saddle-to-scission region. The above scenario suggests that the net effect in driving a system to higher asymmetry as it evolves from saddle-to-scission will be higher for lighter nuclei than for heavier ones. In fact, comparison of mass variances at saddle and scission in Fig. 6.15 shows that while the mass dispersion grows during saddle-to-scission transition for lighter nuclei, it shrinks for heavier nuclei. It may be pointed out here that the first observation in the above, namely, the reduction of mass variance at scission when η^{asym} is not included in the calculation, was also made in Ref. [180]. In the present work, we are able to make further observations regarding the changes in mass variances during saddle-to-scission transition since the variances at both saddle and scission are obtained from dynamical calculations.

We have considered different compound nuclei in the above in order to study the effect of saddle-to-scission dynamics in FFMD over a broad range of saddle-to-scission distances. The
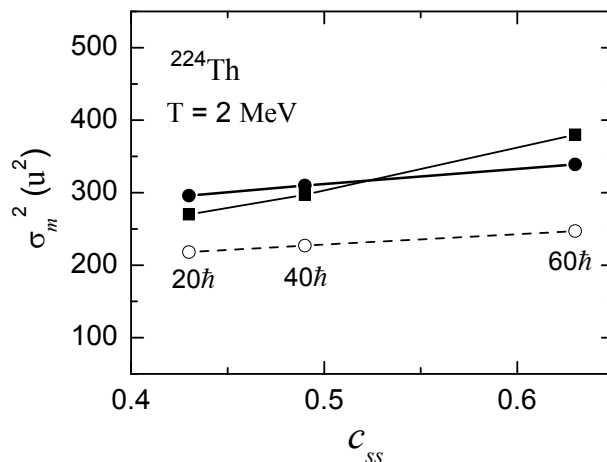
Figure 6.16: The mass variances σ_m^2 calculated with (filled symbols) and without (empty symbols) the η^{asym} term for ^{224}Th at different spins. The circles represent the variances at scission while the squares represent the variances at the saddle. The variances at the saddle for both the cases (with and without η^{asym}) are nearly the same and are indistinguishable in the plot [103]. Lines are drawn to guide the eyes.

saddle-to-scission distance also varies with spin for a given nucleus though over a limited range. The effects are still discernible as shown in Fig. 6.16, where fission fragment mass variances

of ^{224}Th calculated at three different spin values are shown. The mass variances at saddle and scission are found to depend upon c_{SS} in a manner similar to that obtained while considering a set of different compound nuclei.

The stochastic nature of fission dynamics causes a fission trajectory to cross the saddle ridge a number of times in a to-and-fro motion before it reaches the scission line. In addition to the asymmetry distribution due to the last crossing of the saddle ridge by the fission trajectories, we also obtain the mass asymmetry distribution along the saddle ridge for the following cases. First, we calculate the asymmetry distribution by considering only those asymmetry coordinates which correspond to the first crossing of the saddle ridge by the fission trajectories. Keeping
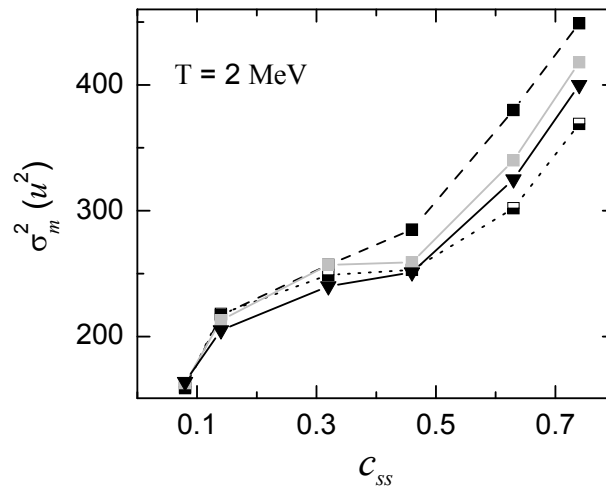
Figure 6.17: The mass variances σ_m^2 corresponding to the first crossing (half-filled square), the last crossing (filled square), and all crossings (gray squares) of the saddle ridge by fission trajectories for different systems. The statistical model predictions are shown by downward triangles [103]. Lines are drawn to guide the eyes.

track of all the successive crossings of the saddle ridge by a fission trajectory, we further calculate the asymmetry distribution by considering the asymmetry coordinates of all such crossings. The corresponding mass variances are given for different systems as a function of c_{SS} in Fig. 6.17. The variances for first and last crossings are found to be very close for small values of c_{SS} while the last crossing values are larger at large c_{SS}. We interpret this observation as follows. In a stochastic process such as nuclear fission, a fission trajectory can return to a more compact

shape even after it crosses the saddle ridge due to the presence of the random forces in the equations of motion. This backstreaming is typical of Brownian motion and has been noted earlier by several authors [27, 105, 174, 168]. In the present analysis of two-dimensional fission dynamics, the scope of to-and-fro motion is highly restricted when the saddle ridge and the scission line are very close together (small c_{SS}). The first and last crossing points of the saddle ridge practically coincide in such cases, giving rise to almost similar distributions. For systems with larger saddle-to-scission separations, however, a larger phase space is available for to-and-fro motion in the saddle region. A fission trajectory therefore experiences the random force for a longer time interval between the first and last crossing of the saddle ridge. Consequently, the system develops higher asymmetry during its evolution from the first crossing to the last crossing of the saddle ridge. We may point out here that the subsequent change in the mass variance of the system as it moves from the saddle to the scission point has already been given earlier in Fig. 6.15.

6.5.1   Comparison with statistical model calculations

We observe in Fig. 6.17 that the variances of distributions considering all crossings lie in between the variances from first and last crossings, as one would expect. The asymmetry distribution obtained from all crossings of the saddle ridge by fission trajectories also corresponds to the average distribution of fission trajectories over the saddle ridge. This distribution is therefore comparable with the predictions of the statistical model. According to the statistical model [168, 184], the yield of fragments with mass asymmetry α' is given as

$$Y(\alpha') = N \exp[-U(\alpha')/T_{sad}] \tag{6.12}$$

where $U(\alpha')$ is the potential profile along the saddle ridge and N is a normalization constant. Here, T_{sad} represents the average temperature on the saddle ridge. The mass variances according to the statistical model are directly obtained from Eq. (6.12) and are given in Fig. 6.17. The variances of average distributions from the dynamical model are found to be very close to the statistical model predictions. This indicates that statistical equilibrium is almost reached in the saddle region in dynamical calculations. We next compare the mass distributions calculated at scission by the statistical and dynamical models. The statistical model values are obtained from a yield distribution as given by Eq. (6.12), where the potential profile along the scission

126

line is used and the average temperature is calculated on the scission line. The inadequacy of
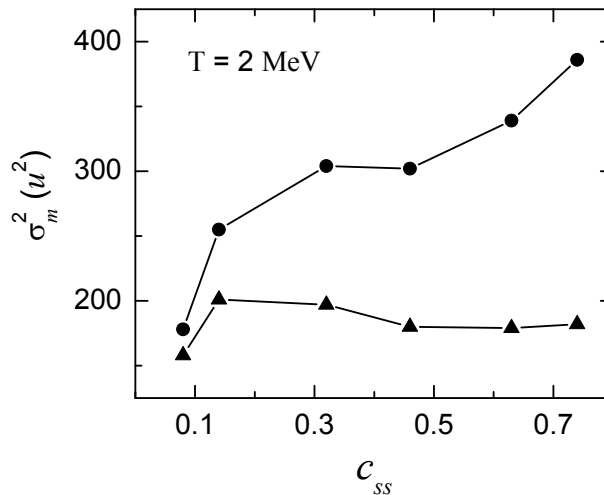

Figure 6.18: The mass variances σ_m^2 at scission from the statistical model (upward triangle) and the dynamical model (circle) for different systems [103]. Lines are drawn to guide the eyes.

the statistical model in predicting the mass variance at scission was shown earlier [117, 180] and it is further illustrated here in Fig. 6.18. The statistical model substantially underestimates the mass variance at scission.

6.6 Summary

In the preceding sections, we have developed a two-dimensional Langevin dynamical model for fission. First, a systematic study of different aspects of dynamical fission width is performed. A comparison with the corresponding Kramers' fission width is also demonstrated. Then, we have studied the growth in shape asymmetry of a fissioning nucleus as it evolves from the ground state to the scission configuration. A number of systems spanning a broad range of saddle-to-scission distances have been considered for this purpose. In particular, the role of the dissipative resistance to change the mass asymmetry degree of freedom (η^{asym}) during the saddle-to-scission transition has been investigated. By comparing the asymmetry coordinate distributions at saddle and scission, it has been shown that while the conservative force guides a CN toward symmetric fission, the random force associated with η^{asym} substantially counteracts it and drives the system toward higher asymmetry during saddle-to-scission transition. This

observation has been made using asymmetry distributions at saddle and scission when both are obtained from dynamical model calculations.

The role of multiple crossing of the saddle ridge by a stochastic fission trajectory in giving rise to the asymmetry coordinate distribution at the saddle has also been investigated. It has been shown that the mass variance increases between the first and the last crossing of the saddle ridge by a fission trajectory. The subsequent development in the asymmetry coordinate distribution as the system approaches scission takes place in a manner as given in the above.

We have also examined the validity of the statistical model in the context of FFMD by comparing the statistical model predictions at the saddle with dynamical model results. It has been shown that the average distribution of fission trajectories over the saddle ridge obtained from the dynamical model closely follows the statistical model predictions.

Chapter 7

Summary, discussions and future outlook

7.1   Summary and discussions

In the present thesis, different aspects of statistical and dynamical models of heavy-ion induced nuclear fission are investigated in detail with the objective to understand the nature of nuclear dissipation and its importance in the fission dynamics. A general overview of the theoretical models and their applications in the study of fission processes is presented in Chapter 1. Specifically, we have elaborated on the two different chronological scenarios corresponding to the developments which happened before and after the advent of dissipative dynamics in the study of fission. We next discussed, in Chapter 2, the Langevin dynamical model for fission and the collective properties of an excited nucleus required for the dynamical calculations. The one-dimensional Langevin dynamical calculations are applied as benchmark in the subsequent chapters.

In Chapter 3, a statistical model calculation for the decay of a compound nucleus is presented where the compound nuclear spin dependence of the Kramers' modified fission width is included [108]. Specifically, the spin dependences of the frequencies of the harmonic oscillator potentials osculating the rotating liquid-drop model potential at equilibrium and saddle regions are considered. First, the method of obtaining these frequencies is explained with the

view that the approximated potential resembles closely the corresponding liquid drop model potential over a wide range of nuclear deformation. Subsequently, statistical model calculations are performed for the $^{16}O + ^{208}Pb$ system. Results show that the energy dependence of the dissipation strength extracted from fitting experimental data is substantially reduced when the spin dependence of the frequencies is properly taken into account.

In Chapter 4, it is shown that Kramers' fission width, originally derived for a system with constant inertia, can be extended to systems with a deformation-dependent collective inertia, which is the case for nuclear fission. The predictions of Kramers' width for systems with slowly varying inertia are found to be in very good agreement with the stationary fission widths obtained by solving the corresponding Langevin equations [27]. In general, the inertia associated with a collective coordinate depends on the choice of the collective coordinate and the underlying microscopic motion. We therefore extend the work on shape-dependent inertia and obtain an expression for stationary fission width for systems with steep shape-dependent nuclear collective inertia [109]. The domain of validity of this modified expression is examined by comparing its predictions with widths obtained from the corresponding Langevin equations.

In Chapter 5, we have examined the validity of extending Kramers' expression for fission width to systems with shape-dependent dissipations [110]. For a system with a shape-dependent dissipation, Kramers' width obtained with the presaddle dissipation strength is found to be different from the stationary width obtained from the corresponding Langevin equations. It is demonstrated that the probability of a hot compound nucleus undergoing fission depends on both the presaddle and the postsaddle dynamics of collective nuclear motion. The predictions for prescission neutron multiplicity and evaporation residue cross section from statistical model calculations are also found to be different from those obtained from Langevin dynamical calculations when a shape-dependent dissipation is considered. For systems with shape-dependent dissipations, we conclude that the strength of presaddle dissipation determined by fitting experimental data in statistical model calculations does not represent the true strength of presaddle dissipation.

In Chapter 6, the fragment mass distribution from fission of hot nuclei is studied in the framework of two-dimensional Langevin equations. The mass asymmetry coordinate distribution is obtained from the dynamical calculation both at the saddle and the scission regions in order to investigate the role of saddle-to-scission dynamics in fission fragment mass distribution [103]. First, the collective properties are calculated in two dimensions. Subsequently, Langevin dynamical trajectories are obtained on the two-dimensional potential contours of different nuclei having a broad range of saddle-to-scission distances. Role of different dynamical forces in the fission fragment mass distribution during the saddle-to-scission transition are then examined quantitatively. Before that, a systematic study of the two-dimensional fission width is also presented in this chapter. At the end, statistical model predictions of mass asymmetry distributions at saddle and scission are compared with the dynamical model results. we point out that the observed near cancellation of the effects due to conservative and random forces during the descent of a CN from saddle to scission in determining the fission fragment mass distribution is specific to the collective fission coordinates and the nature of dissipation used in the present work. Questions may naturally arise regarding the consequences of including more collective degrees of freedom or changing the nature of dissipation on the saddle-to-scission dynamics and the resulting fission fragment mass distribution. It was shown earlier [181] that inclusion of the neck degree of freedom substantially increases the most probable fission path from saddle to scission. Consequently, one may expect that a fission trajectory will be subjected to random forces for a longer period, giving rise to a larger mass dispersion. The saddle-to-scission dynamics also changes when one considers a non-Markovian dissipation (and random force) instead of the Markovian dissipation used in the present work. By considering non-Markovian stochastic dynamics of fission, it has been shown [83] that the mean descent time from saddle to scission increases with the relaxation time of the collective coordinates. Thus the introduction of non-Markovian features in stochastic fission dynamics is also expected to increase the fission fragment mass variance. Evidently, more calculations are needed to explore the role of saddle-to-scission descent under different stochastic dynamical models in giving rise to the fission fragment mass distribution.

7.2   Future outlook

Our studies on the statistical and dynamical models of fission open up the following directions of research which can be attempted in future. In the present thesis, the conservative force for the fission dynamics is extracted from the finite range liquid drop model potential. To be more realistic, proper thermodynamic potential can be used for the dynamical evolution instead of the internal energy which is usually calculated from a liquid drop model. Dynamical model calculations are preformed [117] now a days using the free energy as the thermodynamic potential. A statistical model calculation is also developed [105] following the same consideration. However, for these type of calculations, one need to know the shape dependence of the level density parameter very accurately. Also, the choice of a particular thermodynamic potential in case of fission dynamics is not unique [185]. Nevertheless, if free energy is considered instead of liquid drop model potential then the nuclear potential profile becomes flatter along the fission degree of freedom and hence fission happens to be a faster process. As a result, larger dissipation strength will be required to reproduce the experimental data. However, the main findings of the present thesis are expected to remain unchanged with this modification.

Theoretically it is observed [186] that the dynamical fission width increases with the increase in the number of collective degrees of freedom. It therefore gives us the opportunity to study the effects due to the dimensionality of the dynamical modeling on various fission observables. Three dimensional Langevin dynamical calculations have already been performed [99, 101, 117]. Recently, a five-dimensional dynamical model is also developed [79] for strongly damped shape evolution. To this end, our Langevin dynamical model can be extended to perform more realistic calculations by including larger number of collective coordinates. In this way, we can also study the relative importance of different collective coordinates in different fission observables.

One of the major thrusts in the study of heavy-ion induced fusion-fission reactions is the proper estimation of nuclear dissipation. It was found [108] that different values of dissipation strength are required to reproduce the experimental results on the evaporation residue cross section and prescission neutron multiplicity. Consequently, shape dependent dissipation strength was invoked [78] to obtain both of these observables simultaneously. These studies established the importance of shape dependence in nuclear dissipation. However, the shape dependences,

obtained in the above investigations, were completely phenomenological in nature. In a subsequent study, chaos weighted wall friction was introduced [97], where the shape-dependent dissipation of similar nature was observed. All these preceding studies motivate the microscopic quantum mechanical calculation of nuclear dissipation [67] and its application in the fission dynamics.

Another aspect, which is very essential from the perspective of studies related to the super heavy elements and the exotic nuclei, is the incorporation of shell effects in the nuclear potential. A complete microscopic calculation of nuclear potential gives the shell correction in the liquid drop potential, which in effect predicts the existence of super heavy elements. On the other hand, fission is a dominant decay channel for the super heavy elements. For the exotic nuclei, the information regarding the nuclear potential, as well as the inter-nucleonic interactions, are not known very accurately and hence the microscopic models are needed to be tested. Along these lines, nuclear potentials are estimated recently by using microscopic density functional theory [185]. To proceed further, one has to implement theoretical models for the nuclear decay by including microscopic potentials. However, this remains to be tested quantitatively in dynamical calculations.

Appendix A: Evaluation of the nuclear potential

In the present thesis, we have used the finite range liquid drop model (FRLDM) to calculate the nuclear potential energy. In this model, the nuclear density is considered to be uniform within the nuclear surface. Then, the generalized nuclear energy is obtained by double-folding this density with a Yukawa-plus-exponential potential. The six-dimensional double-folding integral for evaluation of the potential is as follows:

$$I = \int d^3 r_1 d^3 r_2 f(\vec{r_1}) f(\vec{r_2}) v(|\ \vec{r_1} - \vec{r_2}\ |) \tag{A.1}$$

where f and v gives the nuclear density and two-body interaction potential, respectively. To calculate I we follow the Fourier transform technique described in the Ref. [66], where it is used to calculate the FRLDM potential for the symmetric nuclear shapes. In the present work, we extend the calculation to asymmetric nuclear shapes. The above integral in Eq. (A.1) reduces to a integral of lower dimensions by the Fourier transform method. The Fourier transform of the charge densities and the two-body interaction are given in k space by the following relations:

$$
\begin{aligned}
f(\vec{r_1}) &= \frac{1}{(2\pi)^3} \int d^3 k_1 e^{-i\vec{k_1}\cdot\vec{r_1}} \tilde{f}(\vec{k_1}) \\
f(\vec{r_2}) &= \frac{1}{(2\pi)^3} \int d^3 k_2 e^{-i\vec{k_2}\cdot\vec{r_2}} \tilde{f}(\vec{k_2}) \\
v(|\ \vec{r_1} - \vec{r_2}\ |) &= \frac{1}{(2\pi)^3} \int d^3 k e^{-i\vec{k}\cdot(\vec{r_1}-\vec{r_2})} \tilde{v}(\vec{k}).
\end{aligned}
$$

Substituting the above expressions in the Eq. (A.1), the six dimensional integral reduces to a three dimensional integral as

$$I = \frac{1}{(2\pi)^3} \int d^3 k \tilde{f}(\vec{k}) \tilde{f}(-\vec{k}) \tilde{v}(\vec{k}). \tag{A.2}$$

To derive the above expression, we exploit the properties of the following delta function relations:

$$\int d^3 r_1 e^{-i(\overrightarrow{k}_1 + \overrightarrow{k}) \cdot \overrightarrow{r}_1} = (2\pi)^3 \delta(\overrightarrow{k}_1 + \overrightarrow{k})$$

$$\int d^3 r_2 e^{-i(\overrightarrow{k}_2 - \overrightarrow{k}) \cdot \overrightarrow{r}_2} = (2\pi)^3 \delta(\overrightarrow{k}_2 - \overrightarrow{k}).$$

If potential is of the Coulomb form, i.e., $v(\vec{r}) = 1/r$, then it can be shown using contour integration that $\tilde{v}(\vec{k}) = \frac{4\pi}{k^2}$. If the potential takes the exponential form, i.e., $v(\vec{r}) = e^{-\mu r}$, then $\tilde{v}(\vec{k}) = \frac{8\pi\mu}{(\mu^2 + k^2)^2}$. For Yukawa type of potential, i.e., $v(\vec{r}) = e^{-\mu r}/r$, $\tilde{v}(\vec{k}) = \frac{4\pi}{(\mu^2 + k^2)}$. The quantities $\tilde{f}(\vec{k})$ and $\tilde{f}(-\vec{k})$ are evaluated in cylindrical coordinate system. Due to axial symmetry in $f(\vec{r})$, $\tilde{f}(\vec{k})$ and $\tilde{f}(-\vec{k})$ will also have axial symmetry in k space. Assuming $\vec{k}$ to lie in $(y-z)$ plane, it can be shown that $\vec{k} \cdot \vec{r} = \rho k_\rho \cos\phi + z k_z$. Hence in cylindrical coordinate system,

$$\tilde{f}(\vec{k}) = \tilde{f}(k_\rho, k_z) = \int e^{(i\rho k_\rho \cos\phi + i z k_z)} f(\rho, z) \rho \, d\rho \, dz \, d\phi$$

$$\tilde{f}(-\vec{k}) = \tilde{f}(k_\rho, -k_z) = \int e^{(i\rho k_\rho \cos\phi - i z k_z)} f(\rho, z) \rho \, d\rho \, dz \, d\phi. \tag{A.3}$$

It is known from the properties of Bessel function, that

$$\int_0^{2\pi} e^{(i\rho k_\rho \cos\phi)} d\phi = 2\pi J_0(\rho k_\rho) \tag{A.4}$$

where J_0 is the zeroth order Bessel function. Then, for a uniform density ($f(\rho, z) = $ constant) within the defined surface, we get

$$\tilde{f}(\vec{k}) = \int_{-z_{max}}^{z_{max}} \exp(i z k_z) \frac{1}{k_\rho^2} I_2(k_\rho \rho(z)) dz$$

$$\tilde{f}(-\vec{k}) = \int_{-z_{max}}^{z_{max}} \exp(-i z k_z) \frac{1}{k_\rho^2} I_2(k_\rho \rho(z)) dz \tag{A.5}$$

where

$$I_2(\beta) = \int_0^\beta I_1(x) x \, dx \tag{A.6}$$

and

$$I_1(x) = 2\pi J_0(x). \tag{A.7}$$

$I_1(x)$ is calculated for $x = 0$ to x_{max}, where $x = \rho k_\rho$, and using these values of $I_1(x)$, $I_2(\beta)$ is calculated for β ranging from 0 to β_{max} ($\beta = \rho k_\rho$). The integral $I_2(\beta)$ is evaluated at small

135

intervals of the argument and the required value at any β is extracted later by interpolating from the table. The function $I_2(\beta)$ is thus required to be computed only once and can be used as a standard input for any subsequent double folding calculation. These values are used to evaluate $\tilde{f}(\vec{k})$ and $\tilde{f}(-\vec{k})$ in Eq. (A.5) and their product can be written as

$$\tilde{f}(\vec{k})\tilde{f}(-\vec{k}) = A^2 + B^2 \tag{A.8}$$

with

$$A = \int_{-z_{max}}^{z_{max}} \cos{(zk_z)}\frac{1}{k_\rho^2}I_2(k_\rho\rho(z))dz \quad and \quad B = \int_{-z_{max}}^{z_{max}} \sin{(zk_z)}\frac{1}{k_\rho^2}I_2(k_\rho\rho(z))dz. \tag{A.9}$$

The integral in Eq. (A.2) is finally evaluated in spherical polar coordinates. This is done for numerical convenience so that convergence can be obtained with respect to only one coordinate. The final form of Eq. (A.2) is given by

$$I = \frac{1}{(2\pi)^2} \int_0^\pi \int_0^{k_{max}} k^2 dk \sin{\theta} d\theta (A^2 + B^2)\tilde{v}(k). \tag{A.10}$$

The upper cut-off k_{max} is chosen after ensuring a very good convergence of the integral. The k integration is done by dividing the range in two parts, i.e, from 0 to k_1 and k_1 to k_2. Since the integrand for lower values of k is highly oscillating, the integration here (from 0 to k_1) is done with very small step size, while for the second part (from k_1 to k_2), the integration is performed with a bigger step size. The stability of the potential calculation by this method is of the order of 1 in 10^8.

Appendix B: The dynamical and statistical model codes for fission

B.1   Introduction

After the formation of a fully equilibrated compound system in a heavy-ion fusion reaction, the decay of the compound nucleus (CN) can follow two different routes. In the first route the nucleus undergoes fission, i.e, it predominantly separates into two heavy fragments (binary fission) which is called a fusion-fission process. During a fission process, the intermediate system evaporates light particles (n, p, α) and statistical γ-rays until the scission configuration is reached. These evaporated particles are called pre-scission particles. Then, after the fission has happened, the heavy fission fragments are still excited enough to continue the evaporation of light particles and γ-quanta. These are called the post-scission particles. It is possible to distinguish experimentally between the pre- and post-scission particles. Along the second decay route the nucleus does not undergo fission and the excitation of the CN is removed solely by the evaporation of light particles and γ-rays. The evaporation of light particles of a particular kind stops when the excitation energy has dropped to a value below the corresponding binding energy. The deexcitation of the system thus ends with the formation of the so-called evaporation residue. A schematic diagram for the decay of a CN is shown in Fig. B.1. For γ-rays the emission process continues until Yrast-line is reached. During the formation process of the compound system, some light particles can also be emitted, which are of increasing importance with increasing bombarding energy. These particles are called pre-equilibrium particles. Since our model starts from the formation of a equilibrated CN, we do not have the opportunity to take into account these pre-equilibrium particles. On the other hand, in a heavy-ion induced reaction, the intermediate compound system may decay without forming a fully equilibrated
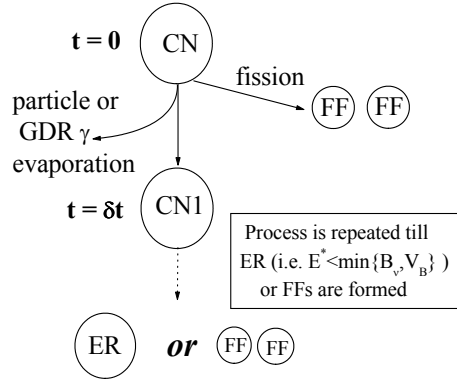
137

Figure B.1: A schematic diagram of the decay of an excited CN.

compound system. Such a process is categorized as the fast-fission or the quasi-fission. In our model we always assume that an equilibrated CN is formed and, hence, the possibilities of fast-fission and quasi-fission are not considered.

B.2 Initial condition

The dynamical and statistical model calculations are event-by-event simulation of the decay of an ensemble of CN formed with different values of spin (ℓ). In a particular event, the state of the CN is completely specified by (A, Z, E^*, ℓ) where A and Z are mass number and atomic number of the CN, respectively. E^* is the initial excitation energy calculated at the ground-state configuration of the CN and it can be written as

$$E^* = E_{cm} - Q - V_{gs}(\ell) - \delta$$
$$Q = \triangle_{CN} - (\triangle_{Target} + \triangle_{Projectile}) \tag{B.1}$$

where E_{cm} is the center of mass energy for the target-projectile combination, $V_{gs}(\ell)$ is the ground-state potential with ℓ as the compound nuclear spin and $\triangle$ is the mass defect of the respective nuclei and it is taken from Ref. [187]. The quantity δ is the pairing energy of the CN. For the dynamical calculations, initial collective momenta are sampled from a Gaussian distribution function and the associated kinetic energy is also subtracted form E_{cm} in Eq. (B.1) to get E^*. The spin ℓ is sampled from the distribution,

$$\frac{d\sigma(\ell)}{d\ell} = \frac{\pi}{k^2} \frac{(2\ell + 1)}{1 + \exp\left(\frac{\ell - \ell_c}{\delta\ell}\right)} \tag{B.2}$$

138

where k is the wavenumber for the relative motion of the target-projectile combination. Here, ℓ_c and $\delta\ell$ are obtained by reproducing the experimental total fusion cross section σ which is given by $\int [d\sigma(\ell)/d\ell]d\ell$. Equation (B.2) represents the simplest model for the fusion spin-distribution. However, one can use other distributions like that obtained with a Coupled-Channel calculation for this purpose.

B.3 Light-particles and statistical γ-ray emissions

In the present statistical and dynamical models, neutron, proton and α emissions are considered as possible evaporation channels in competition with fission. The emission of a particle of type ν (neutrons, protons and α-particles) is governed by the partial decay width Γ_ν which is defined as $\Gamma_{nu} = \hbar/\tau_\nu$, τ_{nu} being the corresponding decay time. Several theoretical approaches have been proposed in order to describe the emission from a deformed, highly excited and rotating nucleus [90, 188, 189]. In the present work, we have used the statistical theory of Weisskopf [38], where the partial decay width for emission of a light particle of type ν is given by

$$\Gamma_\nu = (2\ell_\nu + 1)\frac{m_\nu}{\pi^2\hbar^2\rho_{CN}(E^*)}\int_0^{E^*-B_\nu-\Delta E_{rot}} d\varepsilon_\nu \rho_R(E^* - B_\nu - \Delta E_{rot} - \varepsilon_\nu)\varepsilon_\nu\sigma_{inv}(\varepsilon_\nu) \quad \text{(B.3)}$$

where ℓ_ν is the spin of the emitted particle ν and m_ν is its reduced mass with respect to the residual nucleus. B_ν and ε_ν are the binding energy and the kinetic energy of the emitted particle, respectively. The change of the rotational energy due to the angular momentum carried away by the rotating particle is denoted by ΔE_{rot}. In the above expression, ρ_{CN} and ρ_R are the density of states at the ground-state configurations of the CN and the residual nuclei, respectively. The quantities required to calculate the Γ_ν are described in the following paragraphs.

The expression for the binding energy B_ν is given by

$$B_\nu = (B.E.)_{A-A_\nu,Z-Z_\nu} - (B.E.)_{A,Z} \quad \text{(B.4)}$$

where A_ν and Z_ν are the mass number and charge of the emitted particle. The binding energy $((B.E.)_{A,Z})$ of a nucleus with mass number A, proton number Z and neutron number N is given by the liquid drop model of Myers and Swiatecki [41] which is given by the following expression:

$$(B.E.)_{A,Z} = -c_1 A + c_2 A^{2/3} + \frac{c_3 Z^2}{A^{1/3}} - \frac{c_4 Z^2}{A} + \Delta \quad \text{(B.5)}$$

where

$$c_1 = 15.677 \left[1 - 1.79 \left(\frac{A - 2Z}{A} \right)^2 \right]$$

$$c_2 = 18.56 \left[1 - 1.79 \left(\frac{A - 2Z}{A} \right)^2 \right] \tag{B.6}$$

$c_3 = 0.717$ and $c_4 = 1.2113$. The first term on the r.h.s of Eq. (B.5), i.e., $c_1 A$ is the sum of the volume energy term which is proportional to the mass number A and the volume-asymmetry energy term which is proportional to $(A - 2Z)^2/A$. The second term $c_2 A^{2/3}$ is the sum of the surface energy term being proportional to $A^{2/3}$ and the surface asymmetry energy term proportional to $I^2 A^{2/3}$ where I equals $(A - 2Z)/A$. The third term $c_3 Z^2/A^{1/3}$ is the direct sharp-surface Coulomb energy whereas $c_4 Z^2/A$ gives the surface-diffuseness correction to the direct Coulomb energy. Δ gives the pairing energy correction and is given by the following formulas:

$$\begin{aligned} \Delta &= -\frac{11}{\sqrt{A}} && \text{for even-even nuclei,} \\ &= 0 && \text{for even-odd or odd-even nuclei,} \\ &= +\frac{11}{\sqrt{A}} && \text{for odd-odd nuclei.} \end{aligned} \tag{B.7}$$

The level densities of the CN and the residual nucleus are denoted by $\rho_{CN}(E^*)$ and $\rho_R(E_{int} - B_\nu - \Delta E_{rot} - \varepsilon_\nu)$, respectively, and are given by Eq. (1.4). Following the Ref. [40, 190], the inverse cross section can be written as

$$\begin{aligned} \sigma_{inv}(\varepsilon_\nu) &= \pi R_\nu^2 (1 - V_\nu/\varepsilon_\nu) && (\text{for} && \varepsilon_\nu > V_\nu) \\ &= 0 && (\text{for} && \varepsilon_\nu < V_\nu) \end{aligned} \tag{B.8}$$

with

$$R_\nu = 1.21[(A - A_\nu)^{1/3} + A_\nu^{1/3}] + (3.4/\varepsilon_\nu^{1/2})\delta_{\nu,n}, \tag{B.9}$$

The Coulomb barrier is zero for neutron whereas for the charged particles the barrier is given by

$$V_\nu = [(Z - Z_\nu)Z_\nu K_\nu]/(R_\nu + 1.6) \tag{B.10}$$

with $K_\nu = 1.32$ for α and 1.15 for proton.

For the emission of GR γ we take the formula given by Lynn [191]

$$\Gamma_\gamma = \frac{3}{\rho_c(E^*)} \int_0^{E_{int}-\Delta E_{rot}} d\varepsilon \rho_R(E_{int} - \Delta E_{rot} - \varepsilon) f(\varepsilon) \qquad (B.11)$$

with

$$f(\varepsilon) = \frac{4}{3\pi} \frac{1+\kappa}{mc^2} \frac{e^2}{\hbar c} \frac{NZ}{A} \frac{\Gamma_G \varepsilon^4}{(\Gamma_G \varepsilon)^2 + (\varepsilon^2 - E_G^2)^2} \qquad (B.12)$$

with $\kappa = 0.75$, and E_G and Γ_G are the position and width of the giant dipole resonance. In the present thesis, $E_G = 80.0 A^{-1/3} \text{MeV}$ and $\Gamma_G = 5.0 \text{MeV}$ are considered. For the dynamical model calculations, we first check whether an emission process occurs or not in between two successive time steps. The Monte-Carlo sampling technique is used in this purpose. Then, in case of any decay, a particular decay channel is selected by performing another Monte-Carlo sampling between all the particles and γ emission widths. Subsequently, all the input quantities are adjusted accordingly for the successive time steps. However, the values of the collective coordinates are kept unchanged during the evaporation process.

On the other hand, in a statistical model calculation, the fission width (Γ_f) can be calculated either by using the Bohr-Wheeler theory [Eq. (1.4)] or one can incorporate nuclear dissipation by using the stationary fission width from Kramers' formula [Eq. (1.51)]. In our statistical model code, the evolution of the compound nuclear state (A, Z, E^*, ℓ) is followed with time. Therefore, a time-dependent fission width can be used in order to account for the transient time period that elapses before the stationary value of the Kramers' modified width is reached. A parameterized form of the dynamical fission width is given as [156]

$$\Gamma_f(t) = \Gamma_f(t \to \infty)[1 - \exp{-2.3t/\tau_f}] \qquad (B.13)$$

where τ_f is the transient time.

A comparison between the different particle decay widths, γ-decay width and stationary fission width is shown as functions of excitation energy of CN in Fig. B.2 for three different values of ℓ. The fission width (Γ_f) shown here is calculated with the Bohr-Wheeler formula. The competition between neutron and fission width is the main determining factor in deciding the
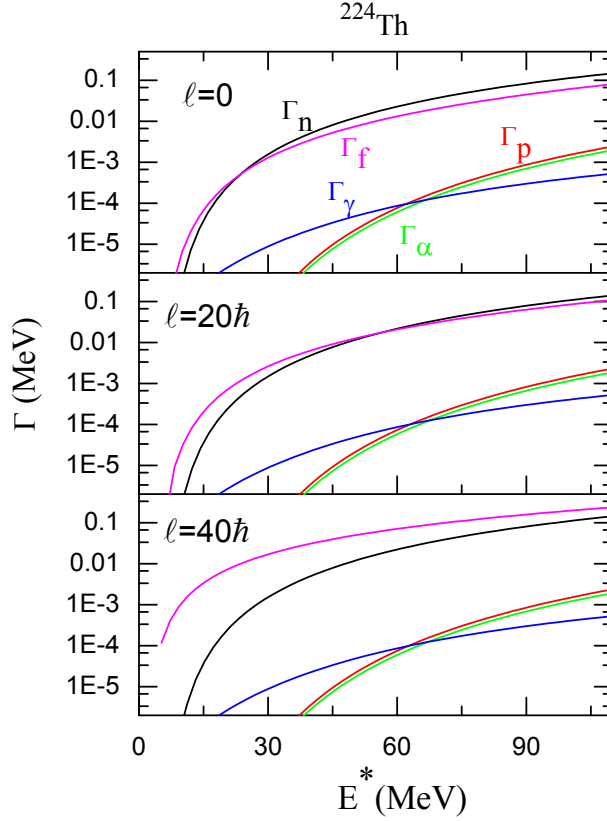
Figure B.2: Different decay widths as functions of E^*.

fate of the CN. At low angular momentum, fission width Γ_f is less than the neutron width Γ_n but with rise of angular momentum the two widths become comparable. These widths depend upon the temperature, spin and the mass number of the CN and hence are to be evaluated at each interval of time evolution of the fissioning nucleus.

B.4 Decay algorithm for statistical model

Once the emission widths and the fission width are known, it is required to establish the decay algorithm which decides at each time step whether the system undergoes fission or a particle is being emitted from the CN. This is done by first calculating the ratio $x = \delta t/\tau_{tot}$ where $\tau_{tot} = \hbar/\Gamma_{tot}(t)$, $\Gamma_{tot}(t) = \sum_\nu \Gamma_\nu + \Gamma_f(t)$, and $\nu \equiv n, p, \alpha, \gamma$. The probability for emitting any light particle or γ is given, for a small enough time step δt, by

$$P(\delta t) = 1 - e^{-\delta t/\tau_{tot}} \approx x. \tag{B.14}$$

142

We then choose a random number r_1 by sampling it from a uniformly distributed set between 0 and 1. If we find $r_1 < x$, it is interpreted as either an emission process or fission during that interval. If the time step δt is chosen sufficiently small, the probability of a decay is small and it guarantees that in each time interval more than one decay process is prohibited. If a decay process happens within δt then a particular decay channel is selected by another Monte-Carlo sampling. Otherwise, the above steps are repeated for the next time step δt. In case of particle or γ evaporation the energy of the emitted particle or γ is obtained by another Monte Carlo sampling of its energy spectrum by choosing another random number following a probability distribution given by the energy distribution laws in Eqs. (B.3) and (B.11). The intrinsic excitation energy, mass, charge and spin of the CN are recalculated after each emission and also the potential energy landscape of the parent nucleus is replaced by that of the daughter nucleus. The magnitude of the angular momentum taken away by a statistical γ-ray is always unity. For particle evaporation, the magnitude of the angular momentum quantum number of the emitted particle is given by [190]

$$\ell_\nu = \ell_{max}\sqrt{\mathcal{R}} \tag{B.15}$$

where $\mathcal{R}$ is a uniform random number between 0 and 1 and

$$\ell_{max} = 0.187(2\mu_\nu\epsilon_\nu)^{\frac{1}{2}}R_\nu\left(1 - \frac{V_\nu}{\epsilon_\nu}\right). \tag{B.16}$$

The angular momentum quantum number of the daughter (ℓ') is sampled between $|\ell - \ell_\nu|$ and $(\ell + \ell_\nu)$ with a probability proportional to the available phase space of the daughter at that value of ℓ'. After assigning the new intrinsic state to the daughter, the same processes as described above are repeated. On the other hand, if fission occurs then the mass, charge and the excitation energy of the CN are divided into two parts for the two fission-fragments. An excited fission fragment decays mainly through neutron evaporation till the excitation energy reduces below the last neutron separation energy. During this process the kinetic energy of the evaporated neutrons are sampled from the corresponding energy spectrum.

An event is completed when the CN undergoes fission or the evaporation residue (when $E^* < V_B$, the fission barrier) is formed. If an event neither fissions nor reaches criterion for the evaporation residue within the total time t_{max} specified for the statistical model calculation, then the calculation is stopped there with the fate of the trajectory still undecided. However,
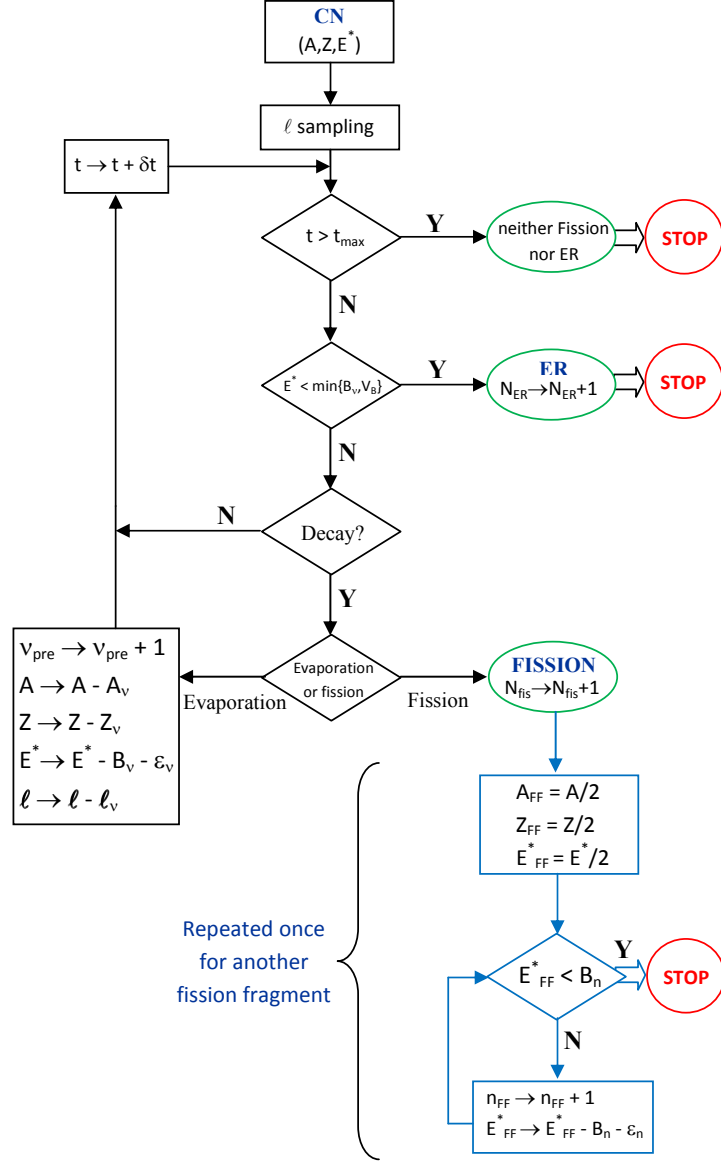
Figure B.3: The flow-chart for an event of the statistical model code. Here, ν specifies the type of the particle evaporated and $A_\nu = Z_\nu = B_\nu = 0$ in case of γ emission.

t_{max} is taken to be sufficiently long so that the number of such undecided trajectories is statistically insignificant. The flow-chart for an event is sketched in Fig. B.3. The code is executed for a large number of events and, in each event, different observables like the particle multiplicities, ER spin and the spin of the evaporated particle etc. are recorded. Finally, the averages of these quantities are taken over a large number of events to reproduce the experimental results with negligibly small statistical fluctuations.

144

B.5 Decay algorithm for dynamical model

The decay algorithm for a dynamical model is similar to the one which is followed in the statistical model, except the fact that the fission event is now decided through dynamical shape evolution of the CN. Therefore, Γ_{tot} required for Eq. (B.14) is given by $\sum_\nu \Gamma_\nu$. As discussed earlier, a fixed value for the time step $\delta t = 0.0005 \, \hbar/\text{MeV}$ is chosen for the dynamical calculations and hence very large amount of computation time is required if the whole evolution
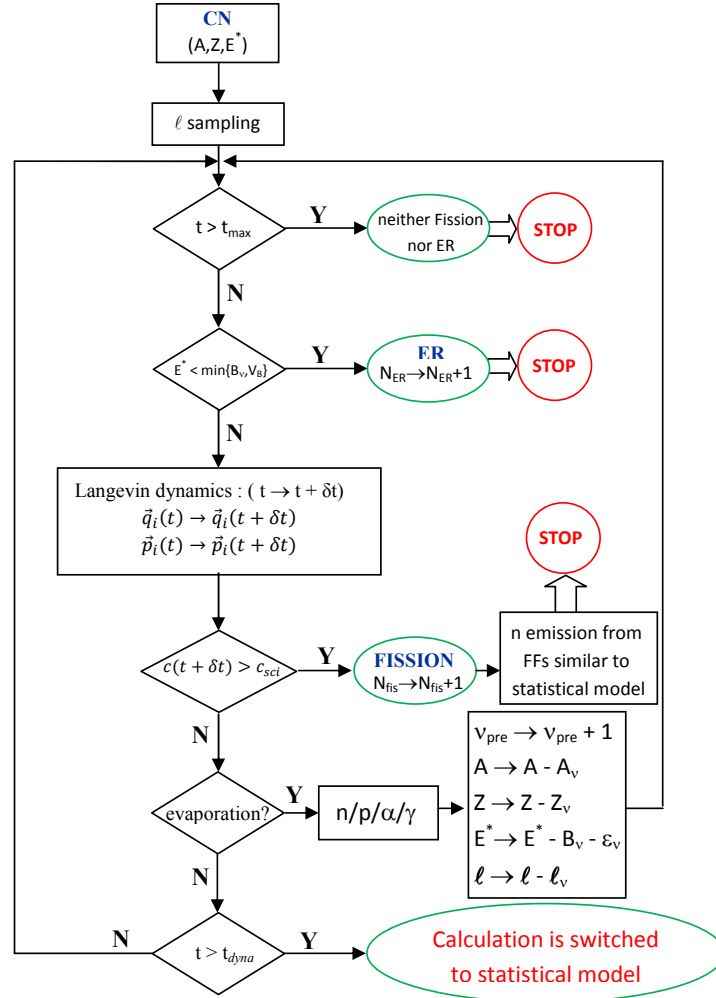

Figure B.4: The flow-chart for an event of the dynamical model code.

up to t_{max} is followed dynamically. To overcome this difficulty, the calculation is switched to the statistical model code if fission does not occur within a time t_{dyna}. The value of $t_{dyna} \approx 100$ $\hbar/\text{MeV}$ which is sufficiently large so that the fission width reaches a stationary value. In the

statistical model part, the fission width is determined either by using the Kramers' formula or it can be interpolated from previously calculated Langevin dynamical widths. The flow-chart of a Langevin dynamical event is given in Fig. B.4.

Bibliography

[1] E. Fermi, Nature **133**, 898 (1934).

[2] E. Amaldi, O. D'Agostino, F. Rassetti, and E. Sergè, Proc. Roy. Soc. A146, 483 (1934).

[3] O. Hahn and F. Strassmann, Naturwiss. **27**, 11 (1939).

[4] L. Meitner and O. R. Frisch, Nature **143**, 239 (1939).

[5] O. R. Frisch, Nature **143**, 276 (1939).

[6] L. Meitner and O. R. Frisch, Nature **143**, 471 (1939).

[7] E. Feenberg, Phys. Rev. **55**, 504 (1939); J. Frenkel, Phys. Rev. **55**, 987 (1939); G. Young, Phys. Rev. **55**, 1102 (1939).

[8] N. Bohr and J. A. Wheeler, Phys. Rev. **56**, 426 (1939).

[9] N. Bohr, Nature **143**, 330 (1939).

[10] P. Demetriou and S. Goriely, Nucl. Phys. A **695**, 95 (2001).

[11] S. Hilaire and S. Goriely, Nucl. Phys. A **779**, 63 (2006).

[12] B. Nerlo-Pomorska and K. Pomorski, Int. J. Mod. Phys. E **15**, 471 (2006).

[13] B. Nerlo-Pomorska, K. Pomorski, and J. Bartel, Phys. Rev. C **74**, 034327 (2006).

[14] B. Nerlo-Pomorska, K. Pomorski, J. Bartel, and K. Dietrich, Phys. Rev. C **66**, 051302(R) (2002).

[15] T. D. Newton, Can. J. Phys. **34**, 804 (1956); B. Krusche and K. P. Lieb, Phys. Rev. C **34**, 2103 (1986); A. J. Koning, S. Hilaire, and S. Goriely, Nucl. Phys. A **810**, 13 (2008).

[16] A. Gilbert and A. G. W. Cameron, Can. J. Phys. **43**, 1446 (1965).

[17] H. A. Bethe, Rev. Mod. Phys. **9**, 69 (1937).

[18] A. Bohr and B. R. Mottelson, Nuclear structure Vol. I (Benjamin Press, New York, 1969).

[19] J. P. Lestone, Phys. Rev. Lett. **70**, 2245 (1993); I. Diószegi, D. J. Hofman, C. P. Montoya, S. Schadmand, and P. Paul, Phys Rev C **46**, 627 (1992).

[20] A. V. Ignatyuk, G. M. Smirenkin, and A. S. Tishin, Sov. J. Nucl. Phys. **21**, 255 (1975).

[21] J. Tōke and W. J. Światecki, Nucl. Phys. **A372**, 141 (1981).

[22] W. Reisdorf, Z. Phys. A **300**, 227 (1981).

[23] R. Balian and C. Bloch, Ann. Phys. **60**, 401 (1970); R. Balian and C. Bloch, Ann. Phys. **64**, 271 (1971); R. Balian and C. Bloch, Ann. Phys. **69**, 76 (1972).

[24] K. T. Brinkmann, A. L. Caraley, B. J. Fineman, N. Gen, J. Velkovska, and R. L. McGrath, Phys. Rev. C **50**, 309 (1994).

[25] L. Corradi *et al.*, Phys. Rev. C **71**, 014609 (2005).

[26] K. Mahata, S. Kailas, and S. S. Kapoor, Phys. Rev. C **74**, 041301(R) (2006).

[27] J. Sadhukhan and S. Pal, Phys. Rev. C **79**, 064606 (2009).

[28] L. A. Turner, Rev. Mod. Phys. **12**, 1 (1940).

[29] S. Frankel and N. Metropolis, Phys. Rev. **72**, 914 (1947).

[30] D. L. Hill, Phys. Rev. **79**, 197 (1950).

[31] P. Fong, Phys. Rev. **89**, 332 (1953).

[32] V. M. Strutinsky, Yad. Fiz. **3**, 614 (1966); V. M. Strutinsky, Nucl. Phys. A **95**, 420 (1967); V. M. Strutinsky, Nucl. Phys. A **122**, 1 (1968).

[33] P. Moller and J. R. Nix, IAEA Third Symp. Phys. and Chem. of Fission, Rochester (Paper SM-174/202) (1973).

[34] M. G. Mustafa, U. Mosel, and H. W. Schmitt, Phys. Rev. C **7**, 1519 (1973).

[35] P. Fong, Phys. Rev. **102**, 434 (1956); P. Fong, Phys. Rev. Lett. **11**, 375(1963); P. Fong, Phys. Rev. C **10**, 1122(1974).

[36] H. J. Specht, Rev. Mod. Phys. **46**, 773 (1974).

[37] D. L. Hill and J. A. Wheeler, Phys. Rev. **89**, 1102 (1953).

[38] V. Weisskopf, Phys. Rev. **52**, 295 (1937).

[39] F. Puhlhofer, Nucl. Phys. A **280**, 267 (1977).

[40] M. Blann, M. Beckerman, Nucleonika **23**, 34 (1978).

[41] W. D. Myers, W. J. Swiatecki, Nucl. Phys. **81**, 1 (1966).

148

[42] J. R. Nix and W. J. Swiatecki, Nucl. Phys. **71**, 1 (1964).

[43] A. Gavron *et al.*, Phys. Rev. Lett. **47**, 1255 (1981), erratum: **48**, 835 (1982).

[44] P. Grangé and H. A. Weidenmüller, Phys. Lett. B **96**, 26 (1980).

[45] P. Grangé, Li Jun-Qing, and H. A. Weidenmüller, Phys. Rev. C **27**, 2063 (1983).

[46] D. J. Hinde, R. J. Charity, G. S. Foote, J. R. Leigh, J. O. Newton, S. Ogaza and A. Chatterjee, Phys. Rev. Lett. **52**, 986 (1984), erratum: **53**, 2275 (1984).

[47] A. Gavron *et al.*, Phys. Lett. B **176**, 312 (1986).

[48] D. J. Hinde, R. J. Charity, G. S. Foote, R. J. Leigh, J. D. Newton, S. Osaza, A. Chatterjee, Nucl. Phys. A **452**, 550 (1986).

[49] A. Gavron. *et al.*, Phys. Rev. C **35**, 579 (1987).

[50] W. P. Zank, D. Hilscher, G. Ingold, U. Jahnke, M. Lehmann, H. Rossner, Phys. Rev. C **33**, 519 (1986).

[51] D. J. Hinde, H. Ogata, M. Tanaka, T. Shimoda, N. Takahashi, A. Shinohara, S. Wakamatsu, K. Katori, and H. Okamura, Phys. Rev. C **39**, 2268 (1989).

[52] H. Rossner, D. Hilscher, D. J. Hinde, B. Gebauer, M. Lehmann, M. Wilpert, and E. Mordhorst, Phys. Rev. C **40**, 2629 (1989).

[53] D. J. Hinde, D. Hilscher, H. Rossner, B. Gebauer, M. Lehmann, and M. Wilpert, Phys. Rev. C **45**, 1229 (1992).

[54] H. Rossner, D. J. Hinde, J. R. Leigh, J. P. Lestone, J. O. Newton, J. X. Wei, and S.Elfström, Phys. Rev. C **45**, 719 (1992).

[55] D. J. Hofman, B. B. Back, and P. Paul, Phys. Rev. C **51**, 2597 (1995).

[56] J.P. Lestone *et al.*, Phys. Rev. Lett. **67**, 1078 (1991).

[57] M. Thoennessen, D. R. Chakrabarty, M. G. Hermann, R. Butsch, and P. Paul, Phys. Rev. Lett. **59**, 2860 (1987).

[58] R. Butsch, M. Thoennessen, D. R. Chakrabarty, M. G. Herman, and P. Paul, Phys. Rev. C **41**, 1530 (1990).

[59] I. Dioszegi,N. P. Shaw, A. Bracco, F. Camera, S. Tettoni, M. Mattiuzzi and P. Paul, Phys. Rev. C **63**, 014611 (2000).

[60] I. Dioszegi, N. P. Shaw, I. Mazumdar, A. Hatzikoutelis and P. Paul, Phys. Rev. C **61**, 024613 (2000).

[61] C. R. Morton, D. J. Hinde, J. R. Leigh, J. P. Lestone, M. Dasgupta, J. C. Mein, J. O. Newton, and H. Timmers, Phys. Rev. C **52**, 243 (1995).

[62] B. B. Back, D. J. Blumenthal, C. N. Davids, D. J. Henderson, R. Hermann, D. J. Hofman, C. L. Jiang, H.T. Penttilä, and A. H. Wuosmaa, Phys. Rev. C **60**, 044602 (1999).

[63] H. A. Kramers, Physica (Amsterdam) **7**, 284 (1940).

[64] J. O. Newton, D. J. Hinde, R. J. Charity, J. J. M. Bokhorst, A. Chatterjee, G. S. Foote, S. Ogaza, Nucl Phys. A **483**, 126 (1988).

[65] M. Thoennessen, G.F. Bertsch, Phys. Rev. Lett. **71**, 4303 (1993).

[66] G. Chaudhuri, Ph.D. Thesis, arXiv:nucl-th/0411005 (2004).

[67] J. Blocki, Y. Boneh, J. R. Nix, J. Randrup, M. Robel, A. J. Sierk, and W. J. Swiatecki, Ann. Phys. **113**, 330 (1978).

[68] H. Hofmann and P. J. Siemens, Nucl. Phys. A **257**, 165 (1976).

[69] H. Hofmann, Phys. Rep. **284**, 137 (1997).

[70] S. E. Koonin and J. Randrup, Nucl. Phys. A **289**, 475 (1977).

[71] K. T. R. Davies, A. J. Sierk, J. R. Nix, Phys. Rev. C **13**, 2385 (1976).

[72] Y. Abe, S. Ayik, P.-G. Reinhard, and E. Suraud, Phys. Rep. **275**, 49 (1996).

[73] V. E Viola, K. Kwiatkowski, and M. Walker, Phys. Rev. C **31**, 1550 (1985).

[74] T. Wada, Y. Abe, N. Carjan, Phys. Rev. Lett. **70**, 3538 (1993).

[75] D. H. E. Gross, Nucl Phys. A **240**, 472 (1975).

[76] W. N¨orenberg, Z. Phys. A **274**, 241 (1975); W. N¨orenberg, Z. Phys. A **276**, 84 (1976).

[77] D. Hilscher, I. I. Gontchar and H. Rossner, Physics of Atomic Nuclei **57**, 1187 (1994).

[78] P. Fröbrich and I. I. Gontchar, Phys. Rep. **292**, 131 (1998).

[79] J. Randrup, P. Möller, and A. J. Sierk, Phys. Rev. C **84**, 034613 (2011).

[80] H. A. Weidenmüller, Prog. Part. Nucl. Phys. **3**, 49 (1980).

[81] S. Hassani and P. Grangé, Phys. Lett. B **137**, 281 (1984).

[82] Y. Abe, C. Gregoire, H. Delagrange, J. Phys. (Paris), Colloq. **47**, C4-329 (1986).

[83] V. M. Kolomietz and S. V. Radionov, Phys. Rev. C **80**, 024308 (2009).

[84] S. Chandrasekhar, Rev. Mod. Phys. **15**, 1 (1943).

[85] V. M. Strutinsky, Phys. Lett. B **47**, 121 (1973).

[86] Z. Jing-Shang and H. A. Weidenmüller, Phys. Rev. C **28**, 2190 (1983).

[87] Wu. Xi-Zhen and Zhuo Yi-Zhong, Chin. Phys. **1**, 671 (1981).

[88] H. Delagrange *et al.*, Z. Phys. A **323**, 437 (1986).

[89] C. Gregoire, H. Delagrange, K. Pomorski, K. Dietrich, Z. Phys. A **329**, 497 (1988).

[90] E. Strumberger, K. Dietrich and K. Pomorski, Nucl. Phys. A **529**, 522 (1991).

[91] G. D. Adeev, I. I. Gontchar, V. V. Pashkevich, N. I. Pischasov, and O. I. Serdyuk, Sov. J. Part. Nucl. **19**, 529 (1988).

[92] U. Eckern *et al.*, J. Stat. Phys. **59**, 885 (1990).

[93] J. Randrup, Nucl. Phys. A **327**, 490 (1979).

[94] K. E. Rehm, Phys. Lett. B **86**, 260 (1979).

[95] V. C. Barbosa, P. C. Soares, E. C. Oliveira, L. C. Gomes, Rev. Bras. Fiz. **15**, 211 (1985).

[96] P. Fröbrich, in: H. Feldmeier(Ed.), Proc. Gross properties of nuclei and nuclear excitations XV, Hirschegg, Austria, 230 (1987).

[97] G. Chaudhuri and S. Pal, Phys. Rev. C **63**, 064603 (2001).

[98] G. Chaudhuri and S. Pal, Phys. Rev. C **65**, 054612 (2002).

[99] A. V. Karpov, P. N. Nadtochy, D. V. Vanin, and G. D. Adeev, Phys. Rev. C **63**, 054610 (2001).

[100] P. N. Nadtochy, A. V. Karpov, D. V. Vanin, and G. D. Adeev, Phys. Atom. Nucl. **64**, 861 (2001).

[101] G. D. Adeev, A. V. Karpov, P. N. Nadtochii, and D. V. Vanin, Phys. Part. Nucl. **36**, 378 (2005).

[102] Y. Aritomo and M. Ohta, Nucl. Phys. A **744**, 3 (2004); Y. Aritomo, Nucl. Phys. A **780**, 222 (2006).

[103] J. Sadhukhan and S. Pal, Phys. Rev. C **84**, 044610 (2011).

[104] J. P. Lestone, Phys. Rev. C **59**, 1540 (1999).

[105] S. G. McCalla and J. P. Lestone, Phys. Rev. Lett. **101**, 032702 (2008).

[106] J. P. Lestone and S. G. McCalla, Phys. Rev. C **79**, 044611 (2009).

[107] J. P. Lestone, Phys. Rev. C **51**, 580 (1995).

[108] J. Sadhukhan and S. Pal, Phys. Rev. C **78**, 011603(R) (2008), erratum: **79**, 019901(E) (2009).

151

[109] J. Sadhukhan and S. Pal, Phys. Rev. C **82**, 021601(R) (2010).

[110] J. Sadhukhan and S. Pal, Phys. Rev. C **78**, 031602(R) (2010).

[111] G. D. Adeev and P. A. Cherdantsev, Phys. Lett. B **39**, 485 (1972).

[112] J. Maruhn and W. Greiner, Z. Phys. **251**, 431 (1972).

[113] M. Brack, J. Damgaard, A. S. Jensen, H. C. Pauli, V. M. Strutinsky, and C. Y. Wong, Rev. Mod. Phys. **44**, 320 (1972).

[114] P. N. Nadtochy and G. D. Adeev, Phys. Rev. C **72**, 054608 (2005).

[115] P. Möller, D. G. Madland, A. J. Sierk, and A. Iwamoto, Nature (London) **409**, 785 (2001).

[116] H. C. Pauli, Phys. Rep. **7**, 35 (1973).

[117] E. G. Ryabov, A. V. Karpov, P. N. Nadtochy, and G. D. Adeev, Phys. Rev. C **78**, 044614 (2008).

[118] V. M. Strutinsky, N. Ya. Lyashchenko, and N. A. Popov, Nucl. Phys. **46**, 639 (1962).

[119] S. Cohen and W. J. Swiatecki, Ann. Phys. (N.Y.) **22**, 406 (1963).

[120] A. Mamdouh, J. M. Pearson, M. Rayet, and F. Tondeur, Nucl. Phys. A **644**, 389 (1998).

[121] H. C. Pauli, T. Ledergerber, and M. Brack, Phys. Lett. B **34**, 264 (1971).

[122] S. Cohen, F. Plasil, and W. J. Swiatecki, Ann. Phys. (N.Y.) **82**, 557 (1974).

[123] W. J. Swiatecki, Phys. Rev. **100**, 937 (1955).

[124] J. L. Egido, L. M. Robledo, and V. Martin, Phys. Rev. Lett. **85**, 26 (2000).

[125] V. Martin, J. L. Egido, and L. M. Robledo, Phys. Rev. C **68**, 034327 (2003).

[126] E. Khan, N. V. Giai, and N. Sandulescu, Nucl. Phys. A **789**, 94 (2007).

[127] J. C. Pei, W. Nazarewicz, J. A. Sheikh, and A. K. Kerman, Phys. Rev. Lett. **102**, 192501 (2009).

[128] A. J. Sierk, Phys. Rev. C **33**, 2039 (1986).

[129] H. J. Krappe, J. R. Nix, and A. J. Sierk, Phys. Rev. Lett. **42**, 215 (1979); Phys. Rev. C **20**, 992 (1979).

[130] M. Beckerman, M. Blann, Phys. Rev. Lett. **38**, 272 (1977); M. Beckerman, M. Blann, Phys. Rev. C **17**, 1615 (1978).

[131] F. Plasil, R. L. Ferguson, R. L. Hahn, F. E. Obenshain, F. Pleasonton, and G. R. Young, Phys. Rev. Lett. **45**, 333 (1980).

[132] M. Blann and T. T. Komoto, Phys. Rev. C **24**, 426 (1981).

[133] D. J. Hinde, J. R. Leigh, J. O. Newton, W. Galster, and S. Sie, Nucl. Phys. A **385**, 109 (1982).

[134] M. Blann, Phys. Rev. Lett. **49**, 505 (1982).

[135] I. Kelson, Phys. Rev. **136**, 1667 (1964).

[136] M. Mirea, R. C. Bobulescu, and M. Petre, Rom. Rep. Phys. 61, 646 (2009).

[137] A. Baran, Z. Lojewski, K. Sieja, and M. Kowal, Phys. Rev. C **72**, 044310 (2005).

[138] A. J. Sierk and J. R. Nix, Phys. Rev. C **21**, 982 (1980).

[139] P. N. Nadtochy, G. D. Adeev, and A. V. Karpov, Phys. Rev. C **65**, 064615 (2002).

[140] J. Blocki, J. Skalski, W. J. Swiatecki, Nucl. Phys. A **594**, 137 (1995).

[141] J. Blocki, J.-J. Shi, and W. J. Swiatecki, Nucl. Phys. A **554**, 387 (1993).

[142] J. Blocki, F. Brut and W. J. Swiatecki, Nucl. Phys. A **554**, 107 (1993).

[143] J. Blocki, C. Jarzynski and W. J. Swiatecki, Nucl. Phys. A **599**, 486 (1996).

[144] C. Yannonleas, Nucl. Phys. A **439**, 336 (1985).

[145] J. J. Griffin and M. Dowrzecka, Nucl Phys. A **455**, 61 (1986).

[146] S. Pal and T. Mukhopadhyay, Phys. Rev. C **54**, 1333 (1996).

[147] T. Mukhopadhyay and S. Pal, Phys. Rev. C **56**, 296 (1997).

[148] G. Chaudhuri and S. Pal, Eur. Phys. J. A **18**, 9 (2003).

[149] J. Randrup and W. J. Swiatecki, Nucl. Phys. A **429**, 105 (1984).

[150] G. E. Uhlenbeck and L. S. Ornstein, Phys. Rev. **36**, 823 (1930).

[151] Y. Abe, D. Boiley, B. G. Giraud, T. Wada, Phys. Rev. E **61**, 1125 (2000).

[152] U. Brosa, S. Grossmann, and A. Müller, Phys. Rep. **197**, 167 (1990).

[153] G. D. Adeev and V. V. Pashkevich, Nucl. Phys. A **502**, 405c (1989).

[154] K. T. R. Davies, R. A. Managan, J. R. Nix, A. J. Sierk, Phys. Rev. C **16**, 1890 (1977).

[155] G. D. Adeev and P. N. Nadtochy, Phys. At. Nucl. **66**, 618 (2003).

[156] K. H. Bhatt, P. Grange, and B. Hiller, Phys. Rev. C **33**, 954 (1986).

[157] B. Jurado, C. Schmitt, K.-H. Schmidt, J. Benlliure, and A. R. Junghans, Nucl. Phys. A **747**, 14 (2005).

[158] H. Hofmann and J. R. Nix, Phys. Lett. B **122**, 117 (1983).

[159] P. Grange, S. Hassani, H. A. Weidenmüller, A. Gavron, J. R. Nix, and A. J. Sierk, Phys. Rev. C **34**, 209 (1986).

[160] P. Fröbrich, I. I. Gontchar, and N. D. Mavlitov, Nucl. Phys. A **556**, 281 (1993).

[161] N. Carjan, P. Talou, and O. Serot, Nucl. Phys. A **792**, 102 (2007).

[162] F. Scheuter and H. Hofmann, Nucl. Phys. A **394**, 477 (1983).

[163] J. R. Nix, A. J. Sierk, H. Hofmann, F. Scheuter, and D. Vautherin, Nucl. Phys. A **424**, 239 (1984).

[164] D. Boilley, E. Surad, Y. Abe, and S. Ayik, Nucl. Phys. A **556**, 67 (1993).

[165] B. Jurado, K.-H. Schmidt, and J. Benlliure, Phys. Lett. B **553**, 186 (2003).

[166] N. D. Mavlitov, P. Frobrich, and I. I. Gontchar, Z. Phys. A **342**, 195 (1992).

[167] A. V. Karpov, P. N. Nadtochy, E. G. Ryabov, and G. D. Adeev, J. Phys. G **29**, 2365 (2003).

[168] I. I. Gontchar and P. Fröbrich, Nucl. Phys. A **551**, 495 (1993).

[169] G.-R. Tillack, Phys. Lett. B **278**, 403 (1992).

[170] M. Thoennessen, Nucl. Phys. A **599**, 1c (1996).

[171] H. Hofmann, F. A. Ivanyuk, C. Rummel, and S. Yamaji, Phys. Rev. C **64**, 054316 (2001).

[172] J. R. Nix, Nucl. Phys. A **130**, 241 (1969).

[173] G. G. Adamian, N. V. Antonenko, A. Diaz-Torres, and W. Scheid, Nucl. Phys. A **671**, 233 (2000).

[174] J.-D. Bao and Y. Jia, Phys. Rev. C **69**, 027602 (2004).

[175] W. Ye, Phys. Rev. C **76**, 041601(R) (2007).

[176] W. Ye, Phys. Rev. C **80**, 011601(R) (2009).

[177] N. P. Shaw, I. Dioszegi, I. Mazumdar, A. Buda, C. R. Morton, J. Velkovska, J. R. Beene, D. W. Stracener, R. L. Varner, M. Thoennessen, and P. Paul, Phys. Rev. C **61**, 044612 (2000).

[178] F. Plasil, D. S. Burnett, H. C. Breit, and S. G. Thompson, Phys. Rev. **142**, 696 (1966).

[179] D. V. Vanin, G. I. Kosenko, and G. D. Adeev, Phys. Rev. C **59**, 2114 (1999).

[180] I. I. Gontchar, A. E. Gettinger, L. V. Guryan, and W. Wagner, Phys. At. Nucl. **63**, 1688 (2000).

[181] S. Pal, G. Chaudhuri, and J. Sadhukhan, Nucl. Phys. A **808**, 1 (2008).

[182] E. G. Ryabov, A. V. Karpov, and G. D. Adeev, Nucl. Phys. A **765**, 39 (2006).

[183] M. V. Borunov, P. N. Nadtochy, and G. D. Adeev, Nucl. Phys. A **799**, 56 (2008).

[184] A. Ya. Rusanov, V. V. Pashkevich, and M. G. Itkis, Phys. At. Nucl. **62**, 547 (1999).

[185] J. A. Sheikh, W. Nazarewich, and J. C. Pei, Phys. Rev. C **80**, 011302(R) (2009).

[186] P. N. Nadtochy, A. Kelić, and K.-H. Schmidt, Phys. Rev. C **75**, 064614 (2007).

[187] Nuclear Wallet Cards, Isotope Project, NNDC, Lawerence Berkeley Laboratory.

[188] P. Fröbrich, Nucl. Phys. A **545**, 87c (1992).

[189] K. Pomorski, J. Bartel, J. Richert, K. Dietrich, Nucl. Phys. A **605**, 87 (1996).

[190] M. Blann, Phys. Rev. C **21**, 1770 (1980).

[191] J. E. Lynn, Theory of Neutron Resonance Reactions, Clarendon, Oxford, 1968, p. 325.

155